2013

APPLICATION OF REMOTE SENSING IN AQUATIC ECOSYSTEMS

Foad Yousef
Michigan Technological University

APPLICATION OF REMOTE SENSING IN AQUATIC ECOSYSTEMS

By

Foad Yousef

A DISSERTATION

Submitted in partial fulfillment of the requirements for the degree of

DOCTOR OF PHILOSOPHY

In Biological Sciences

MICHIGAN TECHNOLOGICAL UNIVERSITY

2013

This dissertation has been approved in partial fulfillment of the requirements for the Degree of DOCTOR OF PHILOSOPHY in Biological Sciences.

Department of Biological Sciences

Dissertation Advisor:	*Dr. W. Charles Kerfoot*
Committee Member:	*Dr. Robert A. Shuchman*
Committee Member:	*Dr. Sarah A. Green*
Committee Member:	*Dr. Amy M. Marcarelli*
Department Chair:	*Dr. Chandrashekhar P. Joshi*

To my wife, Elaheh, and our parents

Contents

List of Figures

List of Tables

List of abbreviations

ALB = Airborne LiDAR Bathymetry
ANCOVA = Analysis of Co-Variance
ArcGIS = A GIS software package
ASD = Analytical Spectral Devices
AVHRR = Advanced Very High Resolution Radiometer
CASI = Compact Airborne Spectrographic Imagery
CD = Change Detection
CDOM = Colored Dissolved Organic Matter
CHARTS = Compact Hydrographic Airborne Rapid Total Survey
Chl-*a* = Chlorophyll *a* concentration
CTD = Conductivity, Temperature, and Depth
CZMIL = Coastal Zone Mapping and Imaging LiDAR
DEM = Digital Elevation Model
EAARL = Experimental Advanced Airborne Research LiDAR
EEGLE = Episodic Events Great Lakes Experiment
ENVI = An image processing software package
ERDAS IMAGIN = Earth Resources Data Analysis System
ERDC = Development Center-Environmental Laboratory
GIS = Geographical Information System
GLIFWC = Great Lakes Indian Fish and Wildlife Commission
GLNPO = Great Lakes National Program Office
GLPPM = Great Lake Primary Production Model
GLRI = Great Lakes Restoration Initiative
GPS = Global Positioning System
GSWIC = Groundwater Surface Water Interface Criteria
IDL = Interactive Data Language (a programming language)
INU = Internal navigation Unit
JALBTCX = Joint Airborne LiDAR Bathymetry Technical Center of Expertise
$\mathbf{K}_d$ = Light attenuation coefficient
$\mathbf{K}_{d490}$ = Light attenuation coefficient for 490nm wavelength
$\mathbf{K}_{dPAR}$ = Light attenuation coefficient for PAR spectrum
KBIC = Keweenaw Bay Indian Community
LiDAR = Light Detection and Ranging
LND = Lateral Nutrient Displacement
MDEQ = Michigan Department of Environmental Quality
MODIS = Moderate-Resolution Imaging Spectroradiometer
MrSID = Multiresolution Seamless Image Database
MSS = Multi-Spectral Scanner
MTRI = Michigan Tech Research Institute
NAIP = National Agriculture Imagery Program
NOAA = National Oceanic and Atmospheric Administration
NSF = National Science Foundation
NSRDB = National Solar Radiation Data Base
NWRI = National Water Research Institute
OC = Ocean Color
OC2 = Ocean Color Algorithm (Version 2)
OC4 = Ocean Color Algorithm (Version 4)
OPC = Optical Plankton Counter

PAR = Photosynthetic Available Radiation
P-E = Photosynthesis - Irradiance
QA/QC = Quality Assurance/ Quality Control
R_{rs}555 = Remote sensing reflectance for 555nm wavelength
RRS = Remote Sensing Reflectance
SeaDAS = Image processing software
SeaWIFS = Sea-viewing Wide Field-of-view Scanner
SHOALS = Scanning Hydrographic Operational Airborne LiDAR Survey
SYSTAT = A statistical software package
TSM = Total Suspended Matter
USDA = United States Department of Agriculture
USGS = United States Geological Survey

Preface

This dissertation is a collection of four journal articles. **Chapter 1**, "*Approaching storm: Disappearing winter bloom in Lake Michigan*", was published in the Journal of Great Lakes Research, 2010. My contribution to this paper includes remote sensing data analysis, chl-*a* and suspended sediment maps, shipboard sampling (2008) and counting, as well as taxonomic identification of zooplanktoon species in the laboratory. I also performed the Quality Assurance/Quality Control (QA/QC) on both satellite and shipboard collected data. C. Kerfoot led the research and prepared the manuscript. S. A. Green arranged and preformed CTD (Conductivity, temperature, depth) and Acrobat (Wet Lab ECO-AFL) casts and data analysis. J. Budd, D. Schwab, and H. Vanderploeg revised the manuscript and provided us with critical comments.

Chapter 2, "*Trends in bio-optical properties and primary production of the changing Lake Michigan: 13-years of SeaWiFS imagery document a mussel mediated collapse*", is a continuing effort to document the over-a-decade long effects of quagga mussels on Lake Michigan primary production. I prepared the manuscript and carried out the data processing, verification and analysis. C. Kerfoot, R. Shuchman, and G. Fahnenstiel kindly provided me with critical advice as well as helped to edit the manuscript. I intend to submit this article to the Journal of Great Lakes Research in June 2013.

Chapter 3, "*Light detection and ranging (LiDAR) and multispectral studies of disturbed Lake Superior coastal environments*", focuses on the application of LiDAR imagery to study the dynamics of coastal erosional processes and lakebed substrate classification. This work was published in Limnology and Oceanography in 2012. I was thoroughly involved with bottom substrate sampling, spectral data collection, data analysis, remote sensing imagery analysis, and coastal sediment dynamic analysis. C. Kerfoot prepared the manuscript and also put the context of the study into environmental, geological, paleolimnological and historical perspectives. S. A. Green collected light spectral observations and prepared figure 4a. R. Regis provided access to a series of historical aerial imagery from the study area. R. Shuchman, C. Brooks and M. Sayers from MTRI (Michigan Tech Research Institute) provided the terrestrial LiDAR imagery and also prepared figure 8a and 10a. B. Sabol and M. Grave from ERDC(Engineer Research and Development Center)-Environmental Laboratory provided the opportunity to collect LiDAR and MSS (Multi-Spectral Sensor) imagery.

Chapter 4, "*Using LiDAR to reconstruct the history of a coastal environment influenced by legacy mining*", is the follow up of chapter 3 and is published in the Journal of Great Lakes Research, 2013. I prepared the manuscript and preformed the data analysis, imagery preparation and mapping. C. Kerfoot edited the manuscript and also linked the study to local and regional paleo -limnological and -geological events. C. Brooks and R. Shuchman kindly reviewed the LiDAR and MSS data analysis. B. Sabol and M. Graves from ERDC-Environmental Laboratory collected and provided the raw LiDAR and MSS

data.

Acknowledgments

There is not enough space here to acknowledge the many good things that have happened to me for the past 6 years. However, I would truly like to thank my adviser Dr. Kerfoot and his wife, Lucille. They were both very generous and patient with me. Charlie is a true gentleman, extremely supportive and caring and I learned a great deal from him, both in science and life. I need to thank him for setting me free to follow my dream; lakes from space. I would also like to thank Dr. Shuchman, who I found very inspiring and supportive when it came to education and research. I would like to thank Dr. Green and Dr. Marcarelli for giving me extra helpful comments along my career as a graduate student, although I always felt more like a colleague around them. I am also always grateful for having many dear friends who helped me to stay sane and positive. Last but definitely not least, I would like to thank my wife, Ehaheh, for being with me and loving me more than I deserve. Without her, I would not have been able to finish my degree at Michigan Tech.

Abstract

I utilized state the art remote sensing and GIS (Geographical Information System) techniques to study large scale biological, physical and ecological processes of coastal, nearshore, and offshore waters of Lake Michigan and Lake Superior. These processes ranged from chlorophyll *a* and primary production time series analysies in Lake Michigan to coastal stamp sand threats on Buffalo Reef in Lake Superior. I used SeaWiFS (Sea-viewing Wide Field-of-view Sensor) satellite imagery to trace various biological, chemical and optical water properties of Lake Michigan during the past decade and to investigate the collapse of early spring primary production. Using spatial analysis techniques, I was able to connect these changes to some important biological processes of the lake (quagga mussels filtration). In a separate study on Lake Superior, using LiDAR (Light Detection and Ranging) and aerial photos, we examined natural coastal erosion in Grand Traverse Bay, Michigan, and discussed a variety of geological features that influence general sediment accumulation patterns and interactions with migrating tailings from legacy mining. These sediments are moving southwesterly towards Buffalo Reef, creating a threat to the lake trout and lake whitefish breeding ground.

Introduction

Traditional research in many fields of science has focused on local and spatially limited subjects. However, the scientific community as a whole has realized the limitation of traditional approaches in understanding regional and global processes. Now, remote sensing has been able to explain many large scale processes of the Earth ecosystem. Satellites and many airplane-mounted sensors cover vast spatial and temporal aspects of many important ecosystems. Remote sensing has also helped in discovering many unknown ecological phenomena that were impossible to discover before. Today, there is an urgent call in many fields of ecosystem research to extrapolate the findings into regional or global scales.

This dissertation is my effort to apply remote sensing and GIS to better understand freshwater aquatic ecosystems. One of the motivations for my research was to bring remote sensing techniques to bear on large scale biological and ecological processes in freshwater ecosystems. I took advantage of these techniques to discover, verify and quantify biological, physical and ecological processes of coastal, nearshore and offshore waters of Lake Michigan and Lake Superior. These processes ranged from chlorophyll *a* concentration and primary production time series analysis in Lake Michigan to assessing the threat of monitoring coastal stamp sands against fish breeding grounds in Lake Superior.

Lake Michigan: Quagga mussels (*Dreissena bugensis*) were transported via ship ballast waters into the Laurentian Great Lakes in late 1980's. They reached Lake Michigan in 2001 and spread to the southern basin by 2004. In chapters 1 and 2 remote sensing was used to understand the over-a-decade long events in Lake Michigan. Satellite imagery was used to discover, verify, and quantitatively measure the changes in water quality parameters of the lake. Satellite imagery helped to understand and illustrate the spatial and temporal trends in chlorophyll concentration before and after the mussel invasion (**chapter 1**). Quagga mussels successfully removed over 50% of the spring bloom chl-*a* between 1998-2010. The results from this analysis (chapter 1) suggested that quagga mussel literally wiped out the spring bloom. Consequently, in **chapter 2**, and using additional satellite imagery, we continued to follow the effects of mussels have on primary production as well as water transparency, photosynthetic available radiation and chl-*a*. The results suggest a 46-49 % decrease in primary production of Southern Lake Michigan basin between 1998 and 2010. Water transparency increased due to strong filtering effects of quagga mussels. Spatial statistical analysis and change detection were successfully applied to connect quagga mussel population to the observed changes.

Lake Superior: **Chapter 3** and **4** demonstrate the use of remote sensing to resolve anthropogenic effects of mining on ecologically and commercially important aquatic habitats of Lake Superior. Copper mining wastes (stamp sands) located along the Lake Superior shoreline were subject of this study. These stamp sand are located in the vicinity of a commercially important fishing grounds. Using one of the latest remote sensing

technologies, Light-Detection and Ranging (LiDAR), we were able to study and answer many critical questions about the fate of the legacy stamp sand. We used LiDAR in combination with historical aerial photos and Multi-Spectrl Scanner (MSS) imagery to estimate the rate of coastal stamp sand erosion and define the net accretional or erosional trends at different locations along the coast. We also mapped the bottom substrate type and identified underwater stamp sands whereabouts relative to Buffalo Reef (**Chapter 3**). LiDAR also helped to document many underwater features and promontories (e.g. Buffalo Reef, underwater stamp sand bars) as well as to characterize the movement underwater stamp sand bars (**Chapter 4**). This feature again emphasized that the erosion and movement of the stamp sand is very active and threatening to Buffalo Reef and its lake trout and lake whitefish spawning habitats. The results from this study helped to prompt a $16M restoration project initiated by the Army Corps of Engineers in 2012.

Chapter 1

Approaching storm: Disappearing winter bloom in Lake Michigan[1]

W. Charles Kerfoot[a,*], **Foad Yousef**[a], **Sarah A. Green**[b], **Judith W. Budd**[c], **David J. Schwab**[d], **Henry A. Vanderploeg**[d]

[a]Lake Superior Ecosystem Research Center and Department of Biological Sciences, Michigan Technological University, Houghton, MI 49931, USA

[b]Department of Chemistry, Michigan Technological University, Houghton, MI 49931, USA

[c]Department of Geological Engineering and Sciences, Michigan Technological University, Houghton, MI 49931, USA

[d]NOAA Great Lakes Environmental Research Laboratory, 2205 Commonwealth Blvd., Ann Arbor, MI 48105, USA

[*]Corresponding author: wkerfoot@mtu.edu

Index words: Winter chlorophyll, SeaWiFS, Lake Michigan, Quagga

E-mail addresses: wkerfoot@mtu.edu (W.C. Kerfoot), fyousef@mtu.edu (F. Yousef), sgreen@mtu.edu (S.A. Green), jwbudd@mtu.edu (J.W. Budd), david.schwab@noaa.gov (D.J. Schwab), henry.vanderploeg@noaa.gov (H.A. Vanderploeg).

[1]The material contained in this chapter was previously published in *Journal of Great Lakes Research* 2010, 36 Sp. Iss. SI Suppl. 3 30-41

1.1 Abstract

Between 1990 and 2001, late-winter phytoplankton blooms were common in parts of the lower Great Lakes (southern Lake Michigan, Saginaw Bay and southern Lake Huron, and western Lake Erie), providing resources for over-wintering zooplankton. In Lake Michigan up to 2001, detailed remote sensing and ship studies documented well-developed late-winter blooms in the southern gyre (circular bloom termed the 'doughnut'). However, from 2001 to 2008, the winter blooms in Lake Michigan also supported early season veliger larvae from the introduced, cold-water adapted "profunda" morph of quagga mussels (*Dreissena rostriformis bugensis*). Remote sensing and ship studies revealed that settled mussels caused an extraordinary increase in water transparency and a simultaneous decrease of Chl *a* in the late-winter bloom. Before quagga mussels in 2001, water transparency was 74-85% at deep-water sites, whereas it increased progressively to 89% by 2006 and 94-96% by 2008. Chlorophyll *a* concentrations in the gyre rings were 1.1-2.6 μg/L in 2001, declining to 0.5-1.7 μg/L by 2006 and 0.4-1.5 μg/L by 2008. The reduction of Chl *a* in the winter bloom rings from 2001 to 2008 was 56-78% for the western limb and 74-75% for the eastern limb. Zooplankton species abundance, composition and abundance also changed, as cyclopoid copepods became very scarce and overwintering omnivorous calanoid copepods declined. Reduction in late-winter phytoplankton and zooplankton poses a serious threat to open-water food webs.

1.2 Introduction

Prior to the development of remote sensing, details of winter circulation and production in the Great Lakes were poorly known, in part because of hazardous ship conditions ([58]; [89]). On the National Science Foundation (NSF) and National Oceanic and Atmospheric Administration (NOAA) Episodic Events Great Lakes Experiment (EEGLE) project, we discovered a late-winter algal bloom in southern Lake Michigan (Chl *a* 'doughnut' ring; [36]; [94]). Contrary to expectations of fairly uniform open waters from February to April, sea-viewing wide field-of-view sensor (SeaWiFS) and moderate-resolution imaging spectroradiometer (MODIS) imagery uncovered spatially complex resuspended sediment, Chl *a*, and CDOM patterns in offshore waters. Apparently, phosphorus-rich coastal river waters and nearshore sediments ([24]) were captured by intensified winter currents, entrained along gyre convergence zones and moved into deeper waters, stimulating a ring of offshore production ([93], [94]). Cross-lake surveys (April 2001, 2006) with two separate profiling instruments revealed columnar patterns consistent with a spatially complex, rotating gyre structure. Optical plankton counter (OPC) transects and zooplankton net tows indicated that spatial heterogeneity extended to higher levels of food webs.

Here we note that the late-winter blooms were not peculiar to the southern basin of Lake Michigan, but also occurred regularly in other Great Lake waters, where the

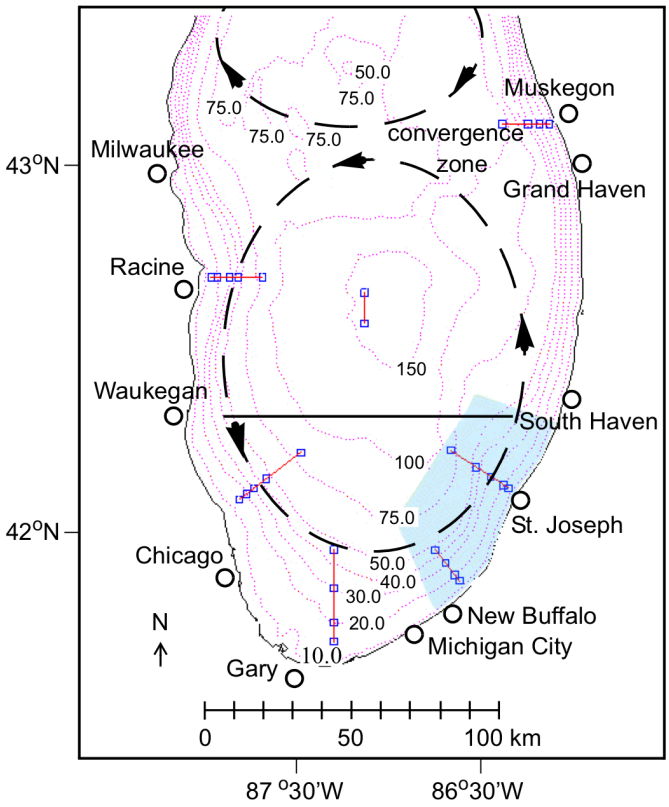

Figure 1.1: Southern Lake Michigan, indicating transect stations for 1998-2000 ship-board TSM: Chl a validation studies (connected squares off various cities) and the April 2001, 2006, and 2008 Seabird CTD/BAT southern transects (62 stations, solid line from South Haven to Waukegan). Gyre circulation of waters after a northwest wind is indicated by arrows, with the position of the convergence zone off Grand Haven/Muskegon noted. Blue area is region of intensified monitoring during the EEGLE project and region of greatest phosphate loading from river discharges.

geometry of bloom patterns differed due to bathymetry, circulation and lake orientation ([15];[16]). In Lake Michigan, there were indications from remote sensing and ship-board studies that the winter 'lateral nutrient displacement' phenomenon had been present for at least 25 years. Up to 2001, the late-winter bloom was probably an important feature that benefited predominately cold, deep-water native taxa (phytoplankton and zooplankton), and that normally supported over-wintering strategies.

The degree that global climate change is involved in accentuating late-winter blooms is unknown, yet global climate change appears to be reducing ice-cover ([11]) and increasing the frequency and intensity of winter storms ([164]), thus promoting the observed lateral displacement of limiting nutrients by capturing river discharges, resuspended sediments, and redirecting coastal algae ([94]). Usually these processes would have enhanced late-winter productivity from 2001 to 2008 in Lake Michigan. However, this has not been the case as cold-adapted veliger larvae of the introduced quagga mussel (*Dreissena rostriformis bugensis*) have also exploited the late-winter productivity pulses. Water column filtration from settled adults is now seriously compromising anticipated late-winter bloom patterns.

It is truly remarkable that one or two species of mussels can so transform the entire ecosystem. During the EEGLE study, zebra mussel effects were confined largely to coastal waters off Chicago ([143]; [180]). In recent years, a 'shallow water morph' of the quagga mussel (*Dreissena rostriformis bugensis*) has begun to replace zebra mussels in shallow areas of the Great Lakes ([140]). In deeper (>30 m), cooler waters, another form of *Dreissena rostriformis bugensis* (the 'profunda morph') has increased tremendously ([140], [141]). Unlike the zebra mussel, the 'profunda morph' is adapted for life on soft sediments (has elongated incurrent siphon and lies on the bottom on one of its valves without attachment with byssal threads). The life history cycle for quagga mussels begins somewhat earlier than zebra mussels and under lower temperatures (e.g., [49]). Quagga mussel spawning occurs in early winter, late spring, late summer, and fall

([160];[49];[141]). The embryos first develop into swimming larvae. In 29 days they develop intestines and a feeding and swimming organ known as the velum. Once the velum appears, the larvae are termed veligers. In the veliger stage they develop D-shaped (straight-hinged) shells about 70-100 μm long ([171]). The settlement of mussels to the bottom varies as a function of temperature and food concentration. At temperatures of 22-26°C, settlement can occur after 32 d ([5]), yet it can take as long as several months at low temperatures and food concentrations.

Moderately high densities of quagga veligers feed on the late winter bloom pulse, and are dispersed by strong currents associated with winter storms ([94]). This soft-sediment species can settle in both shallow and deep waters, reaching 5-15 thousand individuals/m^2. In Lake Michigan, adult quagga mussels increased dramatically in density between 2001 and 2006, spreading below 100 m depth ([140],[141]). At high densities, adult quagga mussels are filtering much of the overlying water column along the coastal shelf ([181]), seriously reducing the typical spring bloom.

Here we first discuss long-term evidence for late-winter blooms in theGreat Lakes between 1998 and 2001, then focus in on Lake Michigan. Remote sensing and coordinated ship studies document how the adult mussel filtration effects are altering late-winter waters and the circular late-winter phytoplankton bloom ('doughnut'). Our observations 1) chronicle the development of a late-winter 'bottleneck' in Lake Michigan and 2) raise grave concerns about the consequences of future productivity losses on winter pelagic foodwebs.

1.3 Methods and materials

1.3.1 Remote sensing (AVHRR, SeaWiFS, MODIS) imagery

As part of the NSF/NOAA EEGLE Project in Lake Michigan, we processed Advanced Very High Resolution Radiometer (AVHRR 1992-2002) and sea-viewing-wide-field-of-view sensor (SeaWiFS 1997-2002) imagery ([183]; [93]). Since becoming routinely available in 1992, AVHRR (NOAA TIROS-N series, NOAA-10 and NOAA-11) imagery has confirmed near-coastal and offshore sediment plumes (channel 1-3 visible bands) and corresponding temperature structure (3-5 bands) every year during late winter (March-April) in Lake Michigan ([111]; [183]; [35]). SeaWiFS and MODIS imagery has also verified late-winter offshore structures, although the spatial extent and duration varies from year to year ([86]; [93], [94]; [172]). Since the sensor swaths included the entire Laurentian Great Lakes region, SeaWiFS image processing (1998-2002) was extended to the other lakes.

During the early EEGLE SeaWiFS processing,we became aware of the 'doughnut-shaped' bloom pattern of Chl *a* in offshore Lake Michigan waters ([36]). The SeaWiFS sensor was located on the PorbView-2-satellite, which imaged the Great Lakes between 17:30 and 19:30 h coordinated universal time ([71]; approximately the same as Greenwich mean time). The instrument had a scan coverage of 2800 km, a nadir resolution

of 1.1 km^2, and contained a passive, eight band multispectral scanner. The scanner picked up reflectance in six visible bands (412 nm, Gelbstoffe; 443 nm, chlorophyll; 490 nm, pigment; 510 nm, chlorophyll; 555 nm, sediments and pigments; and 670 nm, atmospheric correction) used for estimating pigment and total suspended material (TSM) concentrations, and two near-infrared bands (765 nm and 865 nm) used primarily for atmospheric corrections ([129]).

Time series SeaWiFS imagery was processed using SeaWiFS MAP image processing software ([183]) and a modified IDL/SeaDAS (http://seadas.gsfc.nasa.gov/seadas/) code that included the 1998 sensor calibration ([129]) and the coastal atmospheric correction scheme ([175], [174]; [35]). SeaWiFS Chl *a* (OC2) maps were derived from empirical, band-ratioing algorithms, OC2v4 ([148]) and OC4v4 ([147]). The OC2v4 Chl *a* algorithm used a ratio of SeaWiFS bands 3 and 5 ([149]; [183]). See Kerfoot et al. ([94]) for OC2, OC2v4, and OC4v4 equations and more details on procedures.

To check for long-term spatial trends in the southern Great Lakes, we utilized OC2 images and scored the incidence of late-winter bloom patterns between 1998 and 2002. Spectral reflectance (RRS) at 555 nm was used to estimate total suspended matter (TSM; [129]). The ability to observe late-winter blooms is greatly hindered by cloud cover ([172]), but the observations provided strong evidence for past widespread incidence. To provide a quantitative temporal record of Chl *a* concentration decline within the Lake Michigan 'doughnut', we superimposed the southern ship transect on SeaWiFS images between

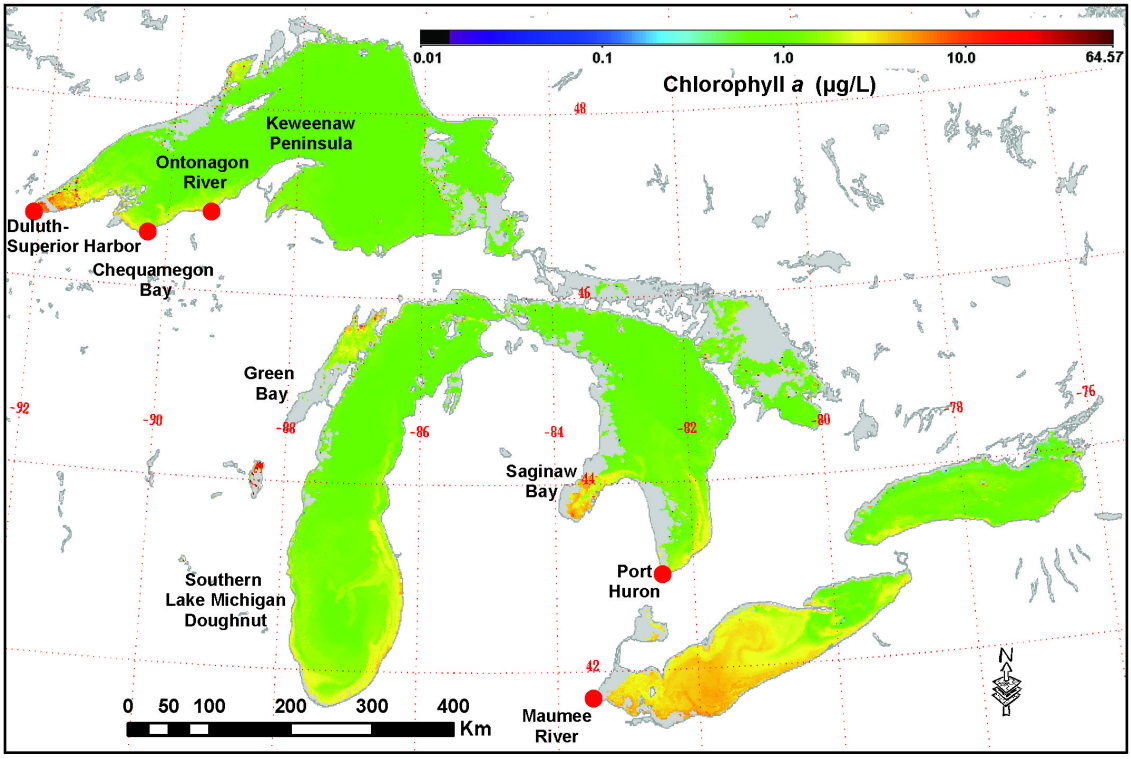

Figure 1.2: Chlorophyll a patterns (SeaWiFS imagery) for the Great Lakes on 24 March 1998, an El Niño year. During this winter, ice development (grey area) was exceptionally scarce. Under prevailing westerly winds, note the movement of Chl *a*-rich waters out of Duluth/Superior Harbor, Chaquamegon Bay, and Ontonagon River in Lake Superior; rotation of Chl *a*-rich waters into a circular ring ('doughnut') in southern Lake Michigan; movement of Chl *a*-rich waters out of SaginawBay and circulation around Port Huron into the southern basin of Lake Huron; intense development in the shallow southwestern basin of Lake Erie off the Maumee River, movement of waters along the northern rim into the middle basin of Lake Erie.

1998 and 2008 and chose Chl *a* pixel values from the inner and outer rims of the eastern and western 'doughnut' bands. We then regressed the mean values against time, over the complete 1998-2008 interval.

Concerns about coastal suspended matter (TSM) and colored dissolved organic

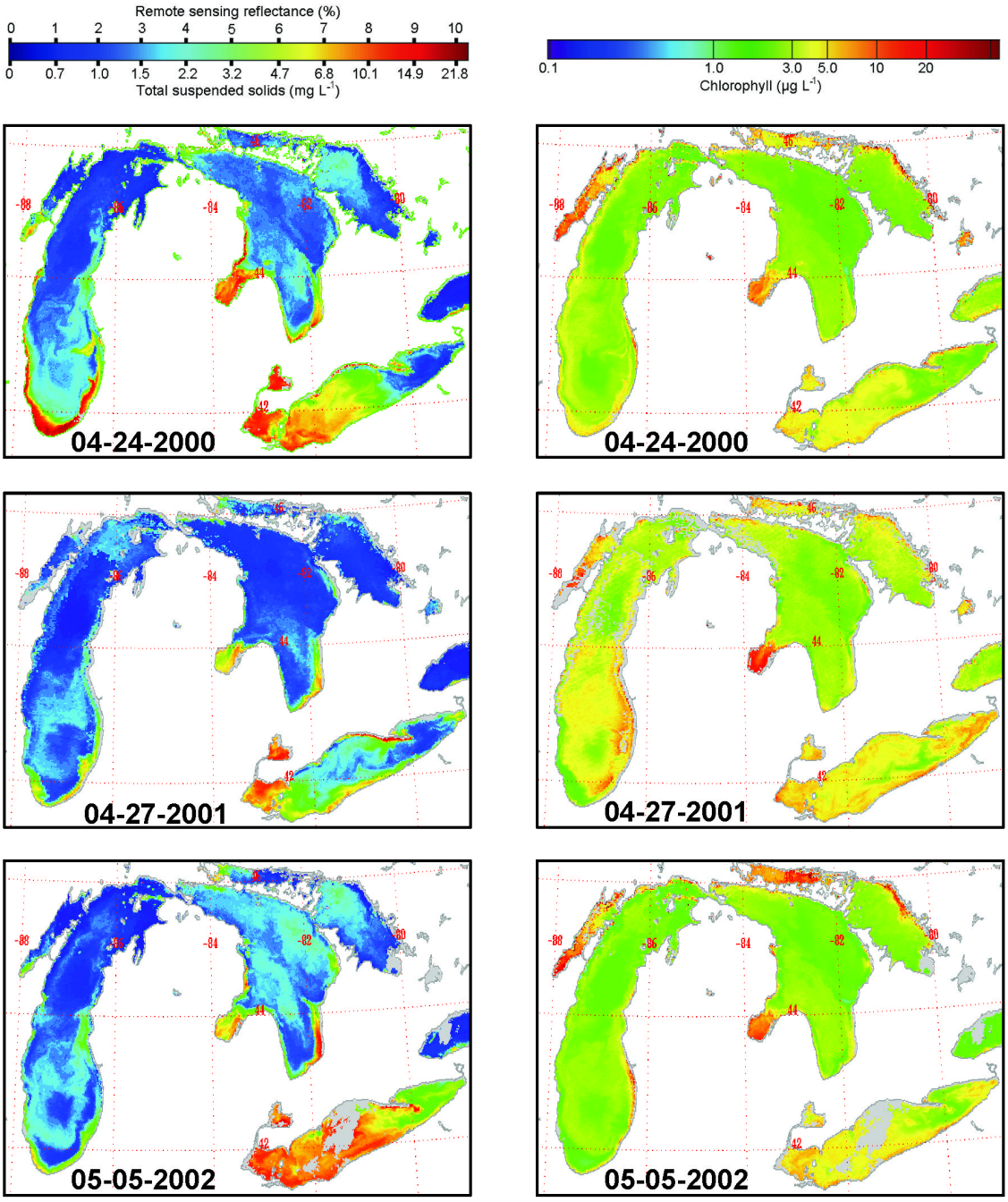

Figure 1.3: Late-winter TSM and Chl *a* patterns, 2000-2002 (SeaWiFS imagery). Left column is total suspended matter (TSM), derived from SeaWiFS 555 nm band reflectance, whereas right column is Chl *a*, from OC2 equation (see methods and materials). Scale bar is given above each column. Dates are provided for the various years.

matter (CDOM) influencing OC2 interpretations are discussed in Stumpf ([173]), Stumpf et al. ([174]) and Budd and Warrington ([35]). CDOM interference was severe for Lake Superior OC2 Chl *a* estimates, but not for Lake Michigan Chl *a* estimates (Budd and Warrington, 2004). The entire set of processed images bearing on pre-quagga conditions from 1998 to 2002 is posted at: http://www.geo.mtu.edu/great_lakes/lakersi/cgi-bin/seawifs.cgi.

1.3.2 Phytoplankton distribution and Chl *a* concentrations

Several cruises were used to validate SeaWiFS imagery and to determine water column variables. Ship-based Chl *a* and TSM samples were collected from January to November 1998-2000 along five transects off Racine, Chicago, Gary, St. Joseph, Muskegon, and at two central stations (Fig. 1.1) and used in initial Chl *a* on C_{SAT} and R_{555} (SeaWiFS) regressions (Table 1.1, regression 1). These initial EEGLE determinations were supplemented in later years by additional cruise measurements along the Lake Michigan southern transect. Field and laboratory calibration curves utilized a pure Chl *a* standard (*Anacystis nidulans*, Sigma C6144). Between 1 and 3 L of lake water from 0, 10, 20, to 25 m depths were filtered (preweighted Whatman GF/F 55 mm filters) at 30-40 stations along the 62-station southern transect. Both field and laboratory values for Chl *a* were run on a Turner TD-700 Fluorometer using the acid (phaeophytin) correction method ([186]) on 90% acetone extracts. The 2006-2008 cruises featured a combination of ship-board Chl

Table 1.1
Validation and empirical relationships for southern Lake Michigan: coefficients of linear (Y=bX-a) regressions relating ship-sampled Chl *a* (μg/L) to CSAT Chl *a* (μg/L) or CTD fluorescence (FL). In the first regression, Chl *a* measurements taken along numerous transect stations at 5-10 m depth from 22 Mar 98-11 Sep 99 are regressed on SeaWiFS CSAT Chl *a* values, whereas the second regression utilizes Chl *a* measurements from the southern transect, 21-23 April 08. In the third to fifth regressions (2001, 2006, 2008), Chl *a* from southern transect stations is regressed on Seabird CTD fluorescence (FL) values. The lowest, log-linear regression (equation 6) relates SeaWiFS R_{555} values to ship-sampled TSM (mg/L; total suspended matter). TSM measurements for R_{555} validation were taken Jan-Mar 1998 and Feb-Apr 1999 from 5 to 10 m depths at various coastal transect stations plotted in Fig. 1.1. All regressions are significant at the $p<0.001$ level.

Linear regression	n	b$\pm$SE	a$\pm$SE	r^2
1. Chl a on CSAT 1998-1999	18	1.079$\pm$0.102	-0.087$\pm$0.171	0.874
2. Chl a on CSAT 2008	51	1.209$\pm$0.058	-0.022$\pm$0.082	0.900
3. Chl a on FL(CTD) 2001	36	23.433$\pm$1.81	-0.501$\pm$0.097	0.836
4. Chl a on FL(CTD) 2006	31	21.331$\pm$2.54	-0.349$\pm$0.196	0.708
5. Chl a on FL(CTD) 2008	52	24.274$\pm$1.29	-0.398$\pm$0.106	0.872
Log-linear regression				
6. R_{555} on *log*(TSM)	32	5.975$\pm$0.387	2.005$\pm$0.15	0.891

a determinations supplemented by later laboratory determinations on additional filtered samples. The field and laboratory filtered samples were used routinely to calibrate CTD and Acrobat (Wet Lab ECO-AFL) fluorescence values (Table 1, regressions 3-6). In addition, CTD and Acrobat Chl *a* measures were checked by running a dilution series of previously calibrated algal cultures (*Chlamydomonas*) through the fluorescence sensors.

Near-surface Chl *a* values were used to validate SeaWiFS OC2v4 reflectance readings. Because field surface samples often showed daylight Chl *a* quenching ([94]), which influenced CTD fluorometry readings, 10-20m Chl *a* determinations were favored

for validation regressions over surface values. However,winter Chl *a* values for 10-25m readings were spatially similar and highly correlated. For example, on the April 2008 cruises, correlations between 10m, 20m, and 25m Chl *a* values along the ship sampling transect were very high (10 m vs 20m r^2=0.976; 10m vs 25m r^2=0.974; 20m on 25m r^2=0.990; N=74), reflecting winter deep-water vertical mixing.

A previously published relationship between SeaWiFS CSAT and R555 estimates and in situ TSM concentrations (regression 6, Table 1.1) was used to look at long-term trends. The ground-truth effort provided an empirical nonlinear relationship between SeaWiFS R_{rs} (555) and ship-based TSM measurements over the observed range of 1-12 mg/L. The logarithmic fit was heuristic for it covered saturating values in nearshore turbidity plumes, while revealing subtle patterns for low-concentration levels in offshore waters. Further discussion of validations used with SeaWiFS imagery during the EEGLE project can be found in Bergmann et al. ([21]) and Lohrenz et al. ([115]). Bergmann et al. ([21]) discuss difficulties in OC2 Chl *a* determinations relating to marine versus freshwater phytoplankton species differences. Additional water column calibrations between CTD fluorometry and Chl *a* are discussed in Vanderploeg et al. ([180]) and Lohrenz et al. ([115]).

1.3.3 Chlorophyll *a* and zooplankton along southern Lake Michigan transect: Developing impact of quagga mussels

Four cruises (April 2001, 2006-2008) aboard the RV Laurentian compared the spatial nature of the late-winter bloom ('doughnut') in southern Lake Michigan, three along the same latitudinal transect (2001, 2006, 2008). All four cruises originated from the eastern port of Muskegon, Michigan. The three E-W cruises (Fig. 1.1) traversed along a mean latitude of 42.372° from South Haven to Waukegon and back, cutting across the center of the circular algal bloom on 19-21 April 2001 and along its southern ring on 12-15 April 2006 and 23-25 April 2008. Over the 3-4 day cruises, Seabird SBE 911plus conductivity-temperature-depth (CTD) full vertical profiles were taken from around 64 stations at 1.85-km (1 nautical mile) intervals (longitude 87.745°W to 86.320°W). The Seabird CTD instrument package recorded depth, temperature, Chl *a* fluorescence, photosynthetically available radiation (PAR), and water transmissivity. The device was equipped with a SeaTech transmissometer, Biospherical Instruments scalar PAR sensor (400 to 700 nm), and Wet Lab ECO-AFL fluorometer. Contour plots were generated from the vertical CTD casts using Matlab (Mathworks). The CTD data were binned at 0.5-m depth intervals from casts every 1.85 km for a total of ca. 10,400 points for each parameter. Data were interpolated in the horizontal dimension using the cubic polynomial function to provide ca. 32,000 points for contouring the cross-sections ([94]). On April 2-3, 2007,

we traversed diagonally towards the 'doughnut hole' from Muskegon harbor, taking CTD vertical profiles, but were forced off the lake by an approaching storm. On April 25, 2008, we traversed diagonally back to Muskegon along a similar transect, and then along the nearshore coastline.

In addition to CTD vertical casts, we towed a BAT (Sea Sciences Acrobat) in tow-yo undulating fashion (5-20-m depth amplitude) behind the ship in 2001 and horizontally (10-20-m depth) in 2006 and 2008. In addition to temperature, Chl *a*, and concentration of dissolved organic matter (CDOM) fluorescence estimates, the BAT contained an optical plankton counter (OPC; Mini Optical Plankton Counter, model OPC-2T, Focal Technologies) that counted and sized zooplankton. The OPC utilized a flow-through tunnel with a thin rectangular light beam (4×20mm cross-section) that measured the profile area of each plankton target, and converted the size into an equivalent spherical diameter (ESD). The device was towed at around 2.5 m/s (ca. 4. 5 knots). Counts were binned in two different size categories (Bin 1, 0.25-0.50 mm; Bin 2, 0.5-1.0 mm). Densities (counts/m^3) were plotted as a 50-interval mean and high-low range of 10-s-duration counts. On 25 April 2008, south of Muskegon, the BAT with the OPC was towed horizontally from offshore, through the thermocline region, and into the nearshore zone to record horizontal patterns for zooplankton densities.

OPC counts in Lake Michigan have been compared with plankton tows ([114]; [94]) and in the laboratory ([114]). In open, dilute waters counts were reliable, whereas in

nearshore turbid waters prior to 2002, they tended to be higher, by virtue of non-living particles being counted along with living plankton ([114]).

In April 2006-2008, vertical zooplankton tows were taken at 24 stations along the E.W transect with a 1-m diameter Puget Sound plankton net (125 μm Nitex). In April 2007, they were obtained along the diagonal transect out of Muskegon harbor. The vertical plankton tows were subsampled with a Hensen-Stempel pipette and counted under a 50$\times$ Olympus SZ30 dissection scope equipped with a 2$\times$ auxiliary adapter. The samples allowed calculation of species densities and indicated changes in community structure from 1998-2001 (EEGLE Project) to 2006-2008. Veliger larvae of quagga mussels also were counted in the 2006-2008 samples, although use of 125 μm mesh meant that smaller sizes were lost. Statistical comparisons utilized Systat ([188]).

1.4 Results

1.4.1 Remote sensing evidence for late-winter phytoplankton blooms

SeaWiFS imagery revealed spatially complex suspended sediment and Chl *a* patterns in several Laurentian Great Lakes during winter (January to April). The spatial patterns were first detected during the low ice-cover El Niño winter of 1998, largely because SeaWiFS imagery became available and the lakes were relatively free of ice. A SeaWiFS image from

March 24, 1998, illustrates elevated Chl *a* (OC2) late-winter plumes in all ice-free lakes, but most pronounced in southern Lake Michigan ("doughnut"), southern Lake Huron and western Lake Erie (Fig. 1.2). In Lake Superior, elevated Chl *a* regions were found off Duluth. Superior Harbors, Chequamegon Bay, and along the southern shallow coastal shelf off the Keweenaw Peninsula. Ice-covered regions are indicated in gray. In the lower lakes, the blooms were even better developed in shallow coastal regions and were sometimes mixed with drifting ice (Green Bay; Saginaw Bay and off Port Huron, Lake Huron; western and middle basins, Lake Erie). The coastal and offshore patterns indicated a previously undetected relationship between storm-induced gyre formation, coastal water plus resuspended sediment capture, and late-winter productivity.

The cold-water blooms were not restricted to abnormally warm, nearly ice-free winters, as images from moderate ice-cover years of 2000-2002 also showed very strong suspended sediment (R_{rs} 555) and Chl *a* (OC2) bloom patterns in late March to early May (Fig. 1.3, Table 1.2). Again, cloud or ice-covered regions (high albedo) are indicated in gray in the images. In Lake Michigan, ship surveys showed that the patterns temperature, and other variables (colored dissolved organic matter, transmissivity) associated with the spatially complex, rotating surface gyre structure ([36]; [94]).

The precise circulation patterns appeared to be basin-specific, subject to ice-off dates, bathymetry configuration, and prevailing wind stress and propagated currents ([15]). For example, multiple images showed that in southern Lake Huron, following ice-off,

Table 1.2
Using SeaWiFS imagery, we noted the number of days that winter algal blooms were seen in southern Lake Michigan, Saginaw Bay in Lake Huron, and western Lake Erie. With SeaWiFS imagery, there were two overpasses per day. The table suggests that late winter algal blooms were relatively common in the lower Great Lakes and in lower Lake Michigan before quagga mussels began increasing. Daily cloud cover obscured many of the scenes in January and February, accounting for low early season totals, whereas clear skies were more common in March and April, allowing better detection of algal blooms.

Year	Lake Michigan				Lake Erie				Lake Huron			
	J	F	M	A	J	F	M	A	J	F	M	A
1998	-	-	5	4	2	-	5	9	-	-	6	7
1999	-	1	11	5	1	3	12	13	-	1	9	13
2000	-	-	7	12	1	2	11	8	-	4	10	12
2001	1	1	5	11	-	2	8	15	-	-	2	10
2002	-	5	5	5	3	10	7	9	-	2	4	11

sediments moved out of Saginaw Bay counterclockwise (cyclonic) around the southern basin. They also rotated counterclockwise off Port Huron, delivering sediments and phytoplankton into deeper waters. In Lake Erie, again following ice-off, Maumee River discharges and resuspended sediments from the shallow western basin combined and moved northward and eastward (anticyclonic) into the central and eastern basins (Figs. 1.2 and 1.3). Algal growth was most pronounced in Saginaw Bay and in the western and middle basins of Lake Erie, as the latter achieved surface Chl *a* concentrations as high as 5.15 μg/L. Circulation of sediments and algae was also evident in southern Lake Michigan, moving off the eastern coastline near the convergence zone (Figs. 1.1-1.3). Algal activity within the circular offshore ring ("doughnut") in Lake Michigan appeared more diffuse than in Saginaw Bay or Lake Erie, and reached maximum Chl *a* concentrations of 2.3 μg /L during 1998-2002. The important point here is that these phytoplankton blooms

were late winter phenomena (Table 1.2), distinct from the traditional warmer water spring blooms that developed behind the coastal 'thermal bar' in late April to early June, and that peaked in May-early June.

1.4.2 Details of "doughnut" in Lake Michigan before quagga mussels

In Lake Michigan, we studied late-winter bloom rings ("doughnut") in much greater detail than in the other lakes. In southern Lake Michigan, water circulation appeared highly episodic, because it was strongly wind driven. Wind direction during winter was predominantly from the north to northwest, propagating two counter-rotating gyres: a counterclockwise-rotating (cyclonic, south basin) gyre to the right of the wind and a clockwise-rotating (anticyclonic, north basin) gyre to the left of the wind (Fig. 1.1; [16]; [17]; [163]). After a large storm, the gyres were separated by a convergence zone (Figs. 1.1-1.3) along the downwind shore (Grand Haven to Muskegon) with resulting offshore flow and a divergence zone along the upwind shore with onshore flow. Offshore flow in the convergence zone could be seen to extend into the rotating offshore gyre (Figs. 1.2 and 1.3). Turbid water captured in the convergence zone contained very fine-grained material (grain size b20 μm), in concentrations between 1 and 5 mg/L, which could stay in suspension for weeks. Within about 2.7 days after capture, the nutrient-rich water created a doughnut-shaped algal bloom in water depths roughly between 40 and 100 m. A subsequent

strong storm could create a new nearshore turbid (resuspended sediment) region, or in the absence of a storm, the offshore “doughnut” ring could close and dissipate.

How long has the “doughnut” late-winter bloom been occurring? Remote sensing studies (AVHRR, SeaWiFS) in the Laurentian Great Lakes are hindered during winter by cloud cover, particularly in January-February ([172]; also see Table 1.2). Yet inspection of AVHRR imagery confirmed TSM and temperature spatial patterns from 1992 to the present (16 years). Similar scrutiny of SeaWiFS imagery revealed winter bloom structures from 1998 until the present, a continuous 10-year interval. April sampling by GLNPO (Great Lakes National Program Office) from 1982 until the present (26 years) indicates strong horizontal patterns for Chl *a* along our E-W transect region that are very consistent with the “hole” and circular “doughnut” bands seen in SeaWiFS images (Glenn Warren, unpubl. data). That is, values are lowest in the “doughnut hole”, higher in the left turbid limb, and highest in the right turbid limb, where PO_4 loading from rivers is known to be greatest (St. Joseph, Kalamazoo, Grand, and Muskegon Rivers, [104]; [150]).

The “doughnut” structure can be present in January, but is most pronounced in March-April (Table 1.2). It can also persist through multiple storms. For example, in 2000, the circular bloom feature was present from March 7 until April 25, whereas in 2001, it extended from April 8 until April 24. If storms are not strong, or near the end of April, the structure would dissipate as rings expand to fill in the central "hole". On 19-22 April 01 the “doughnut” was well formed and the cruise path cut across the hole of the structure,

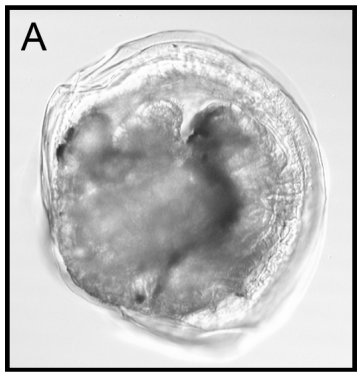

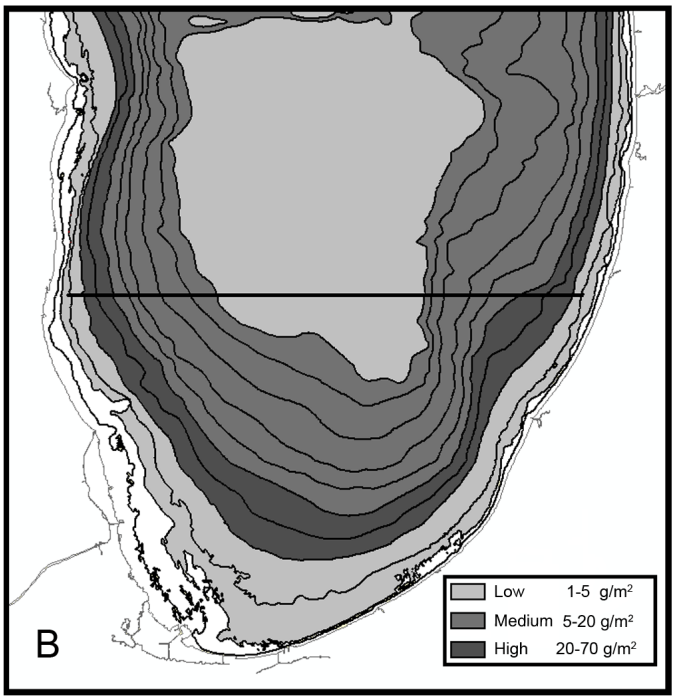

Figure 1.4: Dreissenid mussels in Lake Michigan waters: A) veliger stage from April southern transect sampling; B) depth distribution of settled quagga mussels (*D. rostriformis bugensis*) in southern Lake Michigan (after [140]).

whereas on 12-15 April 06 and 21-23 April, 08, the ring pattern was more diffuse.

Phytoplankton in net tows and water samples from 2001 to 2008 dates documented

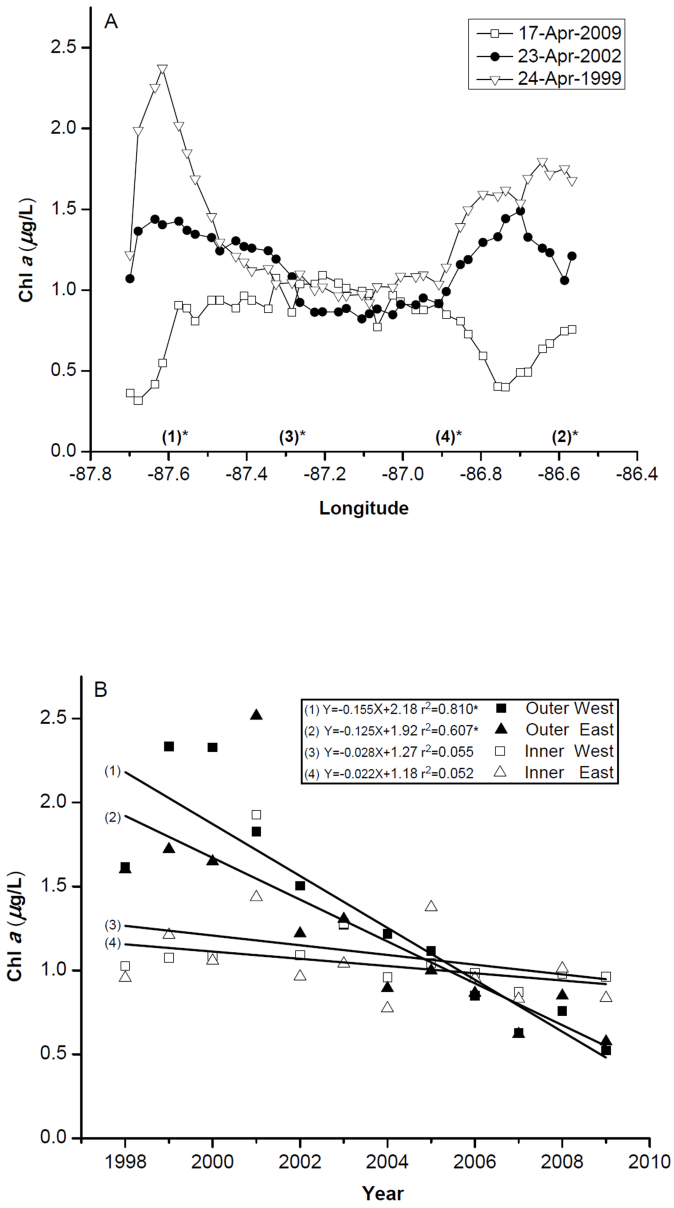

Figure 1.5: Reduction of Chl a around the outer edge of the 'doughnut', estimated from SeaWiFS images: A) Chl *a* values along southern Lake Michigan transect in 1998, 2006, and 2009, taken from SeaWiFS images (mean of 4 nearby pixels per site). Numbers on top of x-axis indicate longitudinal position of the "inner" and "outer" edge regression values plotted in (B). B) Linear regressions are fit to yearly Chl *a* values in outer edge versus inner edge of rings. Paired linear regressions represent east and west limbs of the 'doughnut', contrasting reduction in outer (solid symbol) versus inner (hollow symbol) margin. Regression equations are given for each line (*highly significant slope, $p<0.01$).

that the species composition in the doughnut had large-bodied diatom species [*Aulacosira* (*Melosira*), *Asterionella*, *Tabellaria*, *Fragilaria*; [94]], in addition to open-water small centric diatoms (*Cyclotella*), cryptophytes, and flagellates typically found in deep waters ([21]). Deep net tows were often clogged with *Aulacosira*. However, zooplankton samples from 2006 included substantial concentrations of quagga mussel veliger stages (Fig. 1.4a), although counts were low-biased because we used 125 μm netting. However, dramatic differences have now appeared in the late-winter and early spring spatial distribution of Chl *a* patterns. These transformations appear due to the spread of settled, filtering quagga mussels.

1.4.3 Disappearing "doughnut" in Lake Michigan

Both remote sensing images and ship-board measurements record a major reduction in Chl *a* and a dramatic increase in water transparency since 2002, coincident with increase in dreissenid mussels. Winter veliger larvae from *D. rostriformis bugensis* were detected during the 2006 cruise (Fig. 1.4a). These larvae were not present during the EEGLE late-winter pelagic collections (1998-2001). In 2006, the veligers were shown to be differentially concentrated in the rings of the “doughnut”, benefiting from the late-winter productivity pulse ([94]). During the last three years, veligers were most abundant in 2006, and declined in 2008 (Table 1.3).

Whereas zebra mussels (*D. polymorpha*) have a preference for hard substrates, the rounded and lighter shell and longer, more vertical siphon of *D. rostriformis bugensis* allows this species to colonize softer substrates. Individual *D. rostriformis bugensis* were capable of colonizing substrate under the "doughnut", just by settling out of suspension. Over the interval from 2002 until 2006, the density of settled mussels increased exponentially ([140]). By 2006-2008, mean densities of attached mussels ranged between 6 and 19×10^3 individuals/m^2 at 16-30m depth, 12 and 13×10^3 individuals/m^2 at 30-50 m depth, and 5×10^3 individuals/m^2 at 51-90m depth ([140][141]). As the ability of settled adults to clear the water column is related to the volume of water over the benthic interface, one would expect filtration effects from settled adults to be most pronounced around the shallow rim of the "doughnut" (Fig. 1.4b; modified from [140]). The clearing in nearshore waters around the outer, shallow rim of the "doughnut" is evident in plots of SeaWiFS Chl *a* values through time (Fig. 1.5). Values from the outer edges of the "doughnut" show pronounced, highly significant (OW $_1$F10=48.0; p=4.05E-05; OE $_1$F10=18.0; p=0.002) declines, whereas values from inner edges show only a modest, nonsignificant decrease (IW $_1$F10=1.6; p=0.228; IE $_1$F10=1.6; p=0.233).

Ship-board studies complemented the remote sensing investigation. Vertical Seabird CTD casts [64 stations at 1.85 km (i.e., 1 nautical mile) intervals] and horizontal BAT tows recorded water column differences across the southern basin on a longitudinal transect, between 86.320°W and 87.745°W. Ship-board vertical CTD profiles for Chl *a* and water transmissivity during 2001, 2006, and 2008 across the southern transect also show

Table 1.3
Mean densities (number/m^3) of zooplankton along cross-lake transect, S. Lake Michigan, comparing 2006 (13-14 April 06), 2007 (2-3 April 07), and 2008 (21-23 April 08) values. Densities are means±95% confidence limits (n=9, 2006; n=7, 2007; n=11, 2008); total nauplii are shown separately. Significant ($p<0.05$; t-test) declines between 2006 and 2008 are marked by an asterisk (*). Although veliger densities are high, these are conservative estimates, because smaller individuals passed through the 120 μm mesh.

Taxa	2006	2007	2008
Nauplii	8142±2309	5721±1776	6016±1360
Diaptomus	3208±950	2807±704	2912±775
*Cyclopoids	223±111	16±19	14±8
**Epischura*	750±445	1682±2468	55±29
**Limnocalanus*	364±198	85±59	30±12
Dreissena	645±381	123±48	448±219

pronounced clearing through time, especially along the shallow edges (Fig. 1.6; compare 2001 with 2006 and 2008). Both Chl *a* and water transmissivity change over the time interval, and shallow waters become less turbid. Mean CTD temperatures, depth-averaged Chl *a*, and mean water transmissivity values emphasize how values have changed (Fig. 1.7). Standard deviations for vertical (CTD) site profiles quantify the statistical variation of values. During the cruises, water temperature ranged between 2.8 and 4°C in offshore waters, and above 4°C behind the thermal bar in coastal waters. Note that the standard deviations around the mean temperature values are very narrow, underscoring the vertical mixing of the winter water column in the rotating gyre. Values for different years document highly significant temporal shifts toward increased water transparency and decreased Chl *a* along the outer edge of the eastern and western "doughnut" rings from 2006 to 2008.

In 2001, before quagga mussels, water transparency (transmissivity) varied between

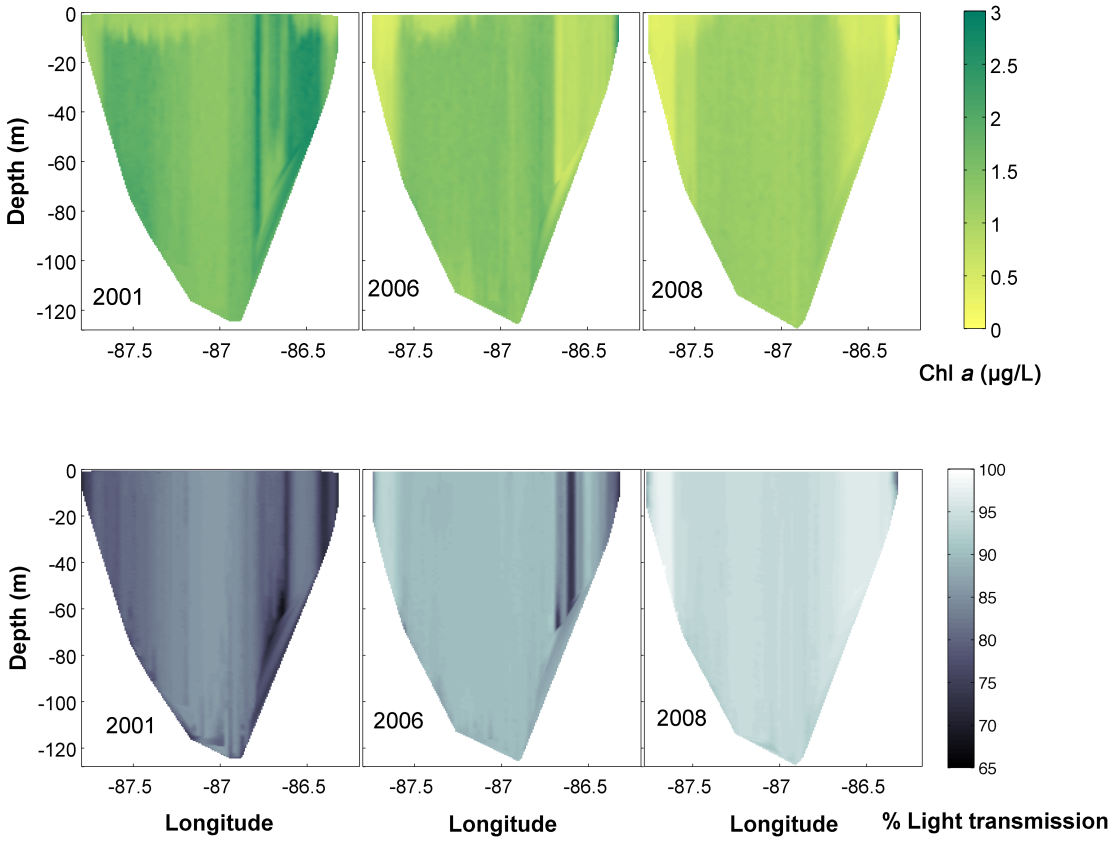

Figure 1.6: Vertical clearing of water column, based on ship-board measurements. Measurements come from Seabird CTD casts taken along the southern transect (see Fig. 1.1) between South Haven, Michigan, and Waukegan, Wisconsin. Compare the Chl *a* and % light transmission values for 2001, 2006, and 2008.

74 and 85% at deep-water sites and was 80 and 82% in the western and eastern 'doughnut' rings. In 2001, Chl *a* ranged between 1.1-2.6 μg/L and 1.8-2.6 μg/L in the western and eastern doughnut rings, respectively. After quagga mussel appearance, water transparency increased progressively to 89% by 2006 and 94-96% by 2008. Chlorophyll *a* concentrations declined to 0.5-1.7 μg/L by 2006 and 0.4-1.5 μg/L by 2008. The reduction of Chl *a* between 2001 and 2008 was 56-78% in the western limb and 74-75% in the eastern limb.

Not only did transparency increase and Chl *a* fall across all sampling stations, the spatial turbidity pattern changed dramatically (Figs. 1.6 and 1.7). The width of the "doughnut" narrowed 26% and transparency at mid-coastal regions (40-80 m depth) reversed from more turbid to less turbid (from 80-82% to 97% transmissivity). Some of the individual values are now extraordinary for Lake Michigan. Along the western shoreline in 2008, water transmissivity reached 97% and Chl *a* dropped to 0.4 μg/L, approaching water clarity and Chl *a* concentrations reported for Lake Superior.

Individual vertical CTD profiles for 2001 and 2008 document the dramatic decline in Chl *a* concentration at the shallower coastal margins of the transect, as compared to the central region, although the decline is present at all stations (Fig. 1.8). When the % reduction is plotted versus longitude along the southern transect, the greater reduction along shallow edges is evident (Fig. 1.9). Reduction of chlorophyll related to water depth and a corresponding transparency pattern suggests progressive filtration effects from settled quagga mussels. The observed results correspond closely to modeled quagga filtration effects expected from a combination of density and water column depth ([181]).

1.4.4 Zooplankton changes

Some zooplankton changes are also apparent from the crosstransect vertical tows (Table 1.3). From 2006 to 2008, nauplii and total herbivorous diaptomid copepods decreased in

density (26% and 9%, respectively). Cyclopoid copepods were dominant in 1998-1999 ([180]), yet by 2008 they were severely depressed over 2006 values (94% decline), and often missing from individual vertical tows. There was also a recent reduction of large-bodied, omnivorous calanoid copepod species from 2006 to 2008 (*Limnocalanus*, 93% decline; *Epischura*, 92% decline). The recent reduction in over-wintering omnivorous (predatory) species may signal reduced energy flow up to higher trophic levels, indicating repercussions of the winter Chl *a* reduction. The *Limnocalanus* reduction from 2006 to 2008 reverses an increasing trend from 2003 to 2006 discussed by Barbiero et al. ([12]). Reduced phytoplankton density may begin to have an impact on veliger densities, although the decline from 2006 to 2008 is not significant.

Comparison of OPC coastal counts also showed some differences. OPC counts were broken down into the two different-sized bins (Bin 1, 0.25-0.5 mm; Bin 2, 0.5-1.0 mm) used previously ([94]). The smallest size category was comprised mainly of rotifers, nauplii, and immature copepodites, whereas the larger was primarily calanoid copepodites. In 2001 OPC transects, Bin 2 coastal densities ranged between 4000 and 5000 counts/m^3 (mean$\pm$SD=$4.8\pm0.4\times10^3$/counts/m^3) whereas 2008 transects ranged between 2000 and 4000 counts/m^3 (mean$\pm$SD=$3.0\pm1.9\times10^3$/counts/m^3), significantly lower than the earlier counts ($p<0.0001$, t-test on 2001 vs 2008 data sets, N=1169, t=206). The significant count reduction occurs in the same region where there were serious reductions in Chl *a* due to quagga activity, again suggesting an impact up the pelagic food-web. This test is region-specific and hence more powerful than the vertical zooplankton tows, which are

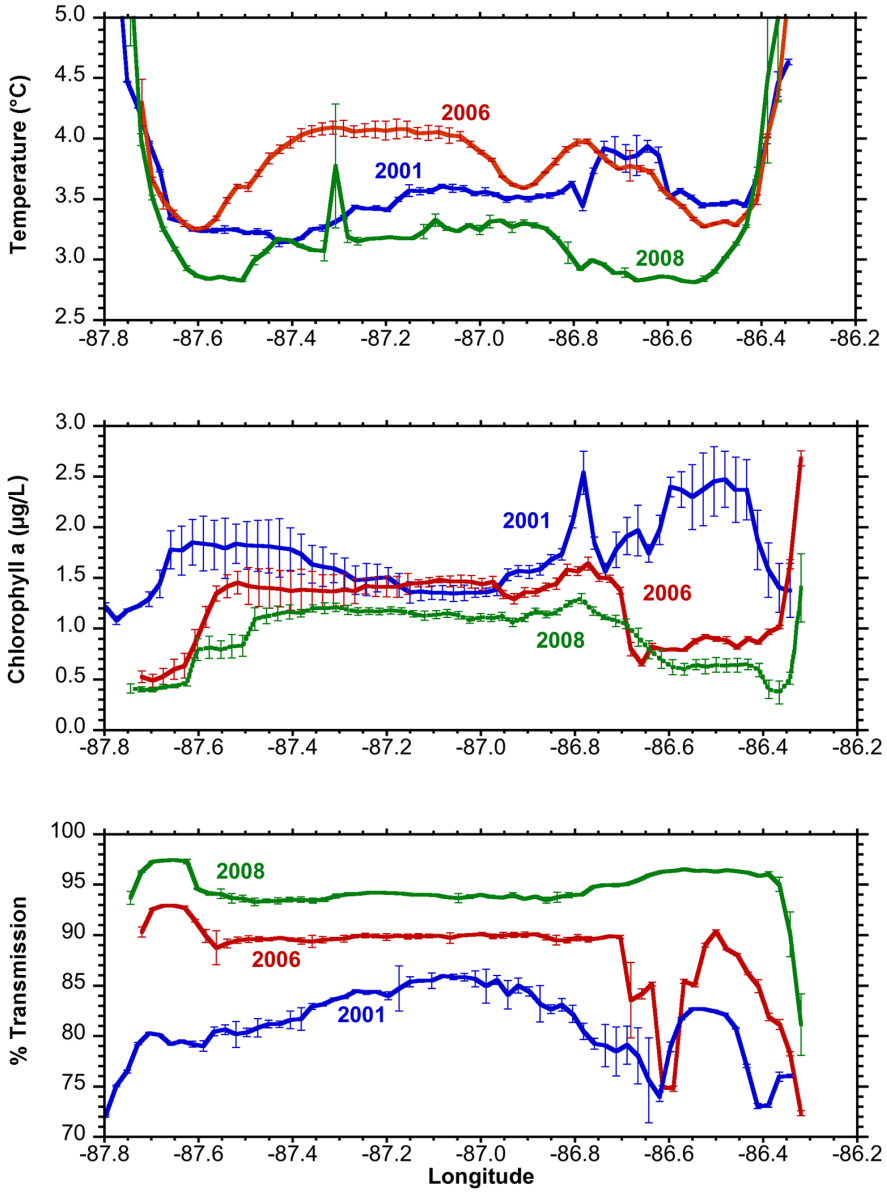

Figure 1.7: Statistical plots for depth-averaged CTD values along southern Lake Michigan transect: (A) temperature, (B) Chl *a*, and (C) % light transmission. Values are means and standard deviations for vertical casts. Note the severe decrease in Chl *a* concentration in both the eastern and western shelf regions (down to 0.4 μg/L), the extreme increase in water transparency (average % transmission 93-98%), and the narrowing of the high-Chl *a* 'doughnut' region.

averaged across the entire transect.

In 2008, across the thermal bar off Muskegon, the smaller size category was 4-fold higher in nearshore waters (Fig. 1.10, Table 1.4) than in offshore waters. The second size category (0.5-1.0 mm) was elevated in deep offshore and declined in nearshore waters, although values peaked near the thermal bar (4°C). Despite the lower Bin 2 values in the coastal regions, the relative Bin values were similar to previous historical comparisons, i.e. rotifers were much more abundant (2-4×) in nearshore regions ([180]).

1.5 Discussion

Remote sensing (SeaWiFS, MODIS) imagery from 1998 to 2003 verified spatially complex suspended sediment and Chl *a* patterns in the Laurentian Great Lakes during late winter. These patterns suggested an important coupling between late-winter storm-induced gyre formation, coastal water plus sediment capture, and deep-water productivity ([94]). Recent resuspended particle-based modeling efforts have successfully reproduced the resuspension and transport dynamics seen on SeaWiFS imagery for Lake Michigan ([109]).

Detailed inspection of river discharges and resuspended sediments along the southeastern coastline of Lake Michigan ([24]) suggested high levels of dissolved organic matter and enhancement of productivity along the coastal shelf in years when the

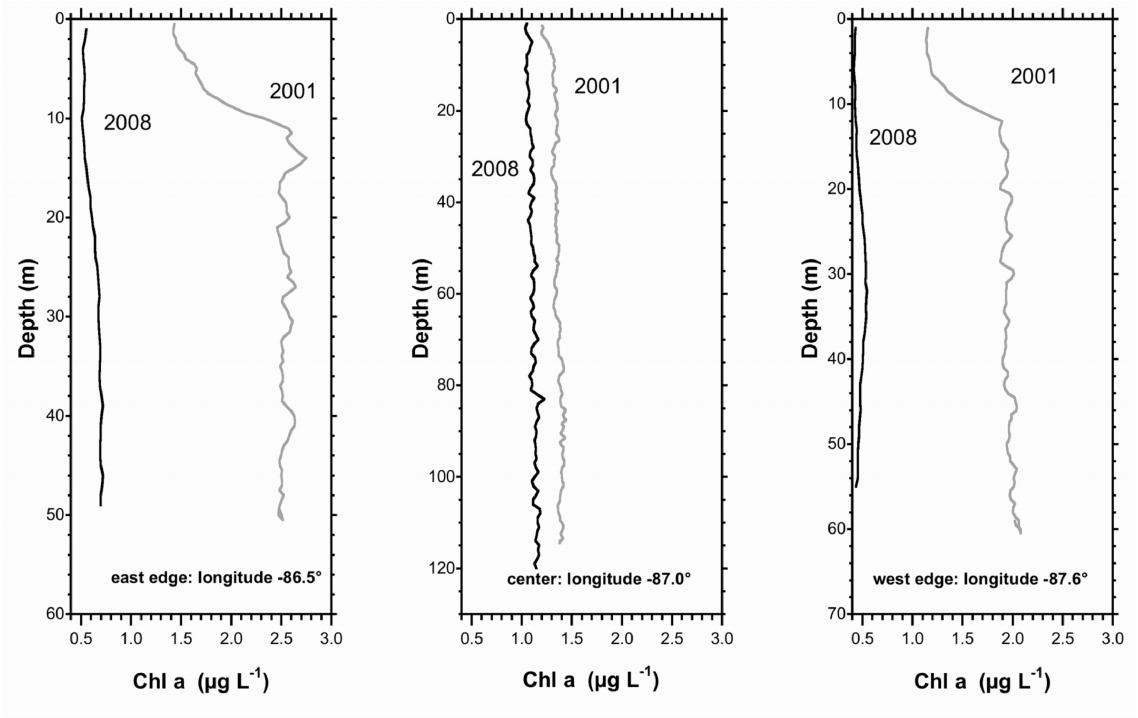

Figure 1.8: Comparative depletion of Chl *a* in shallow shelf versus deep-water, central regions, showing the vertical impact. Vertical profiles for April 2001 (before quagga mussels) are compared with profiles from April 2008 (after quagga mussels) from western shelf, central, and eastern shelf regions.

nearcoastal turbidity plume did not hinder photosynthesis ([133]; [116], [115]). Here we extended the initial Lake Michigan observations to a number of the Laurentian Great Lakes. The remote sensing images revealed an important coastal-offshore linkage, one that normally benefited over-wintering planktonic species characteristic of the large lakes. In Lake Erie, the productivity pulse occurred with scattered ice and persisted into the time of the spring bloom, so that the two phenomena might be confused. High densities of late-winter algae probably contributed to the summer deoxygenation of hypolimnetic waters in the middle (summer 'Dead Zone') and eastern basins.

The magnitude of the offshore transfer of nutrients in Lake Michigan might be exaggerated by climate change, as higher temperatures and more frequent winter storms suppressed coastal ice formation and encouraged movement of nutrient-enriched river waters and sediments into pelagic waters ([94]). The dominant algae associated with the Lake Michigan 'doughnut' ring blooms (*Aulacoseira islandica*) is the same species that recently clogged net tows during 2007-8 Lake Erie ice-breaker studies ([187]). In Lake Erie, *Aulacoseira islandica* was found attached under ice and in open waters near ice, achieving near-bloom conditions (Mike McKay, unpubl. data).

The late-winter blooms were distinct from traditional spring blooms, because they occurred earlier and in cold water, away from the coastal thermal bar. Thermal bar formation and stratification, in fact, disturbs the conditions that promote offshore transfer of river waters and resuspended sediments. During low ice years, phosphorus- rich plumes (river water and coastal sediments) are transported offshore and go through a heterotrophic to autotrophic transformation between January and April in deep waters ([52]; [24]; [94]). The remote sensing and ship studies have stimulated preliminary modeling reconstructions ([86]; [17]; [109]).

Earlier optical plankton counter (OPC) transects and vertical plankton net tows in Lake Michigan documented that the lateral late winter transfers influenced higher levels of food webs (zooplankton). Deep-water, over-wintering zooplankton species (*Leptodiaptomus sicilis*, *Limnocalanus macrurus*, *Eurytemora affinis*,

Senecella calanoides) seemed to benefit from the late-winter production, as they differentially congregated in the rings ([94]). However, the discovery in 2006 that veliger larvae from quagga mussels were also exploiting the late-winter production pulse in southern Lake Michigan, and presumably in the other lower Great Lakes, carried disturbing implications that are now playing out. Deep-water veligers experience a double benefit, relative to spread and growth. Not only do the suspended larvae capitalize on the late-winter productivity pulse, they also disperse in strong winter currents associated with the winter storms. Increased benthic attached mussel abundance in coastal waters behind the thermal bar seems to be severely depleting the spring bloom ([62]; [140], [141]), yet we show here that it is also reducing the winter 'doughnut' pulse in contiguous offshore waters. As suspended material is filtered from overlying waters, remarkable water clarity is achieved along with diminished phytoplankton abundance and productivity. The filtering attached mussels seem to be constricting the winter bloom primarily along the edges and diminishing even the deep-water algae.

Along the coastal regions of Lake Michigan, water transmissivity and Chl *a* values are now approaching Lake Superior values. Primary production estimates in 1998 ranged from 0.18 to 0.48 g C/m^2/d compared to 0.18-0.24 g C/m^2/d for satellite-derived values, and in 2000 shipboard studies gave 0.19-0.37 g C/m^2/d compared to 0.15-0.46 g C/m^2/d for satellite-derived values ([116], [115]). Recent offshore Muskegon site estimates suggest a 66% decline in spring Chl *a* and a 70% reduction in productivity ([62]), whereas GLNPO April ship surveys show about a 72% decrease in April Chl *a* concentrations in southern

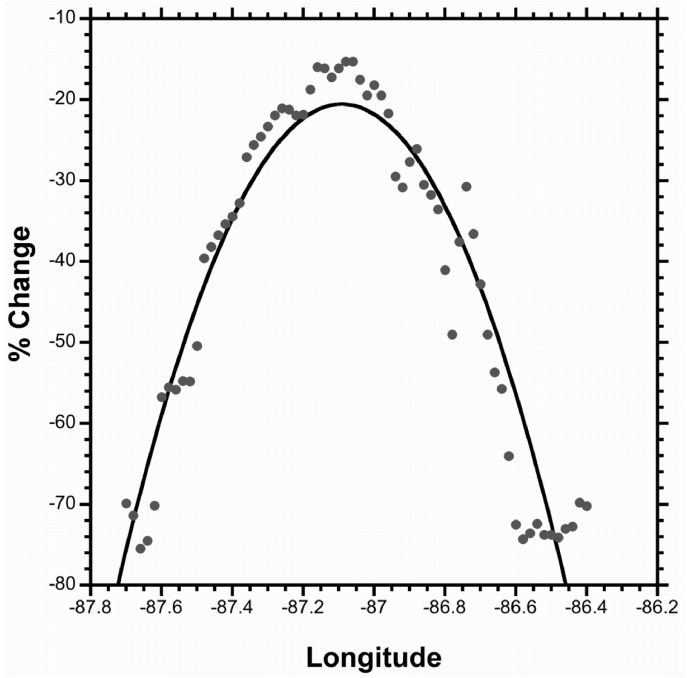

Figure 1.9: Spatial pattern of Chl *a* depletion along southern transect in Lake Michigan, expressed as % change (i.e. reduction) between April 2001 sites (before quagga mussels) and April 2008 sites (after quagga mussels). The difference between the mean Chl *a* site values is plotted against longitude, along the southern ship transect. The Chl *a* reduction occurs most dramatically along the shallower rim ("edges") on both sides, is symmetrical, and is less in the deep central basin. The fit polynomial regression ($Y=-1.127e^{06}-25874X-148.55X^2$) has an $r^2=0.901$; but more important, it shows the depth-dependent symmetry of the severe coastal reductions relative to quagga mussel abundance (see Fig. 1.4).

Lake Michigan ([131]). Both these estimates are similar to our observed declines, although we document the spatial pattern across southern Lake Michigan in much more detail.

Quagga mussel filtration is influencing both nearshore and offshore productivity. Barbiero et al. ([12]) argued that a combination of top-down and bottom-up effects between 1998 and 2006 led to a large increase in *Limnocalanus*. We found that since 2006, filtration from settled mussels seems to be diminishing Chl *a* concentrations for deep

Table 1.4
Grand means and standard deviations for BAT optical plankton counter tallies, nearshore into offshore waters, 14 April 2008, off Muskegon, MI. Grand means are based on a series of 50-interval means for number of individuals counted during a 10-s-duration interval. Estimates of fluid volume flows are then used to convert counts into density estimates given below.

Location	Mean	Std dev
1.0-7.6 km, nearshore		
Total density ($\times 103/m^3$)	26.2	7.9
Bin 1 (0.25-0.5 mm)	24.2	7.4
Bin 2 (0.5-1.0 mm)	2.4	1.5
8.6-16.4 km, thermal bar		
Total density ($\times 103/m^3$	13.0	6.7
Bin 1 (0.25-0.5 mm)	7.3	4.7
Bin 2 (0.5-1.0 mm)	5.4	3.0
16.5-37.9 km, offshore		
Total density ($\times 103/m^3$)	5.6	3.0
Bin 1 (0.25-0.5 mm)	2.5	1.5
Bin 2 (0.5-1.0 mm)	3.0	1.9

water, over-wintering omnivorous zooplankton species (cyclopoid copepods; the calanoid copepods *L. macrurus* and *Epischura lacustris*). The OPC counts in sensitive regions over the coastal quagga beds document a highly significant reduction in counts.We interpret this as a reduction in zooplankton density for medium sized species and size classes (Bin 2, 0.5-1.0 mm). However one must be cautious that the reduced counts might also be correlated with inert particles and increased water transparency, since OPC counts in Lake Michigan can include particles other than live plankton ([114]). The offshore depression of cyclopoid copepods may be linked to severe coastal suppression, as absolute densities of cyclopoid copepods were previously greatest in nearshore waters ([180]). Late winter veliger larvae benefit from the winter production pulses because the late-winter blooms provide a primary source of food at a critical time when starvation could be important. The

late-winter phytoplankton pulse allows deep-water recruitment to begin in April, before the spring bloom ([141]). In our samples, there are some indications of a plateau, or even a modest reduction in veliger density, perhaps suggesting the beginning of a late-winter density-dependent feedback. That is, diminished algae in the 'doughnut' may lower food levels for the April deep-water pulse of veligers, reducing future settlement success. Similar density-dependent feedbacks have been recorded for zebra mussels in Lake St. Clair, Saginaw Bay, Lake Erie, and Lake Champlain ([20]).

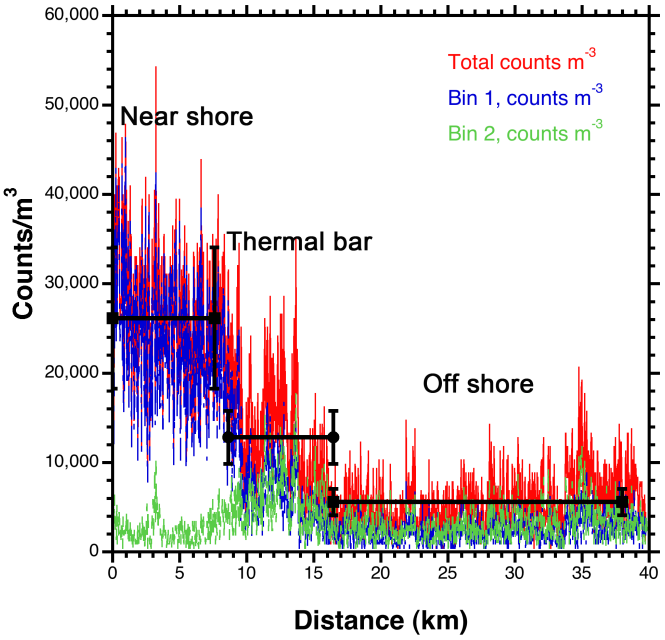

Figure 1.10: Optical plankton counter (OPC) transect from nearshore into offshore waters off Muskegon, Michigan, illustrating differences in zooplankton densities on 14 April 2008. Densities are plotted as a 50-interval mean and high-low range for 10-s-duration interval counts. Total counts (red) and separate densities from two separate size bins (blue, Bin 1, 0.25-0.5 mm; green, Bin 2, 0.5-1.0 mm) are plotted. Dark lines showthemean density (all three bins) for the three intervals: nearshore (left portion), thermal bar region (middle), and offshore region (right). Bin 2 densities increase slightly in the region of the thermal bar (4 °C). Statistics are listed in Table 1.4.

Larger zooplankton (0.5-1.0 mm) seems decreased over coastal waters where quagga mussels are most abundant. Increased smaller zooplankton (especially rotifers) in nearshore waters is expected, and the ratio of small to large size categories appears as skewed in our OPC counts as before. For example, during March-April 2000 EEGLE sampling at four transects (New Buffalo, Gary, Chicago, Muskegon), relative densities of microplankton and small zooplankton to large zooplankton increased from deep to nearshore waters, along a ratio of 1.2-2.3$\times$ ([180]).

The implications of quagga-mediated productivity displacements in the Great Lakes are disturbing. In all probability, in Lake Michigan we are witnessing a major shift of productivity patterns in time and space largely mediated by a single species (i.e. quagga mussels). The spatial and temporal changes resemble shifts documented in Lake Erie for dreissenid filtering ([56]). As quagga and zebra mussels filter the overlying water column, their feces and pseudofeces contribute nutrients and organic matter to the benthic environment ([179]). The increased water transparency allows light to penetrate to the shelf bottom and the displaced nutrients encourage diatom and attached macrophyte growth (e.g. Cladophora). This process has been termed 'benthification' by Mayer et al. ([127]) and the 'shunt' by Hecky et al. ([75]).

The LND ('lateral nutrient displacement') observed in past late winter SeaWiFS images should act opposite to 'benthification' effects, differentially transporting shallow-water river discharges and resuspended nutrients back out to the deep pelagic zone.

Yet descending coastal shoals of quagga mussels appear to have interrupted resuspension of littoral nutrient-rich sediments and lateral transport of organic-rich river discharges. Our observations of greatly enhanced water transparency and severely decreased Chl *a* concentrations along inner (shallow) basin margins suggests serious interference with lateral transport. If the spring bloom collapses along the entire shoreline of Lake Michigan, can the remaining deep-water portion of the late-winter productivity pulse and the summer deep-water Chl *a* maximum adequately sustain the pelagic deep-water food-web?

The presence of dreissenids in the other Great Lakes has caused dramatic increases in water clarity, increased nuisance benthic plant growth, and increased harmful algal blooms, with indications of impacts on many fisheries (e.g. [179]; [75]). We stress that the winter-spring transition is also a critical time for calanoid copepod reproduction. Deep-water calanoid copepods should be the most resilient to nearshore coastal impacts. However, any effect of cold-water dreissenid pelagic veligers or settled adults on 'doughnut' phytoplankton and microzooplankton in Lake Michigan would influence survival and subsequent reproduction of over-wintering calanoid copepods during this period, at a time when food is limiting for over-wintering plankton species, creating a winter bottleneck. Severe reduction of calanoid and cyclopoid copepodite stages would also have serious implications for fish recruitment in the spring, since young of many species draw from these over-wintering planktonic stages as their primary food source. Preliminary evidence on a few pelagic Lake Michigan fishes suggests developing impacts (e.g., alewives; [152]).

1.6 Acknowledgments

Research was supported by NSF OCE-9726680 EEGLE CoOP (National Science Foundation and National Oceanic and Atmospheric Administration Coastal Ocean Program, Episodic Events-Great Lakes Experiment) grant to W.C. K. and J.W. B.; a NOAA Coastal Ocean program grant (NOAA portion of NSF/NOAA EEGLE CoOP Project) to D.J. S. and H.A. V.; an NSF DEB-0083731 (Biocomplexity) grant to W.C. K.; and a NOAA Michigan Seagrant Award NA16RG1145, Project R/ER-19 to Kerfoot, Budd, Green, Vanderploeg, and Schwab. We thank Chris Roussi for the help with the BAT circuitry, Qili Hu and Aaron Hemme for the sampling support, and Jennifer Reed for obtaining additional ship support funds. Lucille Zelazny aided figure preparation. We also acknowledge the crews of the RV Laurentian, who guided us successfully across Lake Michigan during a hazardous time of the year.

Chapter 2

Bio-optical properties and primary production of Lake Michigan: 13-years of SeaWiFS imagery document a mussel-mediated collapse

[a,b]**Foad Yousef**, [a,b]**W. Charles Kerfoot**, [c]**Robert Shuchman**, [a,c]**Gary Fahnenstiel**

[a]Great Lakes Research Center, Michigan Technological University, Houghton, Michigan

[b]Department of Biological Sciences, Michigan Technological University, Houghton, Michigan

[c]Michigan Tech Research Institute, Ann Arbor, Michigan

*Corresponding author: fyousef@mtu.edu

Index words: remote sensing, SeaWiFS, Laurentian Great Lakes, primary production, quagga mussels, dreissenid mussels, PAR, chlorophyll a

running head: Detecting quagga mussels effects via remote sensing

E-mail addresses: fyousef@mtu.edu (F. Yousef), wkerfoot@mtu.edu (W.C. Kerfoot), shuchman@mtu.edu (R. Shuchman), glfahnen@mtu.edu (G. Fahnenstiel).

2.1 Abstract

Remote sensing and GIS techniques were used to document recent changes in water quality parameters of southern Lake Michigan. We utilized 13 years of SeaWiFS data for the early spring isothermal period (March and April) between 1998 and 2010 in order to track trends of Photosynthetic Available Radiation (PAR), PAR attenuation coefficient (K_{dPAR}), chlorophyll *a* (chl-*a*), and phytoplankton primary production after the invasion by quagga mussels (*Dreissena bugensis*). Spatial analysis techniques were employed to link the observed changes in water related parameters to colonization of quagga mussels. Our result demonstrated surface PAR values were unchanged between 1998 and 2010; however, there was an average of a 20% drop in K_{dPAR} values during the March/April periods in 1998 through 2010. We also found a 53% and 45% decline in chlorophyll-*a* concentration (μg*L^{-1}) in March and April, respectively, for the same years. Modeled primary production also exhibited a 42-47% decline during the same period. The decline in K_{dPAR} values resulted in an increase in water transparency of Lake Michigan over the last decade. However, constant PAR during the same time period suggests that surface light availability was not responsible for the observed decreases in chl-*a* and primary production. Using spatial change detection analysis, we detected a statistically significant spatial difference in chl-*a* (μg*L^{-1}) concentrations between nearshore and mid-lake waters (<90 m deep) versus offshore waters (>90 m deep). The results from analysis of co-variance (ANCOVA) test demonstrated that the chl-*a* concentration dropped faster in <90 m waters

compared to offshore waters between 1998 and 2010. Quagga mussels' high filtration rate created a spatial pattern of chl-*a* that matched the dispersal pattern of quagga mussels and bathymetric contours of the lake. We demonstrated that remote sensing not only provides intensive large scale bio-optical information (K*dPAR* and PAR), but through the application of spatial analysis techniques reveals and links long-term changes in chl-*a* and primary production to the responsible invasive specie, quagga mussels.

2.2 Introduction

Remote Sensing has opened many new perspectives in understanding aquatic system dynamics. These tools provide answers to questions related to both physical (e.g. sea surface temperature, sea level, current directions) and biological characteristics (e.g. surface chlorophyll concentration, primary production, algal species composition) of aquatic ecosystems. The temporal and spatial extent of data collected by environmental satellites are very large compared to traditional limnological surveying methods, allowing scientists to follow long term changes in water characteristics of aquatic environments ([97]; [112]; [115]). Remote sensing also provides the opportunity to study aquatic habitats during harsh and dangerous environmental conditions (e.g. during winter storms) and likewise helps to discover and study the spatially large phenomena.

The early spring algal bloom in offshore waters of Lake Michigan was originally

discovered using remote sensing ([94], [97]). This particular algal bloom starts in March and April during the isothermal period when winter storms and high wind stress leads to a complete water column mixing event and eventually forms a chl-*a* ring, termed the "doughnut", in offshore waters ($>$ 90m deep) of Lake Michigan. The southern Lake Michigan counter-clockwise gyre, formed by strong winter storms ([42]), is another unique feature during the isothermal period. These counter-clockwise currents provide necessary mechanisms to transport river discharges and their associated nutrients into offshore waters. The constant vertical and horizontal movement of the water lasts until mid-May or early-June, when summer stratification starts. These physical conditions have profound influences on the biology of Lake Michigan.

Many non-indigenous species have invaded Lake Michigan ([179]). Among these species, zebra mussels (*Dreissena polymorpha*) and quagga mussels (*Dreissena bugensis*), found their way from Lake Huron into northern Lake Michigan in the 1990s and early 2000's. Zebra mussels first populated the shallow region, and then the quagga mussels populated the deep profundal regions and finally began replacing zebra mussels nearshore. Quagga mussels started replacing much of the zebra mussel population by 2005 ([141]). Simultaneously, Fahnenstiel et al. ([62]), using traditional shipboard and *in situ* measurements, reported a 66% drop in chl-*a* and on average a 50% drop in primary production during the spring isothermal period due to the establishment of large quagga mussel populations. It should be noted that the changes described by Fahnenstiel et al. ([62]) were based on only two years of data (2007-2008) after quagga mussel colonization.

In previous studies related to Lake Michigan, remote sensing has been applied to study characteristics such as: determining trends in water clarity of the lower Great Lakes ([25]), delineating bio-optical properties of Lake Michigan ([153]), verification/development of bio-optical models for Lake Michigan ([167];[113]), capturing event driven algal blooms ([112]), and discovering and characterizing the coastal plankton dynamics ([115];[94]). However, remote sensing has not been used to map and characterize the spatio-temporal dynamics of the food-web base, the primary production over the entire southern basin. In this paper, we focused on the southern basin of Lake Michigan and utilized different remote sensing techniques to examine temporal and spatial trends in chl-*a* concentration, surface PAR, and K_{dPAR}. Knowing the trends of these parameters will help to answer the following questions: Can remote sensing be used to document trends in K_d, chlorophyll and primary production in Lake Michigan? Can recent changes in these parameters be related to the recent colonization of quagga mussels? Are there significant regional (nearshore, offshore, etc.) changes in these water quality parameters and are they related to quagga mussel densities?

2.3 Methods

We used daily PAR as an independent variable to analyze the possible effects of solar radiation on primary production. Using change detection (CD) analysis, changes in spatial chl-*a* concentration patterns were studied. Following these analysis, the Great Lakes

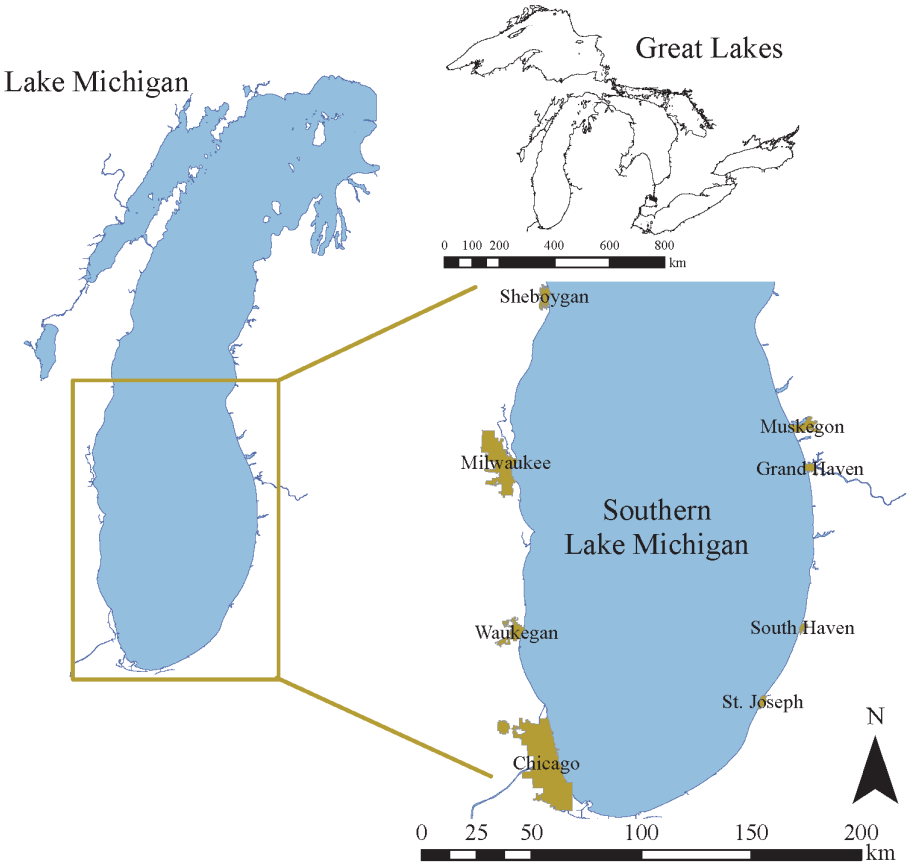

Figure 2.1: Map of study area, southern Lake Michigan basin.

Primary Production Model (GLPPM), was used to estimate the primary production. The entire analytical procedure was focused on the "doughnut" phenomenon in Southern Lake Michigan basin during March and April of years from 1998 to 2010 (Fig. 2.1). Unlike other studies about southern Lake Michigan that divide the lake into three regions (nearshore, mid-depth, and offshore), we use only two regions, >90m waters (offshore) and <90m waters (nearshore and mid-depth waters. This simplification helps to avoid inaccurate comparisons between offshore and nearshore, where (in nearshore) the products of existing bio-optical algorithms can be less accurate.

Data preparation- We used SeaWiFS satellite images between 1998 and 2010. SeaWiFS started its mission in 1997 and after over 13 years of data collection, lost orbit in December of 2010. SeaWiFS data was downloaded from NASA's Ocean Color website. The Ocean Color (OC) group provides 4 different levels of data. We used level1 (L1) and level2 (L2) for our analysis. SeaDAS6.2 (OC software) was used to process and map the acquired data. An IDL code was used to produce and map the monthly average data from different products. Subsequently ENVI, ERDAS IMAGIN and ArcGIS were used to perform image processing, statistical analysis and mapping final products.

The SeaWiFS sensor imaged the Great Lakes 2-3 times a day during its mission. However, not all these images had the necessary quality for our analysis. March and April images usually have a great amount of cloud contamination. The other factor that may disqualify an image is the high satellite viewing angle. This happens when the study area falls near the edges of the image. Under such conditions, fewer numbers of pixels represent the entire study area which eventually leads to erroneous estimates. These images were also discarded from our dataset. By discarding cloud contaminated and distorted images, we worked with approximately 30% of images available for each month. Because of these limitations, monthly averaged images were analyzed.

Three different satellite driven products were used in our analysis: 1) chl-*a*, 2) PAR, and 3) K_{dPAR}. Chl-*a* estimates were the product of NASA's Ocean Color (OC) basic algorithm, OC4v4 ([147]). This band-ratio algorithm has proven to produce consistent

estimates of chl-*a* for Lake Michigan, especially in mid-lake and offshore waters ([97]). However, due to optical complication related to coastal waters (e.g. sediment resuspension, river plumes), we did not apply the OC4V4 results for this region (<30 m). Daily surface PAR data were produced following the Frouin et al. ([66]) algorithm. The attenuation coefficient, or K_{dPAR}, determines PAR within the water column, and the higher the K_{dPAR} the thinner the photic zone. However, the OC's default product for K_d is K_{d490}, which is the attenuation coefficient for the 490 nanometer (nm) band. We used the Morel ([136]) algorithm to converts K_{d490} to K_{dPAR}. This conversion was aimed to ensure that the light attenuation coefficient is representative of the entire PAR spectrum (400-700 nm).

Data processing. Monthly maps of chl-*a*, surface PAR, and K_{dPAR} were generated for every March and April between 1998 and 2010. First, each image was visually inspected to discard distorted and/or cloud contaminated scenes. Then, SeaDAS6.2 was used to convert the remaining raw imagery into L2 images. These scenes were mapped (to a common coordinate system) and averaged to produce monthly average values for the study region.

Change detection analysis. We used change detection (CD) analysis to determine the spatial effects of quagga mussels on chl-*a* concentration in Lake Michigan. The analysis was only performed for the month of April. To make the detected changes statistically more representative, April average chl-*a* maps of southern Lake Michigan were divided into three time periods based on quagga mussel invasion in Lake Michigan: 1998-2001 represents the pre-invasion period, 2002-2006 represents the transitional period,

and 2007-2010 represents the post-invasion period ([141]; T. Nalepa, pers. Comm.). All the April average chl-*a* scenes for each period were combined and averaged. ENVI4.7 (ENVI 2010) was used to construct the change detection map. Finally, bathymetric contours of Lake Michigan were superimposed on the CD map. Additionally, monthly chl-*a* maps were divided (using bathymetric map of Lake Michigan) into nearshore and mid-depth ($<$90 meters depth) and offshore ($>$90 meters depth) regions. Simple linear regression model, F-test, and analysis of co-variance (ANCOVA) were used to compare the $<$90 m and $>$90 m waters. This was in order to test and analyze the hypothetical link between the observed chl-*a* pattern and quagga mussel density.

2.3.1 GLPM model

Primary production model. The Great Lakes Primary Production Model (GLPPM) was used to estimate areal integrated primary production ([168]). Input for the GLPPM included the following parameters: 1) hourly surface solar radiation, 2) depth-varying chlorophyll measurements, 3) depth-varying P-E parameters, and 4) K_{dPAR}. The model outputs integrated daily production (mg C*m$^{-2} * t^{-1}$) over the entire water column.

Hourly solar radiation values, provided by the National Solar Radiation Data Base (NSRDB, 2012) were used in units of Watt*m$^{-2} * h^{-1}$. Watt*m^{-2} represents the power/energy of the solar radiation; however PAR input for the GLPPM model needs to

be in μ Einstein $m^{-2} * \sec^{-1}$ unit which is the number of photons reaching the sensor per unit of space and time. Conversion between these two units was done using Plank's Law. Plank's law calculates the number of photons in every Watt*m^{-2} and is wavelength dependent. Therefore, the results are a series of conversion factors for every wavelength between 400 to 700 nm, converting the power/energy to number of photons reaching the lake surface. Since the NSRDB only output the bulk irradiance (not the spectrum), and because the intensity of solar radiation in visible spectrum is fairly constant, we used the average of all the conversion factors calculated for the PAR spectrum (400 - 700 nm, [137]). NSRDB provides hourly as well as monthly average measurements for solar radiation. Four stations were selected along the eastern and western edges of Lake Michigan and PAR estimates were averaged in order to account for possible spatial variation in solar radiation (Muskegon county Airport, MI; Benton Harbor/Ross, MI; Milwaukee Mitchell Intl. Airport, WI; Chicago/Waukegan, IL).

Chlorophyll *a* concentrations were assumed to be uniform with depth. At this time of the year, the water column is usually isothermal and well mixed (March and April) ([62], [94], [97]), thus our assumption of uniform chl-*a* concentration with depth is reasonable. Depth-varying the P-E parameters were taken from [63] and [62] (Table 2.1).

The GLPPM calculates daily integrated primary production and it accounts for daily variation in surface solar irradiance as well as photosynthesis-irradiance (P-E) curve parameters, chlorophyll concentration and light extinction coefficient (K_{dPAR}). The P-E

Table 2.1
P-E curve parameters used as the input to the GLPPM. For the years between 1998 and 2010, we used the average estimates of P_{max} and α (Gary Fahnenstiel, pers. Comm.).

	P_{max} (mgC•mgChl^{-1}•h^{-1})	α (mgC•mgChl^{-1}•mol Photon^{-1}•m^{-2})
1997-8	1.1	2.9
2007-8	0.9	2.4

curve is an empirical relationship between a range of irradiances and photosynthesis rate. The simplest form of P-E curve is

$$P^B = P_S^B(1 - e^{-\alpha I/P_S^B}) \cdot e^{-\beta I/P_S^B} \tag{2.1}$$

Where P^B is the specific photosynthesis rate at irradiance I, normalized to chlorophyll biomass (mg C*mg chl$^{-1} * h^{-1}$), P_S^B is the saturated rate of photosynthesis (same units as P_S^B), α is the initial linear slope of the P-E curve at low irradiance (mg C*mg chl$^{-1} * Einst^{-1} * m^{-2}$), I is the irradiance at a specific depth (Einst$^{-1} * m^{-2} * h^{-1}$), and β is the negative slope of the P-E curve at high irradiances (mg C*mg chl$^{-1} * Einst^{-1} * m^2$).

By multiplying the normalized photosynthetic rate, P^B, by phytoplankton biomass, B (mg chl-a*m^{-3}), at every specific depth, we can estimate the integrated rate of primary production (mg C*m$^{-3} * h^{-1}$). Since these are discrete estimates of primary production at every specific depth, the GLPPM combines these estimates and produces the daily depth

integrated primary production.

$$P = \sum_{z} \sum_{t} B(z) \cdot P^{B}(z,t) \Delta t \Delta z \tag{2.2}$$

where $B(z)$ represents discrete specific algal biomass value at depth z and $P^{B}(z,t)$ is specific photosynthesis rate at depth z and time t. To correct for surface reflectance, the GLPPM uses Fresnel's equation and Snell's law, and therefore estimates the proportion of light that has transmitted through the air-water interface as a function of solar zenith angle [100].

Solar irradiance at any specific depth is calculated by

$$I_z = (1-r) \cdot I_s \cdot e^{-K_{dPAR} \cdot z} \tag{2.3}$$

whereI_z is the photosynthetic active radiation (PAR) at depth z (Einst$^{-1} * m^{-2} * h^{-1}$), r is surface reflectance (Kirk,1983), I_s is the surface photosynthetic active radiation at surface (Einst$^{-1} * m^{-2} * h^{-1}$), K_{dPAR} is the attenuation coefficient for PAR (m^{-1}), and z is depth (m). After collecting all the required inputs, we ran the GLPPM model for every March

and April between 1998 and 2010.

All estimates for K_{dPAR}, chl-*a*, and primary production were averaged for the entire southern Lake Michigan basin (Fig. 2.1). Finally the average daily primary production estimates for March and April were regressed against time.

2.4 Results

2.4.1 PAR trends

Using linear regression analysis, the monthly estimates of PAR over southern Lake Michigan showed no significant change between 1998 and 2010 (Table 2.2, Fig. 2.2). The average PAR values for the months of March and April were 28.95 and 39.26 Einstein*m$-2 * Day^{-1}$ respectively. PAR estimates during March exhibited large variability in recent years. This likely occurred as a result of SeaWiFS's malfunction during the last few years of its mission.

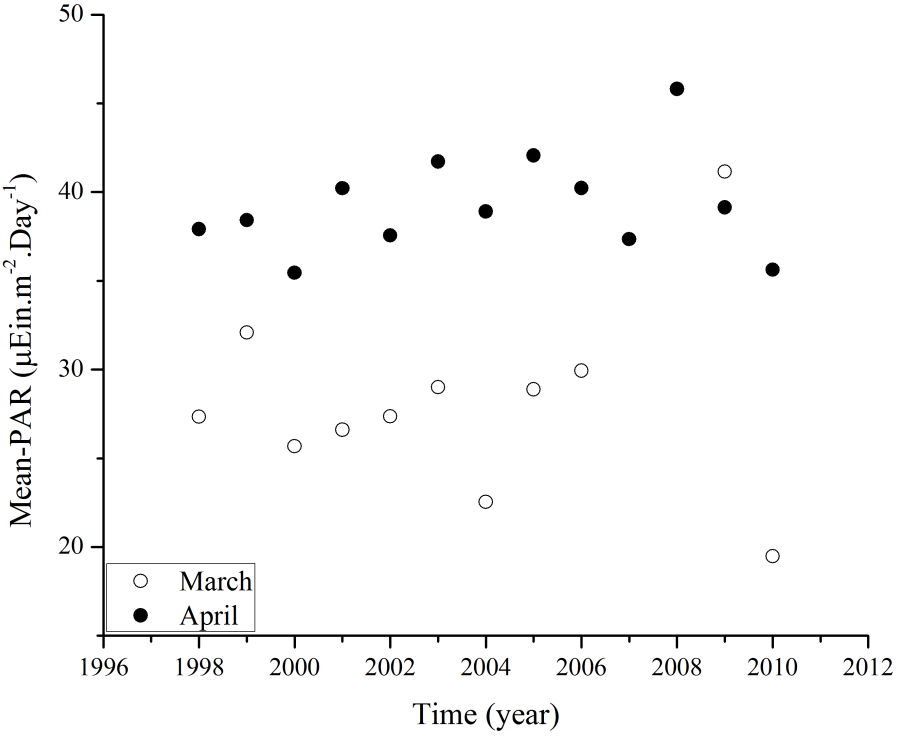

Figure 2.2: Monthly average photosynthetic available radiation, PAR ($Einstein \cdot m^{-2} \cdot Day^{-1}$), values for March and April between 1998 and 2010 collected by SeaWiFS sensor. Solid circles: monthly average values for March; open circles: April monthly average PAR.

2.4.2 K_{dPAR}

Trends analysis of monthly K_{dPAR} values showed a 20% decrease in the mean K_{dPAR} values from 0.18 m^{-1} in 1998 to 0.14 m^{-1}in 2010 for March and a 21% decrease from 0.17 m^{-1} in 1998 to 0.14 m^{-1} in 2010 for April (Fig. 2.3). These decreases were significant for both months, (March R^2=0.678, April R^2=0.867; $p < 0.05$). The overall trend suggests that during the spring isothermal period between 1998 and 2010, water clarity increased, and therefore greater light availability at the same depths. It is interesting to note that rather

than a simple linear response over the entire time period, there appears to be an abrupt decline in K_{dPAR} between 2001 and 2002.

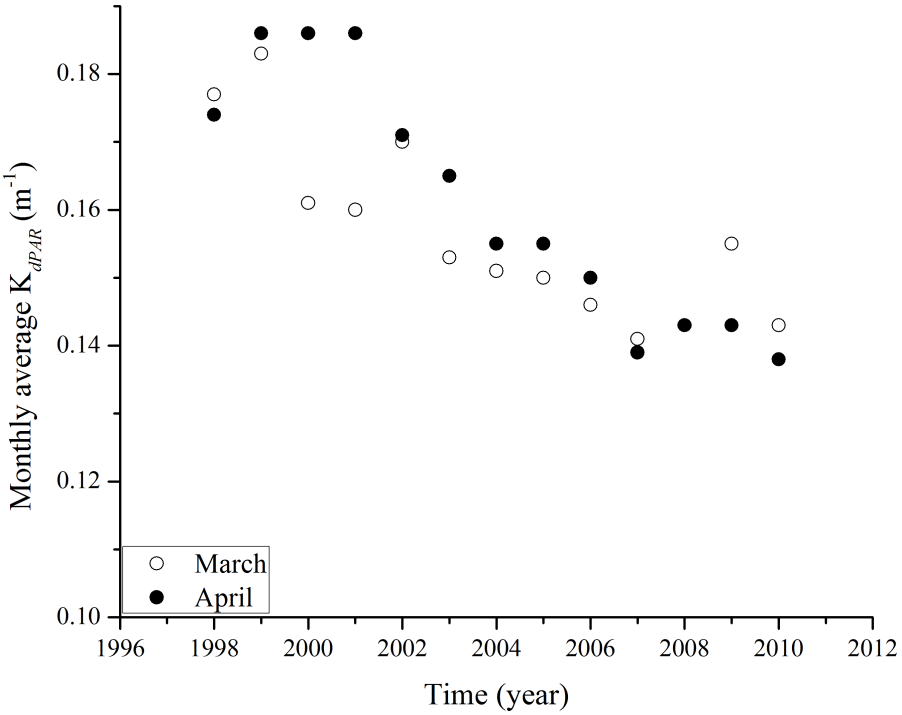

Figure 2.3: Monthly average water-column, PAR light attenuation coefficient, K_{dPAR} (m^{-1}), for southern Lake Michigan between 1998 and 2010. Solid circles: March; open circles: April.

2.4.3 Chl-*a*

The southern Lake Michigan monthly chlorophyll *a* values showed a significant decline from 1998 to 2010. March chl-*a* values dropped from 1.7 μg*L^{-1} in 1998 to 0.8 μg*L^{-1}in 2010 (50.6% decline). April chl-*a* values also showed approximately the same decline from 1.7 μg*L^{-1}in 1998 to 1.0 μg*L^{-1} in 2010 (55.2% drop, *see* Fig. 2.4). The highest

monthly average chl-*a* for March occurred in 1998 (1.7 μg*L^{-1}), however, the greatest chl-*a* for April was recorded in 2000 (2.0 μg*L^{-1}). These changes were significant for both months, (March R^2=0.623, April R^2=0.85; $p<0.05$). Again, there appears to be an abrupt decline in chl-*a* between 2001 and 2003.

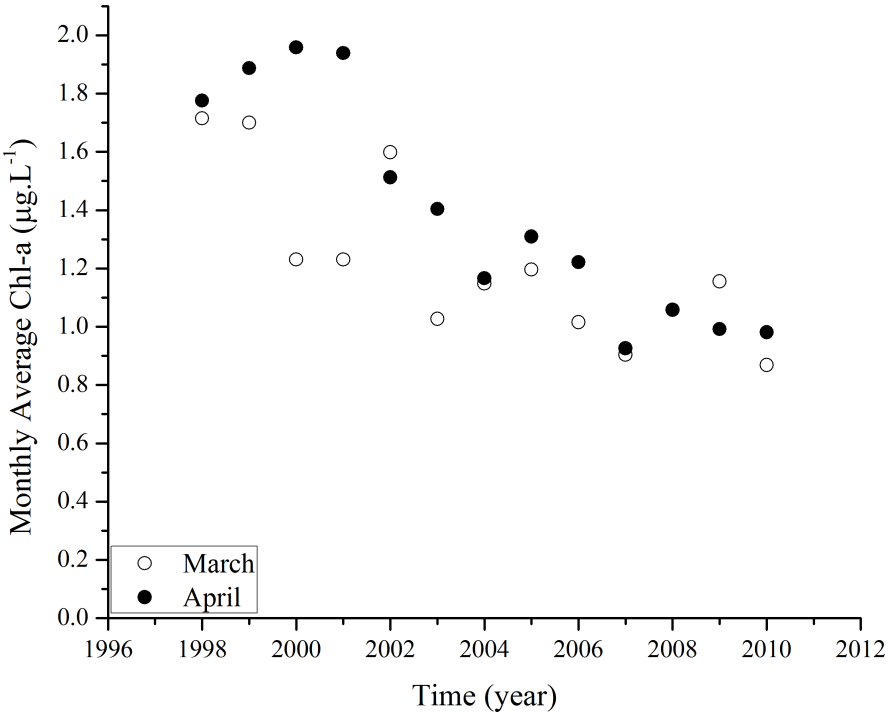

Figure 2.4: Monthly average chlorophyll *a* values ($\mu g \cdot L^{-1}$)for southern Lake Michigan basin between 1998 and 2010. Solid circles: March; open circles: April.

2.4.4 Change detection

CD analysis was used to identify spatial differences in April chl-*a* values between the pre-invasion and post-invasion periods (1998-2001 vs. 2007-2010). Superimposing

bathymetric depth of southern Lake Michigan on top of the CD map produced an intriguing picture. Compared to offshore waters, the CD analysis result revealed a higher chl-*a* drop in nearshore and mid-depth waters (<90m). We observed a 0.2 μg*L^{-1} drop between 1998 and 2010 in offshore waters (the light blue disk is the center of southern Lake Michigan, *see* Fig. 2.5) corresponded to 0.5 μg*L^{-1} on average for nearshore and mid-lake waters (the dark blue surrounding band); however, there are some exceptions to this pattern. In fact, the dark blue band penetrates into > 90m waters in the north-eastern section of the lake (Fig. 2.5). Also from the CD analysis, the eastern coastal edges of Lake Michigan showed an increase of chl-*a* during this period in April.

2.4.5 Region-specific monthly average chl-*a* regression analysis

Separate linear models were fitted to show changes in offshore (>90m) and nearshore (<90m) concentrations of chl-*a* between 1998 and 2010. We used the F-test to compare the average chl-*a* values of these two regions for March and April separately (Table 2.2). Offshore chl-*a* concentrations were significantly lower ($p<0.05$) than values from the nearshore regions in both March and April.

ANCOVA test was used to analyze the linear regression models (Table 2.2). Analyzing these regressions, we found that the slopes (offshore vs. nearshore and mid-lake) were significantly different ($p<0.05$) in April, and marginally not significantly different in

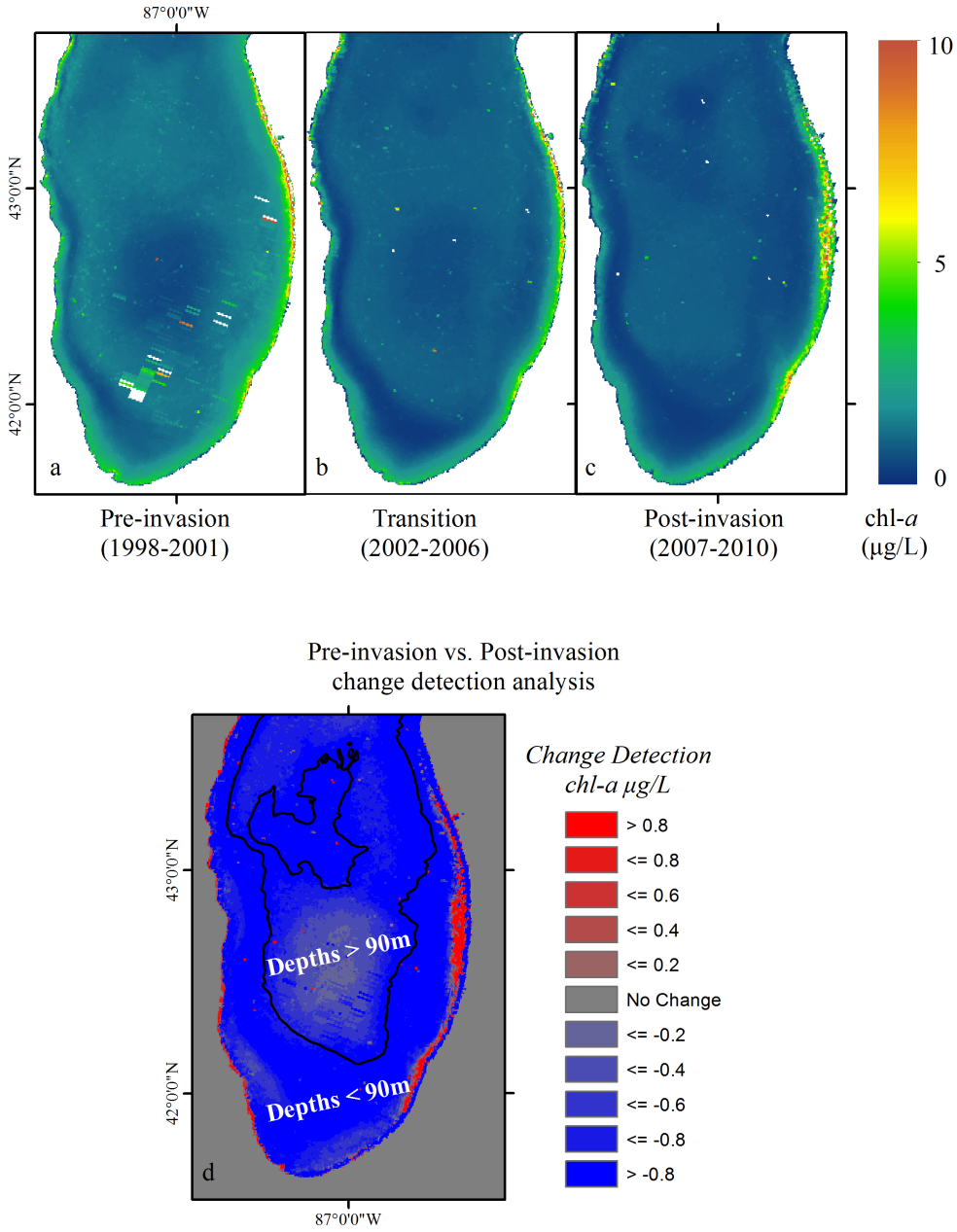

Figure 2.5: Change detection analysis results for southern Lake Michigan. A) Average chl-*a* values for April between 1998-2001, B) April 2000-2006, and C) April 2007-2010. D) Change detection map of chl-*a* concentration between pre-invasion vs. post-invasion period. The black contour line encircles waters deeper than 90 meters. The color scale bar to the right shows the positive and negative changes of chl-*a* concentration ($\mu g \cdot L^{-1}$) between pre- and post-invasion periods.

March (p=0.057). Therefore, between 1998 and 2010, and compared to offshore waters, nearshore to mid-lake waters showed a faster decrease in chl-*a* concentration (Fig. 2.6 and 2.7).

Table 2.2
The linear regression results for various water parameters. PAR, photosynthetic available radiation (Einstein·m^{-2}·Day^{-1}). K_{dPAR}, PAR attenuation coefficient (m^{-1}). Chl-*a*, chlorophyll concentration ($\mu g \cdot L^{-1}$). PP, primary production (mg C·m^{-1}). <90m, depth less than 90 meters. >90m, depth greater than 90 meters.

	Month	R^2	Intercept	Slope	Intercept SE	Slope SE
PAR	March	0.03	-561.2	0.29	947.2	0.47
	April	0.05	-272.6	0.15	427.6	0.21
K_{dPAR}	March	0.68	5.83	-0.003	1.24	6.17
	April	0.87	8.93	-0.004	1.03	5.16
Chl-*a*	March	0.62	120.1	-0.06	29.2	0.02
	April	0.85	183.8	-0.09	23.03	0.01
PP	March	0.87	30281.52	-14.96	34496.2	1.74
	April	0.71	20222.60	-9.98	4044.9	2.02
Chl-*a* <90m	March	0.69	155.2	-0.08	30.21	0.02
	April	0.84	221.9	-0.11	27.59	0.01
Chl-*a* >90m	March	0.49	81.9	-0.04	23.36	0.01
	April	0.80	150.6	-0.07	21.53	0.01

2.4.6 Primary production

We used the Great Lake Primary Production Model (GLPPM, [168]) to estimate the average daily water column integrated phytoplankton primary production (mg C*$m^{-2} * day^{-1}$) over the entire southern Lake Michigan basin. The monthly average primary production was always higher in April than in March during the 13 years between 1998 and 2010. We observed a 42% decrease in primary production in March (from 301.2 mg C*m^{-2} in 1998 to

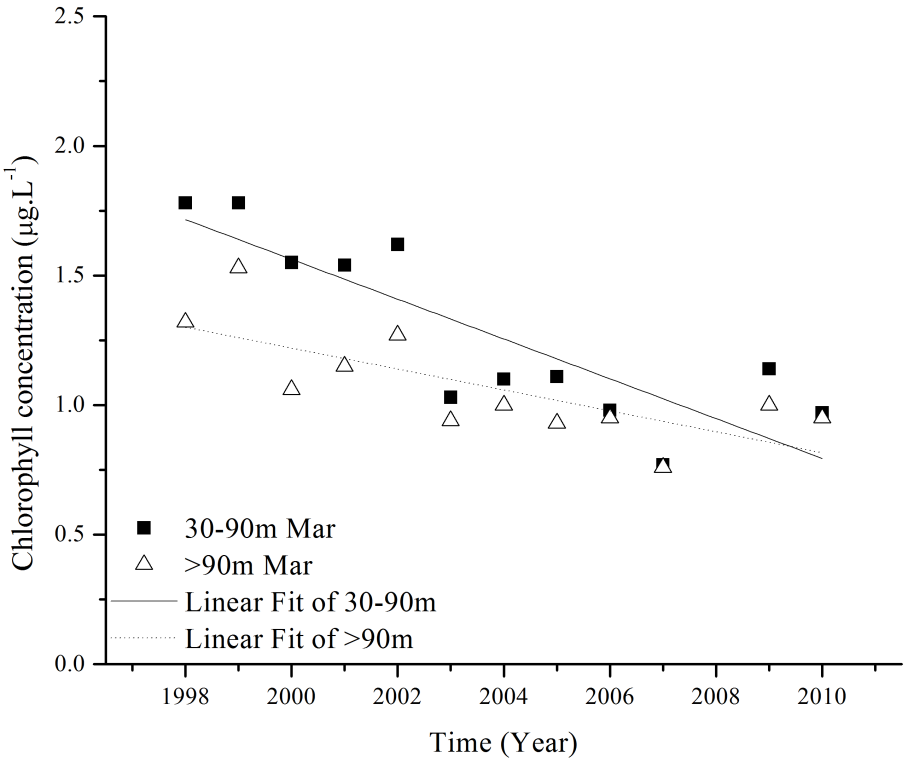

Figure 2.6: March region specific chl-*a* (μg·L^{-1}) concentration between 1998 and 2010. Solid squares: chl-*a* concentration for waters from 30 to 90 meters deep; open triangles: chl-*a* concentration for > 90 meters. The lines are linear regression models fitted to each of these datasets. See table 2.2 for regression equation coefficients.

160.5 mg C*m^{-2}in 2010) and a 46% decrease in primary production for April (from 388.4 mg C*m^{-2} in 1998 to 223.9 mg C*m^{-2} in 2010). Total declines in primary production during both March and April were highly significant ($p<0.01$ $R^2= 0.71$ and 0.87 for March and April, respectively; Fig. 2.8). Similar to chl-*a* and K_{dPAR}, we observed a sharp decline in primary production between 2001 and 2003.

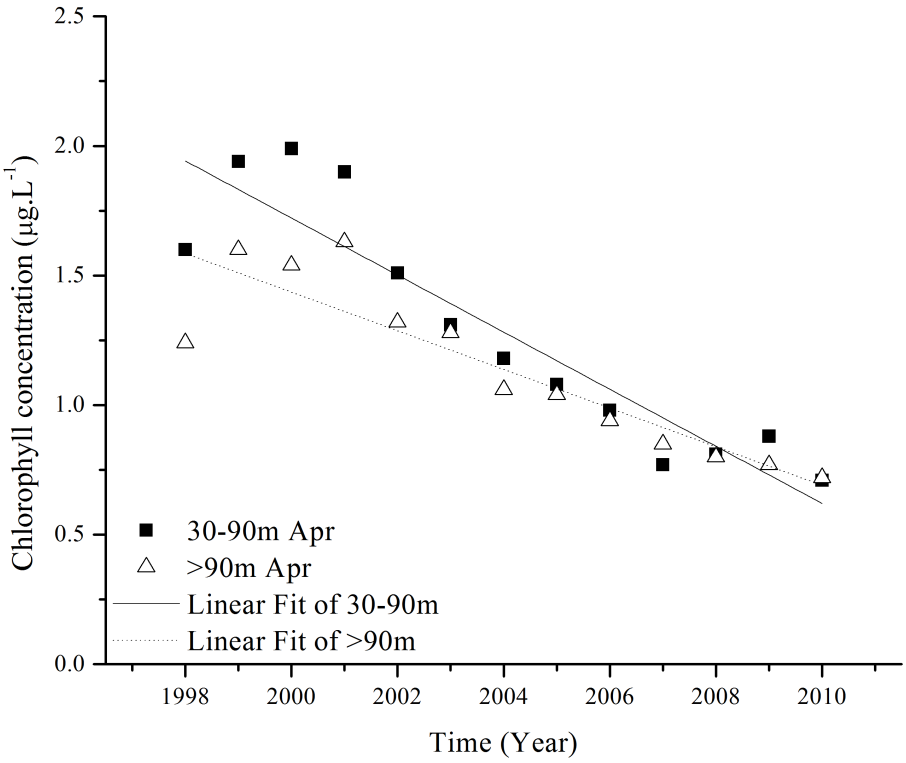

Figure 2.7: April region specific chl-a (μg·L^{-1}) concentration through time. Solid squares: chl-*a* concentration for waters from 30 to 90 meters deep; open triangles: chl-*a* concentration for > 90 meters. The lines are linear regression models fitted to each of these datasets. Regression equations are presented in table 2.2.

2.5 Discussion

Using the "eyes in the sky", remote sensing techniques, we studied the recent changes in water quality properties of southern Lake Michigan during the early spring isothermal period, when isothermal mixing allows mussels located on the bottom to affect phytoplankton abundance throughout the water column ([62]). We tracked the 13 year long trends of various water quality parameters of Lake Michigan during this early

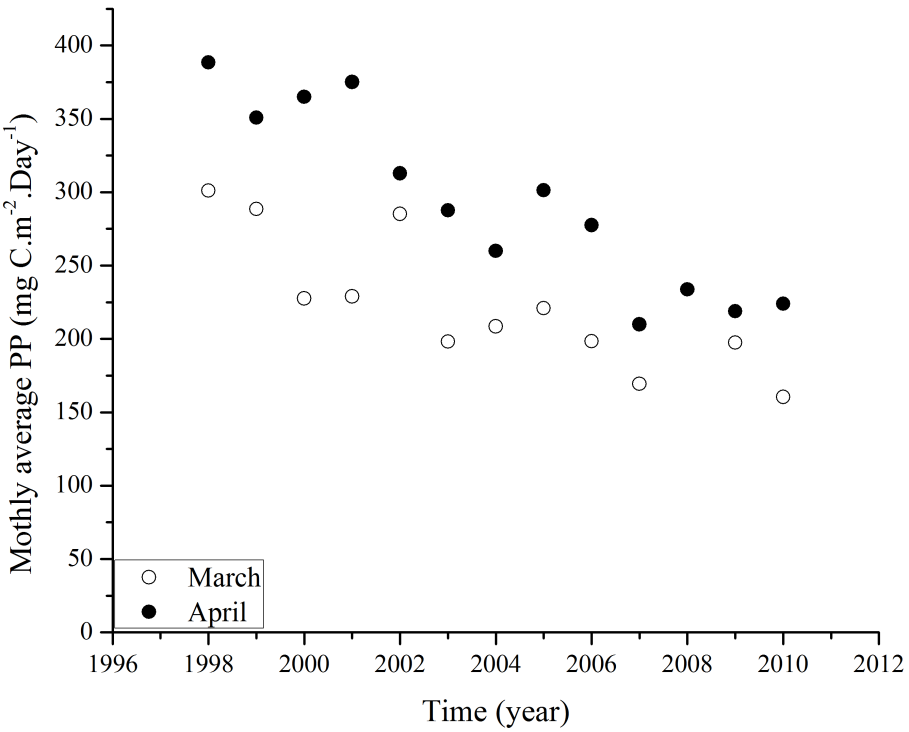

Figure 2.8: Monthly average primary production values (mg $C{\cdot}m^{-2}{\cdot}Day^{-1}$)for southern Lake Michigan basin between 1998 and 2010. Solid circles: March; open circles: April.

spring period. The application of remote sensing allowed us to characterize basin- and region-specific (i.e., offshore and nearshore) changes in water parameters. Following are our interpretations of these changes.

Sea surface solar irradiance is an important factor in production of aquatic systems. One of the objectives of this study was to look at the trend and magnitude of sea surface solar irradiation. PAR represents the quantum flux of solar radiation for wavelengths between 400 and 700 nm. Insensitivity to cloudiness is one of the advantages of the Frouin et al. ([66]) algorithm, producing a rather continuous map of PAR over the study site. The results of our analysis did not show any significant decline or increase in monthly

average values of PAR reaching the surface of Lake Michigan during our study period. These trends suggest that the cloud coverage climate of the lake has not changed, which in turn eliminates any possible contribution of PAR in observed trends of chl-a and primary production.

Although we didn't find any particular changes in the availability of solar radiation between 1998 and 2010, K_{dPAR} values exhibited a significant decline during the same period. We observed a significant drop from 0.17 to 0.14 (m^{-1}) in March (20%) and from 0.17 to 0.13 (m^{-1}) in April (21%). Also a more abrupt decline was observed between 2001 and 2003 (from 0.183 to 0.165 m^{-1}), which is coincident with exponential expansion of quagga mussel ([141]).

Our findings were similar to the recorded *in situ* values of K_{dPAR} by Millie et al. ([133]). In 1998, they recorded a K_{dPAR} of 0.21 (m^{-1}) for southern Lake Michigan. Also, our K_{dPAR} values for the year 2010 matches very closely with the Satlantic (Seabird 2013) measurements from Shuchman et al. ([168]). Similar declines were also noted in Lake Ontario where K_{dPAR} values declined from 0.34 m^{-1} in early 1970's to 0.26 and 0.32 m^{-1} in late 1980's and to 0.18 m^{-1} in 1995 ([177]; [132]; [63]). According to Fahnenstiel et al. ([63]), the lower K_{dPAR} values can be translated as more light availability for phytoplankton and the potential for less light limitation. The downward trend in K_{dPAR} between 1998 and 2010 suggests that light limitation may be alleviated and other factors, i.e, nutrients, may play a more important role for limiting primary production.

Significant changes in chlorophyll were noted across the entire southern basin as well as in regionally specific areas. The basin averaged chlorophyll decreased (for both March and April) from 1.7 μg*L^{-1} in 1998 to 0.9 μg*L^{-1} in 2010 (51-55%). Our results are consistent with those from a long term study by Fahnenstiel et al. ([62]) where a 66% drop in chl-*a* concentration between 1995-8 and 2007-8 was noted in the offshore region of southeastern Lake Michigan. Although relatively similar decreases were noted, our results suggest that regions of the lake responded differently. Fahnenstiel et al. ([62]) results were from the eastern region of the Lake which tends to be somewhat more productive, while our results represent the entire southern Lake Michigan basin and therefore includes less productive waters of the offshore region. Another source contributing to these minor differences might be due to slight differences in the temporal scale of these two studies as the work of Fahnenstiel et al. ([62]) includes data from 1983-1998 and some of these years had higher production than 1998 and our other pre-mussel years.

Change detection (CD) analysis was useful in detecting regional changes in water column parameters. Using CD analysis (Fig. 2.5), a noticeable spatial difference in the amount of chl-*a* was noted. While the only evidence for an increase in chl-*a* was observed along the eastern coastal edges of southern Lake Michigan (probably due to an increase of harmful algal blooms in shallow water or an artifact caused by suspended sediments), the majority of the lake area showed a > 0.8 μg*L^{-1} drop in chl-*a* (above the basin average drop) whereas in a few areas only a 0.2-0.4 μg*L^{-1} drop (below average basin drop) was observed. There are some interesting similarities between the spatial patterns of the chl-*a*

and the Lake Michigan bathymetry. Superimposed over the CD image (Fig. 2.5) is the 90m contour line of the Lake Michigan. The inner parts of the polyline are depths greater than 90 meters (except the semi-triangular section in the upper middle section). As can be seen, the encircled waters have shown a lower decline in chl-*a* during this period, versus $<$ 90m waters that have shown more decline in chl-*a*.

The spatial chlorophyll patterns can be related to differences in quagga mussel density and lake bathymetry. Since their arrival in northern Lake Michigan in 2001, quagga mussels have worked their way south and established populations in southern Lake Michigan by 2003-4 ([141]). Biological and physiological properties of quagga mussels enable them to proliferate in the deep profundal regions of the Great Lakes, regions where zebra mussels cannot reproduce or grow. Quagga mussels, in comparison to zebra mussels, have higher filtration rates and lower metabolic rates and can easily grow in soft mud substrates due to their much longer intake siphon ([141]). By 2008, quagga mussels were most abundant in depths less than 90 m and their population just started dispersing into depths greater than 90 m ([141]). Reaching densities over 15,000 individuals per m^2 in 2008, quagga mussel out competed zebra mussels over the entire southern Lake Michigan basin. Looking closely at the CD image (Fig. 2.5), there is indirect evidence of dreissenids further dispersal into offshore waters in the northeastern section of the CD map. The dark blue band (representing the area affected by quagga mussels) extends into $>$90 m and does not clearly follow the 90 m contour line. It may be caused by the continuous migration of the dreissenids into deeper waters after 2008 (Nalepa, unpub. data, [141]).

Correspondingly, based on observations in 2008, quagga mussels were still expanding into >90 meters waters (T. Nalepa, pers. Comm.).

When the physical properties of the water during isothermal conditions in March and April are combined with high densities of quagga mussels, a much clearer picture of reasons for the observed changes starts to emerge. Wind induced lake overturn is much easier under water column isothermal conditions ([63]; [122]; [180]). In Lake Michigan and during winter storms instantaneous flow could reach 20-50 cm/s. For Lake Michigan as a whole, depth averaged mean winter current speed is 2.5 cm/s where the maximum speed is 10.3 m/s ([181]). Therefore quagga mussels, while residing on the bottom of the lake, have easy access to what's being produced in the photic zone. The other important factor probably lies in the nature of diatoms; the dominant phytoplankton in the water column during this time of year. Fahnenstiel et al. ([63]) noted the abundance of large net diatoms; diatoms which clog the sampling nets due to their high abundance during the early spring period. These large net diatoms have high sinking rates which cause their rapid settling onto to the benthic region ([65]). It has been suggested ([133]; [181]) that these viable diatoms form a considerable epibenthic population and therefore contribute significantly to the water column total phytoplankton biomass when sediments become resuspended during winter storm periods. Nalepa and Quigley ([142]) reported the existence of viable benthic chl-*a* on the surface of benthic sediments, with the largest amount being observed during late spring. Before the presence of quagga mussels in 1998, Millie ([133]) estimated that 0.4 -3.5 x 10^8 grams of viable chl-*a* could be resuspended from the lake floor in nearshore

waters (<60 meters deep). This would result in a potential increase of 0.4 -1.5 μg/L chl-*a* to the overlaying water column during major prolonged events. Therefore quagga mussels not only have access to the entire water column, they can also filter all the settled diatoms and prevent periodic resuspension of the settled diatoms by stabilizing the bottom.

The change detection analysis allowed us to examine the effects of quagga mussel filtration in relationship to the observed patterns in chl-*a* depletion. This was done by comparing the spatial statistics of chl-*a* concentrations associated with two separate parts of the lake; the average chl-*a* of nearshore versus offshore. We used F-test and regression line (slope and Y-intercept) comparison to test the statistical differences between these two regions. The results of the F-test showed that the two regions have statistical differences in their average chl-*a* concentrations. In other words, the difference between the average chl-*a* concentration in depths $<$ 90 m through time (1998 to 2010), is significantly ($p<0.05$) different from the same parameter over depths $>$ 90 m during the same time period, implying links to the high density presence of quagga mussels in $<$ 90 m regions.

The F-test only explains the overall differences between average chl-*a* concentration. To determine the trend and magnitude of the difference we compared slopes of the chl-*a* regression lines. The result showed that the rates of change (slopes) are significantly different between nearshore to mid-lake and offshore regions (both for March and April). Less than 90 m waters, comparing to offshore waters, have had significantly faster chl-*a* concentration drop rates between 1998 and 2010. While the reason for the faster drop in

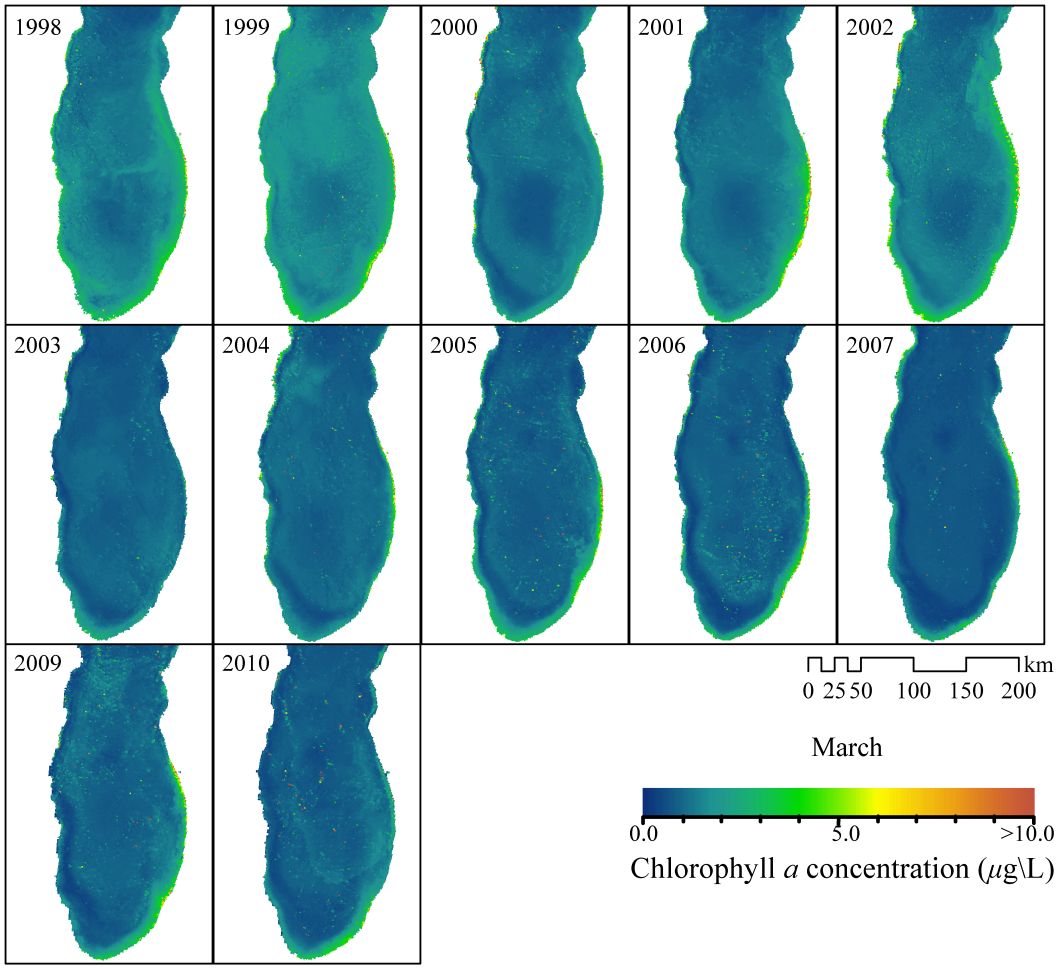

Figure 2.9: March chlorophyll *a* map for southern Lake Michigan. Notice the gradual disappearance of the "doughnut" and simultaneous progress of the dark blue band around the edges of the lake where quagga mussels are most abundant.

$<$ 90 m region is related to the higher density of quagga mussel, the offshore drop in chl-*a* can be described by other scenarios.

Due to the large offshore currents and the relatively slow growth rates of spring diatoms, mussel impacts can be located many kilometers away from large mussel populations ([62]). Figure 2.9 and 2.10 show a large very nearshore phytoplankton

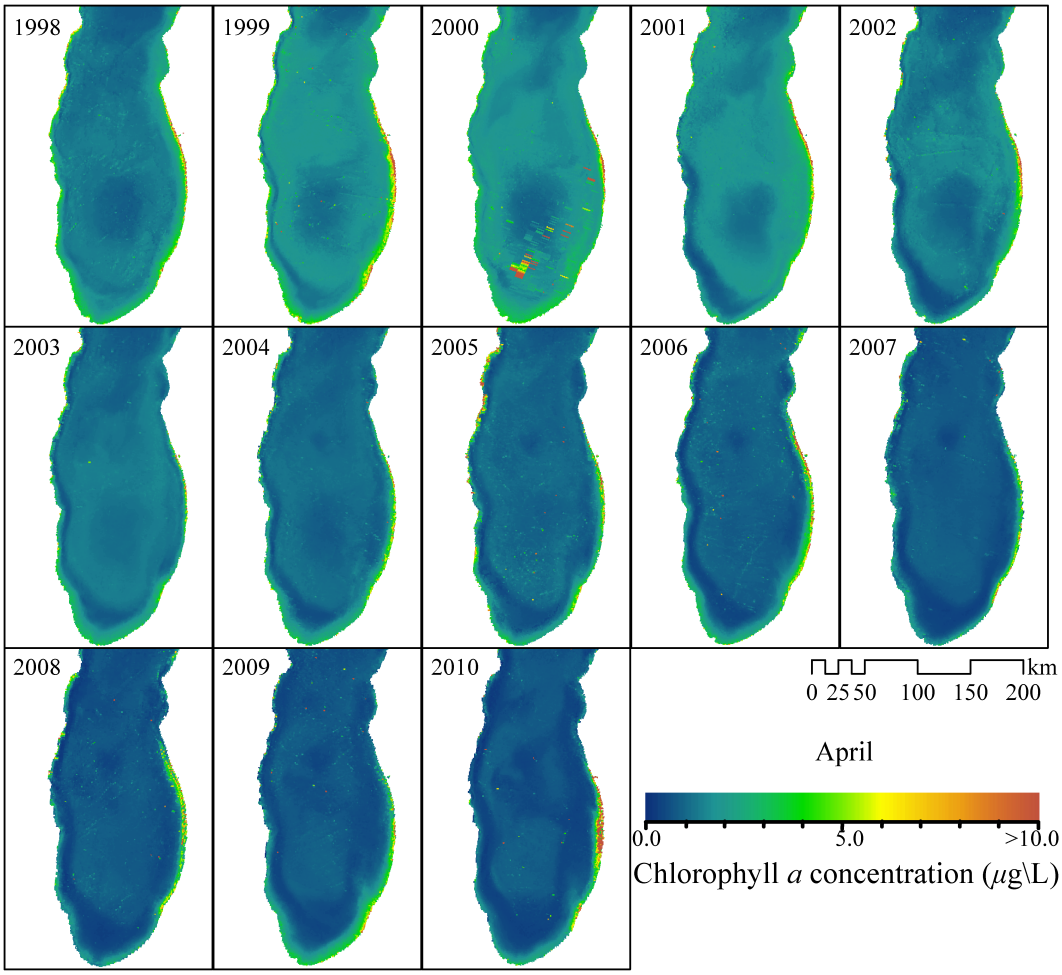

Figure 2.10: April chlorophyll *a* map for southern Lake Michigan. Noticeable are the presence of the "doughnut" (blue-green ring) between 1998 and 2004 and its gradual disappearance afterward. The results of these changes are mostly dramatic around the shallower edges of the lake.

bloom a few miles off the coastline (specially the eastern shoreline) of Lake Michigan during this spring period. This bloom may be related to a nearshore "shunt" ([75]; [181]). Dreissenid mussels filter large volumes of water ([181]) and therefore retain a large pool of phosphorous near the shore line. This scenario helps explain another possible effect of quagga mussels. The eastern shoreline of the southern basin receives up to 70% of the annual phosphorus load ([131]). Quagga mussel's high density in nearshore and mid-lake

regions can prevent a major portion of nutrients, including phosphorous, from migrating to the center of the lake. Thus, although quagga mussels are not present in the center of the lake, their indirect effect (retaining the nutrients in this region) has caused a drop in production in offshore regions as well ([41]; [181]).

The effects of quagga mussels on primary production are dramatic. We observed a 42% decrease in primary production in March (from 301.2 mg C*m^{-2} in 1998 to 160.5 mg C*m^{-2}in 2010) and a 46% decrease in primary production for April (from 388.4 mg C*m^{-2} in 1998 to 223.9 mg C*m^{-2} in 2010). Our findings are consistent with Fahnenstiel et al. ([62]) findings, where they used field measurements to demonstrate similar drops in primary production between 1998 and 2010. They observed a 45% decrease in primary production in March and a 58% drop in April.

Despite the large changes in phytoplankton abundance and productivity during the winter/spring isothermal period, summer and fall phytoplankton abundance and production were similar to values in the 1980 and 1990s ([62]). There are a few factors that can contribute to this pattern. A possibility is related to the suboptimal water temperatures. Cold ($<4°C$) waters do not provide optimal growing condition for phytoplankton and conditions for phytoplankton growth are suboptimal during early spring ([63]). Therefore the filtration rate of quagga mussels is likely higher than the phytoplankton growth rate this time of year ([181]). However, higher summer water temperatures increase the phytoplankton growth rate ([62]). Physics plays a significant role in favor of quagga

mussels as well. During isothermal conditions, quagga mussels have easier access to the entire water column. However, in summer, density difference of water layers (due to thermal stratification) makes it much harder, if not impossible, for the water column to get mixed; thus eliminating the quagga mussel's access to the photic zone and its phytoplankton production.

2.5.1 Ecological consequences of invasion by Dreissenid mussels

The evidence for ecological impacts of dreissenid mussels on primary production also have been observed in other lakes. Analyzing the trends of chl-*a* fluctuations in inland lakes after invasion by dreissenid mussels, Higgins et al. ([77]) found an overall 40-45% decline in chl-*a* concentration. In Lake Huron, using SeaWiFS imagery, Barbiero et al. ([13]) noted that May chlorophyll values for 2003-2006 were 50-60% of 1998-2002 values. Colonial diatoms were among the most depressed phytoplankton in both Lake Michigan ([62]) and Lake Huron ([14]).

The decline in population of diatoms has significant impacts on the silica (Si) and nitrogen (N) uptake rate. Evidence of increased Si concentrations in all basins of Lake Michigan and Lake Huron between 1983 and 2008 are indicators of decreasing growth of dominant diatoms. These declines in Si consumption/uptake rate (or in other words the surplus Si) might be related to other nutrient limitation (e.g. phosphorus, P) as a

consequence of a combination of nutrient loading management (e.g. limiting P loading in Great lakes) and dreissenids bioengineering. Currently the Si and N drawdown rates in Lake Michigan and Lake Huron are similar to values in Lake Superior ([131]; [61]). But not all of their ecological effects has downward trend. By increasing the water clarity and light availability (reduced K_{dPAR}), quagga mussels have indirectly led to increase in cladophora (nuisance benthic algae) population in shallow waters (0-30m deep) of lower the Great Lakes ([6],[78],[79]). However, the ecological impacts of dreissenid mussels are not limited to phytoplankton and primary production.

Density and community composition of organisms in other trophic levels (secondary producers, benthic macro-invertebrates), as well as nutrient utilization and uptake rate are altered due to high filtration pressure by dreissenid mussels. Density of certain zooplankton species showed a major decline after dreissenids between 2006 and 2008; Cyclopoid copepods (94%), *Epischura* (92%), and *Limnocalanus* (93%; [97]). The low densities of predatory species may well be due to less energy flow up to higher trophic levels. In Lake Huron, cyclopoid copepod population and *Daphnia* population egg ratio in August exhibited a major decline between 2003-2006 and has remained depressed since then ([13]). Also in Lake Michigan, while population biomass of *Diporeia* spp., a native amphipod, showed a 90% decline between 1995 and 2005, the biomass of dreissenids showed more than a 7000% increase. The decline in *Diporeia* occurred progressively from shallow to deep regions and was temporally coincident with the expansion of dreissenid mussels into offshore regions ([14]; [140], [141]; [181]). As we know, dreissenids produce both feces

and pseudofeces. In an experiment, Dermott et al. ([57]) conclude that the presence of pseudofeces might have a direct negative effect on *Diporeia* survival, perhaps by interfering with its metabolism. Another example is the overgrowth of Unionid bivalves by dreissenids in the Black Sea, causing mass mortality of these native Bivalves ([38]). *Mysis*, opossum shrimp (*Mysis relicta*), population density in Lake Michigan may be the next victim suffering from this invasion; showing a 70% decline in nearshore waters and an 81% decline in the offshore ([152]). Being herbivorous and highly dependent on phytoplankton as the food source in earlier stages of their life, *Mysis* has been impacted directly by dreissenids. Both *Mysis* and *Diporeia* are among the most important food resources for most of the forage and commercial fish in Lake Michigan ([152]).

Growth rates of forage fish, such as alewives (*Alosa pseudoharnegus*) as well as commercial fish, such as lake whitefish (*Coregonus clupeaformis*), have declined in both Lake Michigan and Lake Huron after the invasion by Dreissenids. Lake whitefish are benthivores and alewives feed on both zooplankton and benthic macroinvertebrates (e.g. *Diporeia* spp., *Mysis relicta*, and Chronomidae). Dreissenid mussels, by affecting the food resources, have indirectly affected these two fish species ([152]).

This paper clearly documents basin-wide changes in water clarity, chlorophyll concentrations and primary production after the establishment of large quagga mussel populations. Based on our evidence and that presented by Fahnenstiel et al. ([64]), quagga mussels are clearly responsible for the disappearance of the spring algal bloom in Lake

Michigan during the recent past years. However, there is already some evidence that quagga mussels are negatively affecting the abundance of their own juveniles in spring time. Although it remains to be verified, it seems that the disappearance of "the doughnut" (which served both as the food source and the distribution vector for quagga mussels) will further hinder their "safe" transportation/reintroduction to new unoccupied habitats in southern Lake Michigan basin.

Remote sensing has proven to be a complementary asset to the current fleet of scientific methods and tools regarding Great Lakes researchers. Nonetheless, its robustness and interpretability depends heavily on field validation ([25]; [94]; [153]; [167]). The observed consistency between SeaWiFS and field measurements of K_{dPAR}, further encourages the research and application of satellite derived K_{dPAR} in the future. Besides the necessary verification of the existing bio-optical algorithms, can we take the next step and explore long term biological and ecological relationships of the Great Lakes ecosystem using remote sensing? Specifically, and regards to recent changes in Lake Michigan, can we explain and relate the important factor behind them? Taking advantage of the great spatial coverage of satellite imagery for the first time, we documented the changing trends of K_{dPAR}, chl-*a*, and primary production in southern Lake Michigan. Focusing on food-web aspects of these recent changes and using spatial analysis of remote sensing data, we demonstrated that highest drops in the chl-*a* concentration between 1998 and 2010 were actually observed where quagga mussels were most abundant. This direct evidence almost rules out the significance of other possible contributing factors (e.g. PAR, phosphorous).

Close similarities between the principle results of this paper and the results from other researchers (e.g. [62]; [141], [131]) demonstrate the advantages of remote sensing and encourages its complementary application in future research. However, abilities to resolve some of the spatially complex phenomena in Lake Michigan (the "doughnut" and its disappearance) and to spatially connect the aquatic food-web links are unique to remote sensing. This ability can serve to answer both scientific and management questions related to water quality of Lake Michigan and other Great Lakes.

Identifying quagga mussels as the cause of these changes puts a new spin on the Lake Michigan ecosystem management. There might be a need to revise some of the aspects of phosphorous loading management. Fishing policies and regulation might face changes to reduce the limits for annual catch of certain fish species (e.g. lake whitefish; [152]). Managers should implement specific regulation and measures to prevent the further transport and spread of other invasives into these valuable freshwater resources (e.g. ship's ballast water treatment).

Chapter 3

Light detection and ranging (LiDAR) and multispectral studies of disturbed Lake Superior coastal environments[1]

W. Charles Kerfoot,[a,b,*] Foad Yousef,[a,b] Sarah A. Green,[c] Robert Regis,[d] Robert Shuchman,[e,d] Colin N. Brooks,[e] Mike Sayers,[e] Bruce Sabol,[f] and Mark Graves [f]

[a]Lake Superior Ecosystems Research Center, Michigan Technological University, Houghton, Michigan

[b]Department of Biological Sciences, Michigan Technological University, Houghton, Michigan

[c]Department of Chemistry, Michigan Technological University, Houghton, Michigan

[d]Department of Geological and Mining Engineering and Sciences, Michigan Technological University, Houghton, Michigan

[e]Michigan Tech Research Institute, Ann Arbor, Michigan

[f]U.S. Army Engineer Research and Development Center (ERDC-Environmental Laboratory), Vicksburg, Mississippi

[*]Corresponding author: wkerfoot@mtu.edu

3.1 Abstract

Due to its high spatial resolution and excellent water penetration, coastal light detection and ranging (LiDAR) coupled with multispectral imaging (MSS) has great promise for resolving shoreline features in the Great Lakes. Previous investigations in Lake Superior documented a metal-rich "halo" around the Keweenaw Peninsula, related to past copper mining practices. Grand Traverse Bay on the Keweenaw Peninsula provides an excellent Great Lakes example of global mine discharges into coastal environments. For more than a century, waste rock migrating from shoreline tailings piles has moved along extensive stretches of coast, damming stream outlets, intercepting wetlands and recreational beaches, suppressing benthic invertebrate communities, and threatening critical fish breeding grounds. In the bay, the magnitude of the discarded wastes literally "reset the shoreline" and provided an intriguing field experiment in coastal erosion and spreading environmental effects. Employing a combination of historic aerial photography and LiDAR, we estimate the time course and mass of tailings eroded into the bay and the amount of copper that contributed to the metal-rich halo. We also quantify underwater tailings spread across benthic substrates by using MSS imagery on spectral reflectance differences between tailings and natural sediment types, plus a depth-correction algorithm (Lyzenga Method). We show that the coastal detail from LiDAR and MSS opens up numerous applications for ecological, ecosystem, and geological investigations.

3.2 Introduction

Light detection and ranging (LiDAR) is an airborne laser-ranging technique that acquires high-resolution elevation and bathymetric data ([7]). The data are collected with aircraft-mounted lasers capable of recording elevation measurements at a rate of 10-200-kHz pulses s^{-1} for above-water topographic stretches and 1-10-kHz for coastal bathymetric surveys, with a maximum vertical precision of 15 cm ([55]). In coastal surveys, the aircraft travels over a water stretch at about 60 m s^{-1}, pulsing two varying laser beams toward earth through an opening in the plane's fuselage: a red wavelength (infrared) beam that is reflected by the water surface and a narrow, blue-green wavelength beam that penetrates the water surface and is reflected from the bottom surface. The LiDAR sensor records the time difference between the two signals to derive measurements of water depth.

An infrared version of LiDAR is used in forest applications, principally for biomass surveys and profiling of canopies ([110]). More recently, attention has expanded to underwater marine and freshwater applications. Under ideal conditions in coastal waters, blue-green laser penetration allows detection of structures down to depths approximately three times greater than passive light reflection. LiDAR has penetrated to a recorded maximum of 35 m in oceanic environments ([67]). Applications of blue-green laser techniques to mapping underwater structures have recently expanded. Marine studies include mapping of coral reefs ([30]), characterization of Atlantic barrier islands ([144])

and studies of Gulf of Mexico estuaries ([29]). In freshwater applications, recent river channel-bed characterizations include erosional surveys along braided streams ([27]). Here we emphasize potential applications in the Great Lakes and marine coastal environments, particularly under circumstances where past and present mine tailings discharges or tailings pond failures are of concern.

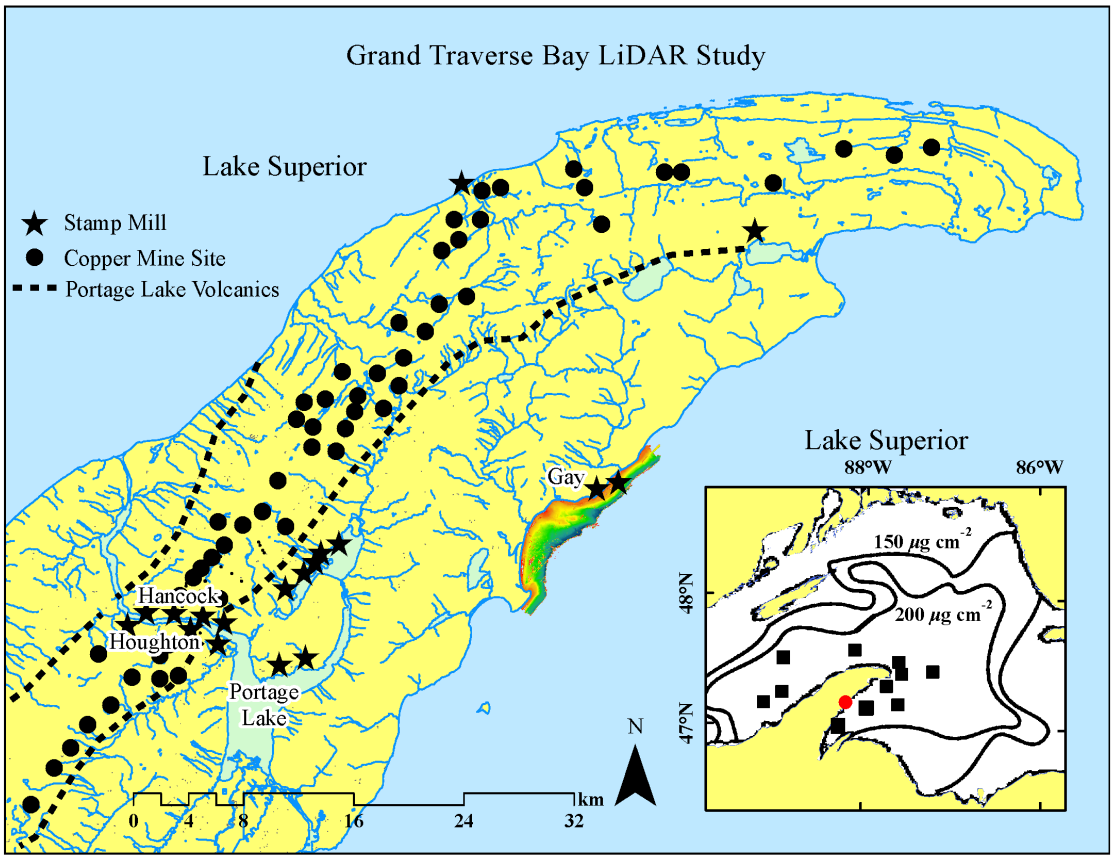

Figure 3.1: Geographic location of Grand Traverse Bay (gray), on the Keweenaw Bay side of the Keweenaw Peninsula, along the southern shoreline of Lake Superior. The boundary of the Portage Lake Volcanics is indicated by dashed lines, copper mines by black dots, and shoreline stamp mills by black stars. Contours in Lake Superior represent copper inventory values (specific core sites from the NSF Keweenaw Interdisciplinary Transport Experiment in Superior KITES: solid black squares indicate 200-400 mg cm^{-2}; [89])

Multispectral sensors (MSS) are instruments that acquire passive reflectance images in many continuous spectral bands throughout the visible, near-infrared, mid-infrared, and thermal portion of the spectrum. These systems can discriminate above- and below-water surface features that have diagnostic absorption and reflectance characteristics. In our case, keying off albedo and spectral differences, they were used jointly with LiDAR to characterize stamp sand dispersal along the shoreline and under the water. Studies were carried out along the southern shoreline of Lake Superior, on the Keweenaw Peninsula. Recent investigations in Lake Superior documented a metal-rich "halo" around the Keweenaw Peninsula associated with past copper mining practices (Fig. 3.1; [89], [95]; [68]). In Grand Traverse Bay (Fig. 3.2), the magnitude of the discarded wastes literally "reset the shoreline" and provided an intriguing field experiment. We used the Compact Hydrographic Airborne Rapid Total Survey (CHARTS) system, one that collects LiDAR and multispectral scanner Compact Airborne Spectrographic Imagery (CASI), to construct detailed coastal maps. Using a combination of historic aerial photography and LiDAR, we estimated the time course and amount of tailings that eroded into Keweenaw Bay and the quantity of copper that contributed to the metal-rich halo.

The Keweenaw Peninsula was one of the first great metal mining regions in North America. Between 1850 and 1929, the district was the second largest producer of copper in the world ([139]; [18]). Native copper in the Portage Lake Volcanic Series came from two principal kinds of ore: basalt lava flows (amygdule deposits) and inter-bedded sediments (conglomerates). Both were crushed with early gravity and later giant steam-driven stamps

to release the native copper and silver ([33]; [19]). During that interval, mill sites and stamp sand piles dotted the regional landscape (Fig. 3.1). More than 140 mines worked the central deposits and 40 mills processed stamp rock ([96]). The unit used here to express mass is the teragram (Tg), equivalent to 10^{12} grams or 1 megatonne (Mt). Smelters produced 4.4 Tg of copper, while stamp mills sluiced around 360 Tg of copper-rich stamp tailings into rivers and waterways, including 64 Tg directly onto Lake Superior shorelines and 25 Tg into Keweenaw Bay ([96],[95]; [101]).

In Grand Traverse Bay, the magnitude of the wastes initiated a perturbation that has played out for more than a century. The coastal stamp sands in the bay were promising for CHARTS studies because albedo and spectral reflectance contrasts between stamp sands and natural sediments afforded opportunities to locate drift of tailings over natural coastal sediments (Fig. 3.3a,b). Here we emphasize that LiDAR and MSS applications have a wide range of uses. These include: (1) identifying drifting sediment inputs from multiple sources (e.g., tailings, shoreline dunes, gravel or cobble beds, river-mouth sediments); (2) characterizing post-Pleistocene features (e.g., Nipissing beach ridges, ancient riverbeds); and (3) quantifying substrate cover from seasonal biological variables (e.g., wetland vegetation, aquatic macrophytes, benthic cover). All these attributes are evident in the Grand Traverse Bay investigation. Yet we must also emphasize that coastal mine tailings, either from direct discharges or from failed tailings dams, are not just local curiosities, they present a genuine global problem ([126]; [120]).

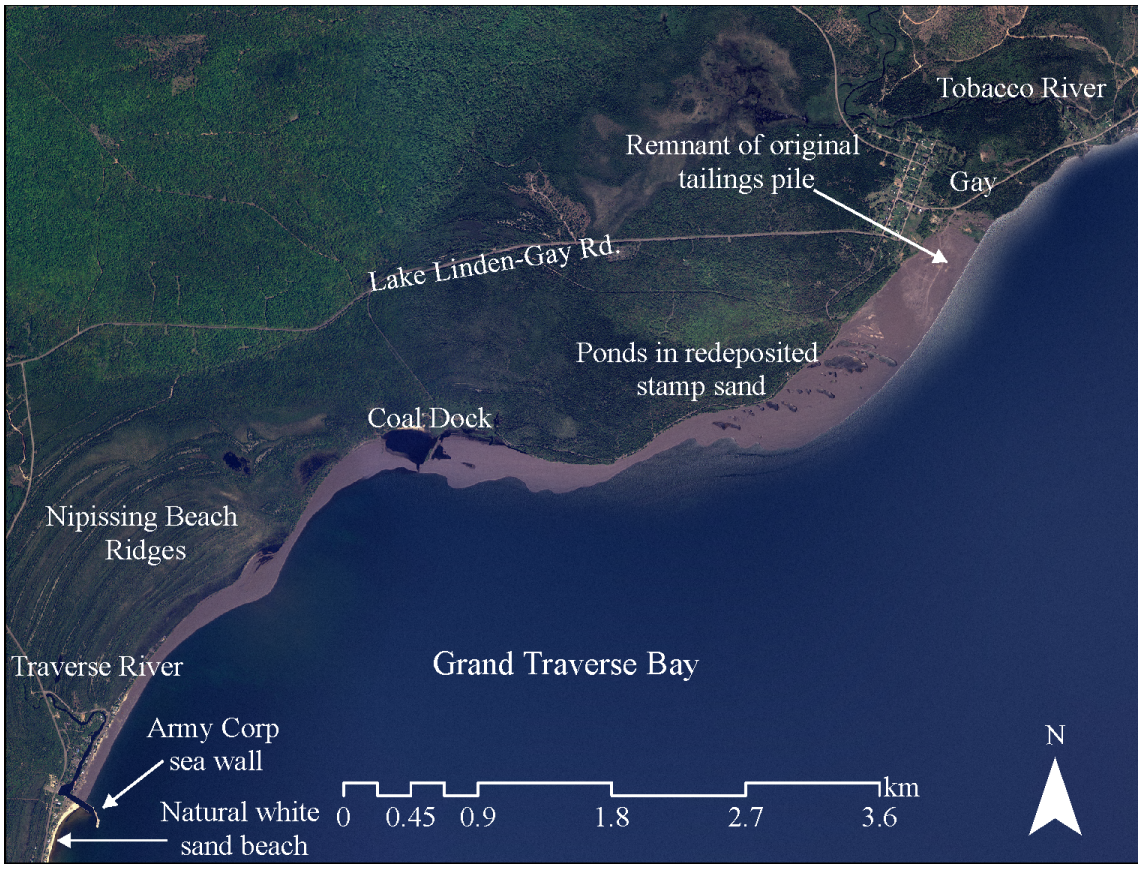

Figure 3.2: Aerial image of Grand Traverse Bay (2005 National Photography Program, MrSID format). Labels indicate local features, including the original tailings pile remnant at Gay, the Coal Dock region, and redeposited stamp sand stretching southward to natural white sands at the Traverse River seawall. Note remnants of natural beach sands behind the Coal Dock and high on the beach north of the Traverse River seawall.

3.3 Methods

Determining discharges into Keweenaw Bay- The Copper Country Archives section of the J. R. Van Pelt Library, Michigan Technological University, retains copies of processing records from mining companies. The archived records include yearly reports of total copper

produced, total amount of rock removed, total amount of stamp rock shipped to stamp mills, and operation details. The tallies allowed us to reconstruct accurate totals for yearly stamp stand discharges from mills into Keweenaw Bay (Table 3.1).

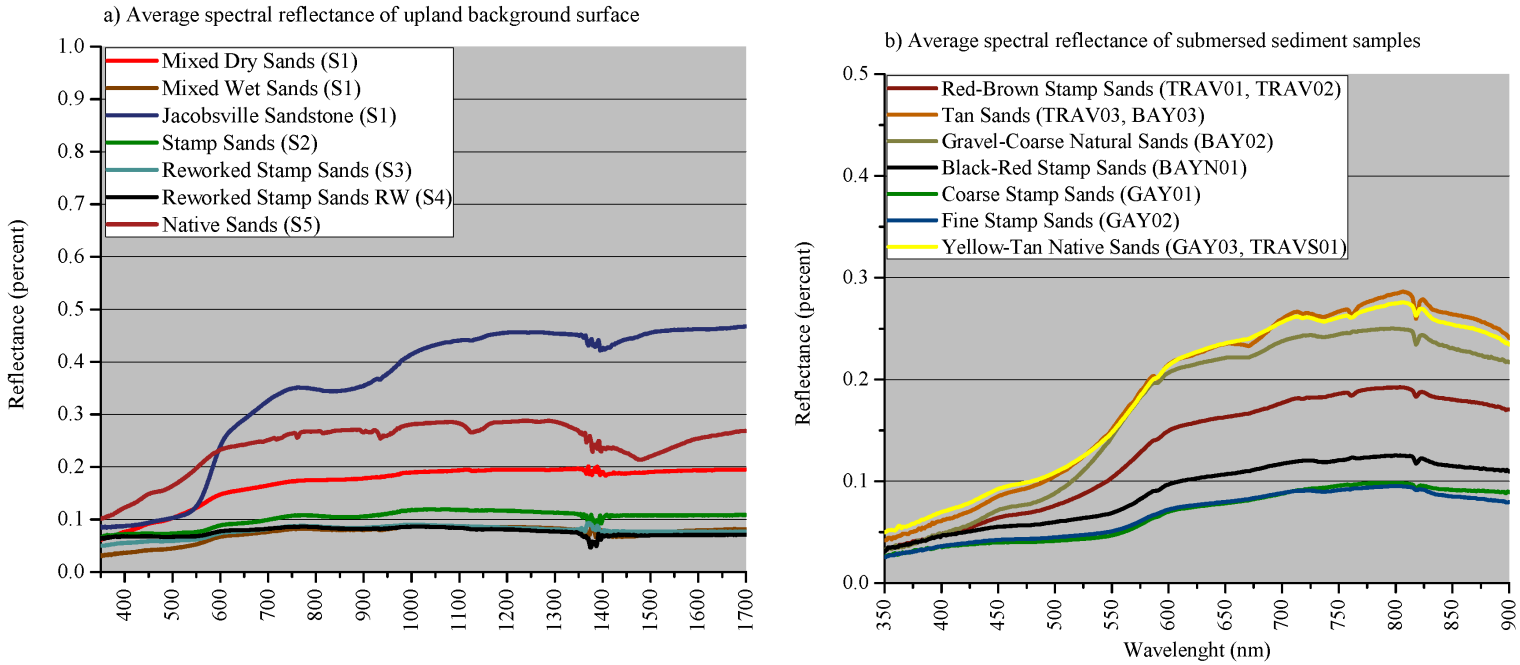

Figure 3.3: (a) Spectral reflectance of shoreline above-water surfaces near Gay. Jacobsville Sandstone has the highest reflectance, whereas native beach sands have intermediate reflectance and stamp sands have the lowest reflectance. Native and stamp sand mixtures have intermediate reflectance values. (b) Spectral reflectance of submersed (1-2-cm) sediment samples collected from the Gay site. Yellow, tan, and gray natural sands show the highest spectral reflectance values, whereas coarse and fine stamp sands from Gay show the lowest. Note that the wavelength scale is shortened.

Estimating erosion of the Gay tailings pile after 1938- Material in the original stamp sand pile consisted of two fractions: a coarse fraction (sand) with a specific gravity around 2.9, and a fine silt-clay fraction (the so-called "slime clays"; [19]). Coarse grain sizes on tailings piles are angular, approximately log-normally distributed, with modal sizes ranging between 0.3 and 3.4 mm (Babcock and Spiroff unpubl.; [85]). Prevailing coastal currents off Gay move strongly southward, with only occasional reversals ([43]; [193]). Currents are maximum during late fall and early winter storms (60-80 cm $\cdot$ s^{-1}; November to early December, National Oceanic and Atmospheric Administration [NOAA] Great Lakes Environmental Research Laboratory and Coastal Current Forecast Model, 2010). During wave erosion, the coarse fraction is redeposited as a beach sand to the south of the main pile (Fig. 3.2), whereas the fine silt clay fraction (an estimated 7-14% of pile mass; Babcock and Spiroff unpubl.) is winnowed out and dispersed far out across the coastal shelf. The tailings are distinctively different in color, mineral content, and physical characteristics from the natural beach and lake sediments, derived from the local Jacobsville Sandstone formation.

LiDAR was used in this project principally for producing digital elevation models (DEMs). During the week of 23 June 2008, CHARTS aerial overflights of the Grand Traverse Bay area were performed by the Joint Airborne LiDAR Bathymetry Technical Center of Expertise. The pulse rates were 1 kHz at 532 nm and 9 kHz at 1064 nm with a scan width of -4° side to side from an altitude of 400 m. The flight speed was 125 knots (64 m $\cdot$ s^{-1}), slower than normal for improved image collection. The

preprocessed CHARTS LiDAR and 8-band multispectral data were forwarded to Michigan Technological University, Houghton, Michigan, and to Michigan Tech Research Institute, Ann Arbor, Michigan. Using the Geographic Information System (GIS)-referenced high-resolution LiDAR DEM portion of the data set, we constructed 2-m^2-resolution LiDAR bathymetry maps. The CHARTS LiDAR had a vertical resolution of 30 cm. At the same time, locations and orientation of the laser source were determined by the Geographic Positioning System and by the Internal Measurement Units, respectively.

For a check on the accuracy of bathymetric measurements, the LiDAR-derived depths were compared with georegistered National Water Resources Institute (NWRI) sonar-derived depths ([23]). Statistical software packages (SYSTAT) were used for determining spatial cross-correlations. The resulting regression matches were very similar (Fig. 3.4b, $R^2 = 0.98$). Notice, however, that LiDAR in 2008 showed slightly less substrate depth in very shallow regions, compared to the 2004 sonar data set. The slight disparity may be real, as the NWRI depth data were collected 4 yr earlier. During the interval, migrating coastal stamp sands might have filled in more of the shallow depths.

Using CHARTS LiDAR data along with several aerial photos from 1938 to 2010, we attempted to reconstruct the 1938 Gay stamp sand pile volume and, with some reasonable assumptions, to calculate the shoreline erosion rate of the pile between 1938 and 2008, concluding with the year of the CHARTS overflight. To measure erosion of the tailings pile and the mass of sands washed into Lake Superior, three estimates were needed: (1) the area and volume of the pile above water level (available from the 2008 LiDAR); (2)

Table 3.1
Copper mill yearly discharges of stamp sands into Keweenaw Bay. Totals compiled from company records (Copper Country Archives, J. R. Van Pelt Library, Michigan Technological University, Houghton, Michigan).

Date	Mass Mill (Tg)	Mohawk Mill (Tg)	Wolverine Mill (Tg)
1898	0	0	0
1899	0	0	0
1900	0	0	0
1901	0	0	0
1902	152,562	7813	253,091
1903	122,611	261,645	284,912
1904	105,614	416,506	291,917
1905	143,430	531,837	310,065
1906	185,789	561,080	312,099
1907	204,599	581,249	316,451
1908	171,268	622,110	338,978
1909	139,404	742,932	354,528
1910	90,747	727,981	352,387
1911	73,475	727,991	364,026
1912	132,891	714,741	352,410
1913	78,250	332,414	165,207
1914	209,354	589,297	360,676
1915	323,335	752,702	352,769
1916	287,900	602,811	320,066
1917	244,671	548,979	275,303
1918	196,456	412,089	270,397
1919	123,780	508,642	233,391
1920	0	394,578	238,615
1921	0	624,332	263,439
1922	0	464,792	221,614
1923	0	367,749	86,545
1924	0	637,269	186,344
1925	0	580,607	39,607
1926	0	654,079	0
1927	0	689,285	0
1928	0	595,728	0
1929	0	562,026	0
1930	0	428,716	0
1931	0	402,698	0
1932	0	196,467	0
1933	0	0	0

the below-water volume, i.e., calculating the true depth of the stamp sand pile above lake bottom bedrock; and (3) the area of the pile lost through time (erosion at the shoreline face, estimated from aerial photos, essentially treated as vertical slices across the pile; Fig. 3.5).

Although discharges ended in 1932 (Fig. 3.6), the original boundaries of the Gay tailings pile were determined from a georegistered 1938 aerial photograph of the region. ArcMap9.3 was used to digitize this aerial photo ([82]). Wave action along the outer edge

erodes the pile, yet the high specific gravity and angular nature of particles helps maintain a near-vertical face along the eroding cliff (Fig. 3.7a). Strong prevailing currents ([105]; [43]; 2010 NOAA Great Lakes Environmental Research Laboratory Now-cast Wind Model) transported stamp sand particles southwestward, covering natural Jacobsville Sandstone outcrops and white beach sands. Seven other aerial photos, taken between 1944 and 2010, provided subsequent shoreline edge changes on the original tailings pile and estimates of redeposition along southern beaches, both quantified with ArcGIS and ENVI ([82]). The photos allowed mapping of the original piles changing boundaries (Fig. 3.8), to which we fit pixel polygons.

To estimate below-water volume, the pile was separated into two regions. One region was the portion of the pile eroded to bedrock, which allowed LiDAR-derived estimates of past bottom contours under the original pile, whereas the second portion was the remaining part covered by stamp sand. In the first portion (eroded area), we assumed a fairly constant yearly water level (183.4 m; Detroit District Corps) to estimate the underwater volume of the pile. To estimate the depth of the stamp sand in the second region, currently covered by stamp sand, we used the slope change of bedrock from the LiDAR bathymetric map adjacent to the pile and extrapolated this slope under the pile. The result of the linear slope analysis produced an average depth below lake level of about 2 m for the currently covered portion.

To estimate volume lost above water (i.e., exposed shoreline component), we also

needed to determine the elevation of the stamp sand pile removed by shoreline erosion. Again we considered the same two regions: current pile and the portion of the pile that was lost. The high resolution 2008 LiDAR DEM provided the height measurement of the 2008 pile. Past pile elevations were reconstructed by extending the height of known existing landmarks (ends of preserved sluiceways) across the aerial photos to estimate depth. Photos and company discussions of the surface sluiceways suggested that most of the original Mohawk-Wolverine pile had been nearly flat, giving the tailings pile a flat-topped mesa, or table, appearance (Fig. 3.7b). The idea of a nearly flat slope (low grade) was compatible with conveyor belt operation. A very slight slope allowed extension as far as possible away from the mine and into Grand Traverse Bay. The average height of the above-water-level (8 m) portion and down-gradient slope was determined from the 2008 LiDAR elevation values along the preserved sluiceway landmarks on the existing pile. Projected extension of the sluiceways was used to estimate the height of eroded portions, and past aerial photos to estimate area dimensions. The underwater volume was added based on estimated depth to bedrock.

The reconstructed pile was first used to calculate the volume and mass of stamp sand in 1938. Procedures employed a pixel spatial resolution of 3 m and an area of 9 m^2. Multiplying area by depth gave an estimate of volume of stamp sand for each pixel. Integration provided an estimate of total volume in cubic meters. An average of Colin's (internal report 2009; accessible from the U.S. Department of Agriculture's [USDA] Natural Resource Conservation Service) Web Soil Survey values

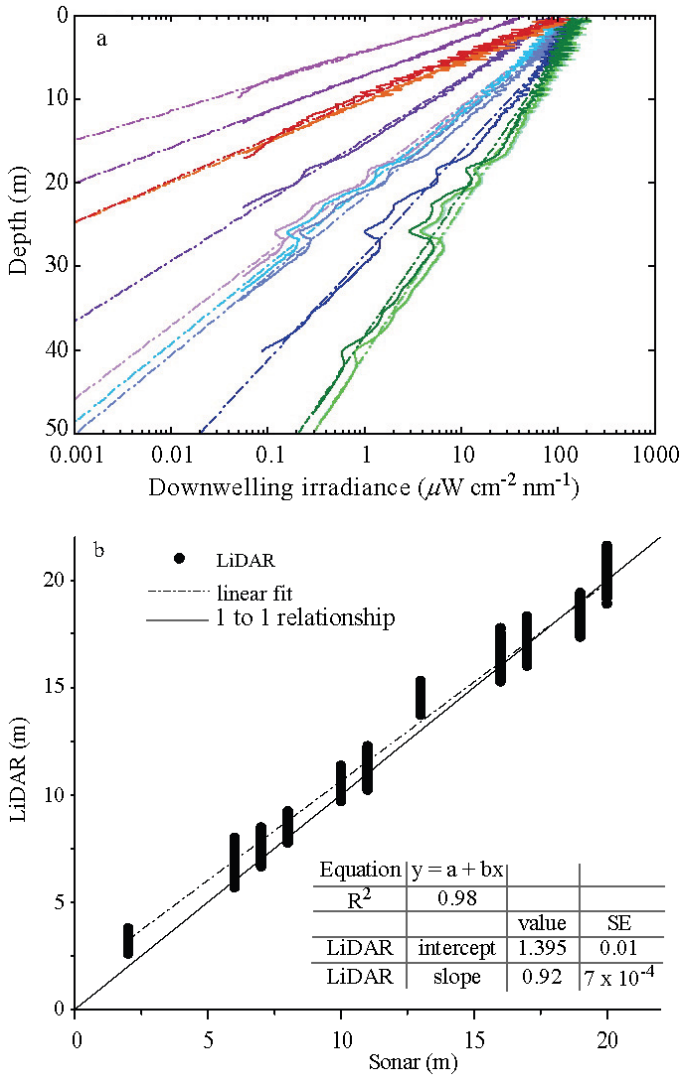

Figure 3.4: (a) Sample data from Satlantic OC P1000 Optical Profiling Radiometer; each color represents a different spectral band. The dashed straight lines represent spectral regression lines using the Beer-Lambert's law equation. Notice how blues and greens (right lines) penetrate deeper than red wavelengths. (b) Regression of LiDAR-derived (2008 CHARTS) depths on sonar-derived (2004 NWRI) depths. Solid line represents a perfect match; dashed line is a linear data-fit line.

(http:// soildatamart.nrcs.usda.gov/Manuscripts/MI605/Keweenaw_MI.pdf) was used to assign mass. Moist bulk density of the Gay stamp sands soil was estimated as between 1.35-1.65 $g \cdot cm^{-3}$ or 1350-1650 $kg \cdot m^{-3}$. We chose the mean bulk density value of 1.65

g cm^{-3} and calculated the mass for each eroded slice. An exponential decay equation was fit to the mean erosion curve, giving an intercept estimate of date when the pile was gone (i.e., zero mass). A separate independent estimate of zero mass intercept came from log-transformed values, after fitting a line to the linear points. However, because of log-transformation, that line estimated loss based on the mode, rather than on the mean. A final estimate came from estimating shoreline regression, i.e., meters of erosion at the shoreline through time for four transect lines (Fig. 3.5) across the Gay pile, extrapolated to intercept the natural shoreline.

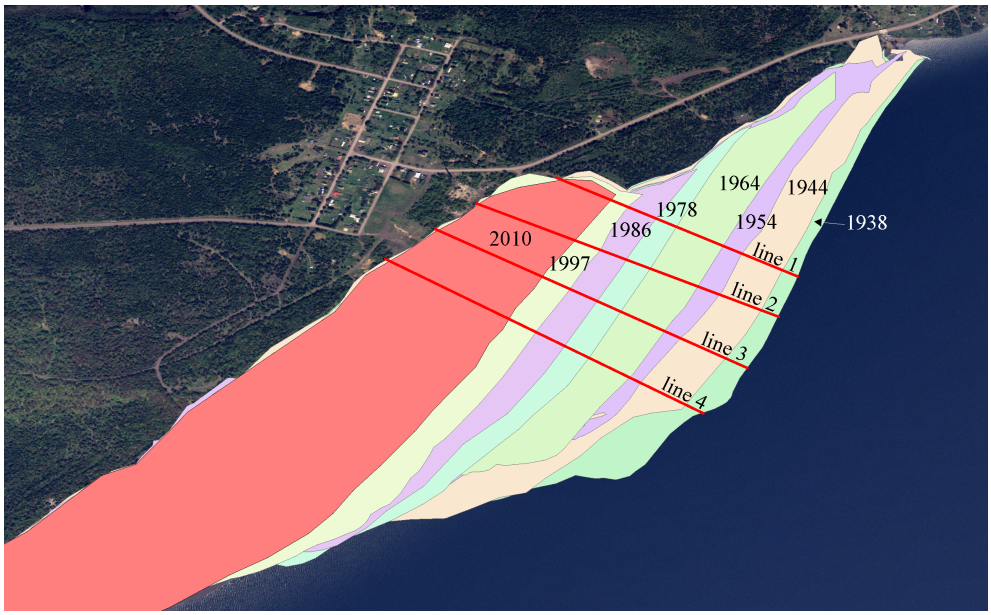

Figure 3.5: Four transect lines across Gay tailings pile, showing shoreline erosion down to 2010 condition. Eroded margins are shaded and dated.

Bathymetric LiDAR and multispectral data- A 1906 bathymetry map (Lake Superior Coast Chart No. 4, Soundings 1906) provided depths at some sites and an estimate of nearshore contours. Although crude, the depth records allowed estimates of underwater

shoreline contours before stamp sand encroachment. Bottom contours of the 1906 map were superimposed on the 2008 LiDAR aboveground aerial map of the shoreline stamp sands to more precisely calculate total shoreline volume of stamp sands south of the main pile. LiDAR imagery was complemented with simultaneously collected MSS imagery on the CHARTS airborne platform. The CASI hyperspectral scanner was configured to acquire data over eight bands uniformly spaced between 375 and 1050 nm, including five visible wavelengths (nominal bandwidth of 84 nm). For distinguishing bay sediments, wavelength studies required the ability to penetrate water and sufficient spectral differences to separate stamp sands from background Jacobsville Sandstone and natural beach sands (Fig. 3.3a,b). Our main focus was on the green and red portion of the visible spectrum-495-750 nm (Fig. 3.4a). Delineation of the land-water boundary was best when using near-infrared bands. Additional images of Grand Traverse Bay were retrieved from the National Agriculture Imagery Program (NAIP) multiresolution seamless image databank (years 2005 and 2009).

LiDAR substrate mapping and upwelling multispectral color data helped resolve substrate features and aided distinguishing stamp sands from natural substrates. Concurrent with overflights, we measured water column and sediment characteristics using Michigan Tech's 11.3-m R/V Agassiz and 7.3-m R/V Polar. Ground-truth Ponar samples clarified the nature of the various substrates in the bay. Samples were photographed and supplemented by underwater video images of sediment surfaces, taken by a MarCum VS620 Underwater Viewing System. Previous underwater images were also available from NWRI surveys ([23]).

Interpretation of 8-band 2008 MSS and 2009 3-band aerial photo images was aided by substrate differences in spectral reflectance. As is evident on aerial photo images (Fig. 3.2), the gray to black stamp sands (crushed basalt) on the beach have a low albedo, whereas the natural white beach sands (derived from Jacobsville Sandstone) have a high albedo. Spectral reflectance of stamp sands, natural beach sands, and Jacobsville Sandstone (coastal rock outcrop) was quantified above and underwater (Fig. 3.3a,b). Procedures followed Sabol et al. ([161]), using an Analytical Spectral Devices (ASD), FieldSpec Pro (model FSP350-2500PJ). Beach substrates included: (1) stamp sands from the primary discharge pile; (2) wave-reworked stamp sands; (3) native beach sands, derived from Jacobsville Sandstone; (4) Jacobsville sandstone; and (5) various mixed stamp sands and natural sands.

Using Lyzenga's techniques to help classify CHARTS MSS substrate types- To quantify downwelling and upwelling spectral irradiance in Grand Traverse Bay, we used a Satlantic OC P1000 Optical Profiling Radiometer at seven sites (Fig. 3.4a). During the week of 23 June 2008, and during the summers of 2009-2010, additional ground- and sea-truth data were collected. Determining depth limitations on the MSS data required three components. The first component was a finished bathymetry map of Grand Traverse Bay, derived from the 2008 LiDAR studies. The second component was a finished MSS mosaic, stitched together from the various overflight tracks. The third component involved calculations from Satlantic spectral radiometer light profiles to help identify upwelling reflectance types and to facilitate substrate classifications.

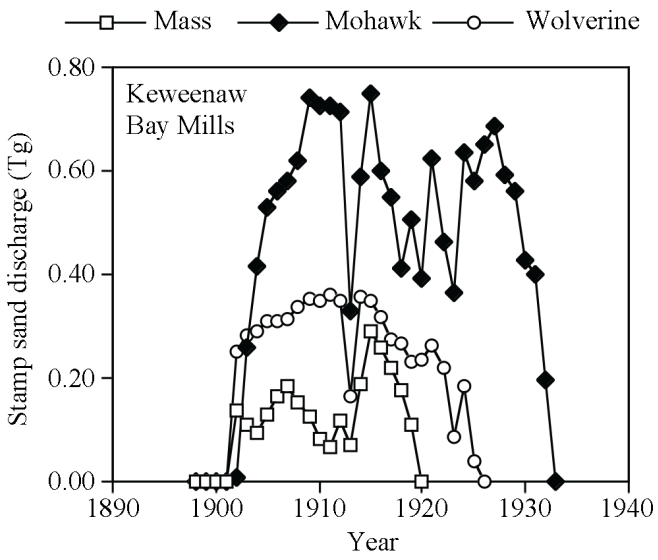

Figure 3.6: Yearly stamp sand discharges from large Keweenaw Bay copper mills (Mass, Mohawk, and Wolverine). Mohawk and Wolverine Mills were located at Gay, whereas the smaller Mass Mill was south, near Assinins, north of Baraga. Total stamp sands discharged were Mass 2.7 Tg, Mohawk 16.2 Tg, and Wolverine 6.5 Tg (see Table 3.1).

Table 3.2
Mass of stamp sands left on the original Gay tailings pile through time.

Year	Mass (Tg)
1938	15.76
1944	14.00
1954	10.72
1964	9.58
1978	7.03
1986	5.63
1997	4.08
2008	3.29

How deep could MSS resolve bottom sediment details? The Satlantic provided attenuation coefficients for downwelling and upwelling spectral bands (Fig. 3.4a). Critical additional variables were surface irradiance energy and coefficients for depth-dependent spectral transmission. From these two parameters, we calculated the maximum water depth

that light can penetrate, according to the simple formula: $I_z = I_0 e^{-\varepsilon z}$, where I_z is irradiance at depth z, I_0 is surface irradiance, and $-\varepsilon$ is the extinction coefficient. However, for MSS resolution, ambient light must reflect off the bottom surface and return a signal to the surface plane, hence the importance of the Satlantic upwelling irradiance measurements. ArcMap software package (version 9.3) was used to create a depth-dependent mask that was superimposed upon the MSS data to check the ability to resolve substrate color contrasts ([82]).

Lyzenga ([119]) provided a method for handling reflectance depth effects in MSS imagery, allowing production of a water depth-independent mosaic:

$$R_w = (A_d - R_\infty) e^{-gz} + R_\infty$$

where R_w is the water column reflectance if the water were optically deep, A_d is the bottom albedo, z is the depth, and g is a function of the diffuse attenuation coefficients for both downwelling and upwelling light.

Ratio-based algorithms determine the relation between different spectral bands over the same bottom type. The polygons were then classified by substrate type. By applying this method, we were able to separate different bottom types based on their reflectance. The MSS images were projected to Universal Transverse Mercator Zone 16 coordinate system and pixel values converted to actual spectral reflectance values ($W.m^{-2}$) for comparison with Satlantic data. ArcGIS or ERDAS (Earth Resources Data Analysis System) IMAGINE

was used to translate data from MSS images.

Although we had a clear path to follow in classifying different bottom types, there were some typical technical problems with flyover images. These problems were due to different sun angles, cloud cover, and sun glints off waves during the 2-d operations, and sometimes to miscalibrated sensors (data gaps). A simple glint-removal algorithm was applied to the 2008 overflight bands to correct for sun glint artifacts ([76]). We obtained another 3-band MSS data from an aerial overflight (2009 USDA; http:// datagateway.nrcs.usda.gov/GDGOrder.aspx) from calmer lake surface conditions to complement the 2008 set. The imagery was obtained from NAIP. Depth-corrected radiance images were produced for each of the visible bands per image strip. Through visible inspection, bands 2 (490 nm, blue) and 3 (581 nm, green) were chosen as optimal channels for bottom type discrimination. We utilized bottom type's attributes (albedo, color, and depth-corrected radiance) to aid classification, and cross-correlated with sites of actual Ponar substrate samples (ground truth). Depth-corrected images were input into the depth-invariant index algorithm ([119]) to produce one combined bottom type image. Level slicing of the derived depth invariant bottom type image created a bottom type classification map. The method appeared to clearly differentiate three different shallow-water substrate types: stamp sands, native yellow sands, and Jacobsville Sandstone (bedrock, cobble).

3.4 Results

General features- Grand Traverse Bay landforms are shown in Fig. 3.2 (2005 NAIP, Multiresolution Seamless Image Database-MrSID format, 1-m-resolution image). The bay includes about 8.5 km of shoreline where dark stamp sands lie over formerly white native beachfront derived from Jacobsville Sandstone. Eroding dark sands have covered around 2.3 km^2 of beach surface over the last 70 yr. The northernmost thousand meters of coastline contain the original tailings pile, an area that appears slightly purple from the Fe-oxidized slime clay fraction, and reaching 6-7 m elevation above water. The pile shoreline features a weathered bluff fronted by a narrow sinusoidal beach (Fig. 3.7a). The beach varies from 5 to 8 m wide. South of the pile, the redeposited stamp sand portion is fairly level and ranges from 45 to 530 m in width, with numerous small ponds. There is residential housing along, 1,125 m of shoreline north of the Traverse River harbor. Immediately south of the harbor break-wall, the shoreline is also residential with typical white sand beach from weathered Jacobsville Sandstone.

The aerial photo (Fig. 3.2) reveals long stretches of stamp sands along the middle beach region that penetrate into the forest margin and wetland edges. About 1.5 km north of the Gay pile is the Tobacco River, which marks the northern drift of stamp sands, whereas 6.9 km south in the bay is the Traverse River, where dark stamp stands stop abruptly, abutting up against an extended Army Corps seawall. In between, in the middle of the bay,

Figure 3.7: (a) Wave erosion of the Gay tailings pile. The near-vertical 7-m bluffs contain wellpreserved remnants of wooden troughs that sluiced stamp sands across the pile. (b) Primary and secondary sluiceways (Wolverine Mill, winter 1922) carry stamp sands over the Gay pile. Lake Superior is on the horizon. Notice melted regions with fresh discharges. Photo courtesy of Michigan Tech Archive.

stamp sands have mounded up south of the pile and around the Coal Dock site, forming a small pond behind the dock. At present, an unnamed intermittent stream floods the pond in early spring and exits through the stamp sand beach margin. Small remnants of the original white beach sands show up behind the Coal Dock and in an elevated fringe north of the Traverse River seawall. Inland there are about 60 alternating post-Pleistocene (Nipissing) beach ridges distinguished by different vegetation types, switching between pines (Pinus)

and spruce (Picea) on upland highs and grasses in lowland swales. The Nippising beach ridge complex demonstrates that the southern portion of the bay is a region where eroded sediments were deposited as beach sands for 3800-900 yr before present (B.P.) during dropping lake levels. Dated cores suggest that a beach ridge formed every 36 ± 7.8 yr, and that the strandline progradation rate was 0.68 ± 0.1 m yr^{-1} ([87]). South of the Traverse River seawall, relatively undisturbed white beach sands stretch for another 5 km.

Historic mill discharges and Gay tailings pile company records document that the Mohawk and Wolverine companies mined the Kearsarge amygdaloidal basalt deposit and constructed new stamp mills at Gay during the summers of 1901-1902. The two operated as twin mills, with a single pumping plant and a joint superintendent. Stamp rock was hauled from the mines to the stamping site via the Mohawk and Traverse Bay Branch (Mineral Range Railroad), a distance of about 21-27 km ([134]). Coal for operations was unloaded south of Gay, requiring construction of a Coal Dock (Fig. 3.2), and laying of a short connecting line. The Coal Dock extended 100 m into the bay, 5.7 m deep at its end ([48]).

Three major mills discharged into Keweenaw Bay (Fig. 3.6; Table 3.1). The Mohawk and Wolverine Mills were located at Gay, whereas the Mass Mill was to the south near Assinins, north of Baraga. Operations at the Mohawk and Wolverine Mills were much larger than at the Mass Mill. The beginning of Keweenaw Bay stamp mill operations was nearly synchronous, as the Mohawk (1901), Wolverine (1902), and Mass (1902) Mills

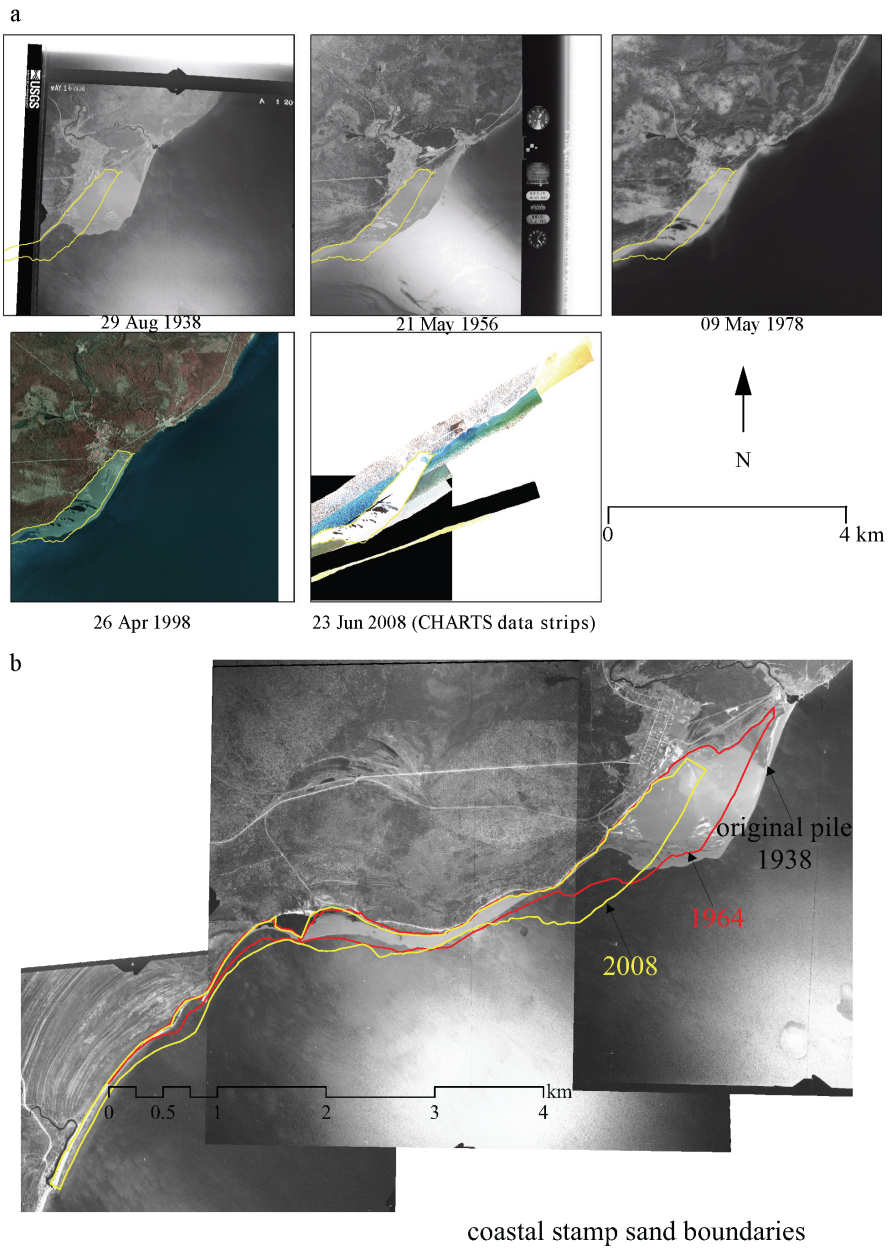

Figure 3.8: Selected aerial photos record erosion of the Gay tailings pile: (a) LiDAR-derived outline of 2008 pile superimposed upon various aerial images; (b) changing boundaries of coastal stamp sands indicated on original 1938 aerial image (red-1964 outline; yellow-2008). Note the diminished original tailings pile and the greater spread southward of stamp sands as time progresses.

opened within 3 yr of each other and closed between 1919 and 1932 (the dates were Wolverine 1925, Mohawk 1932, Mass 1919; [33]; [95]). The Mohawk and Wolverine Mills utilized Nordberg stamps, Harding ball, and Chilean mills. The two stamp mills sluiced a combined 22.7 Tg of stamp sands onto one large pile, covering about 0.9 km^2 originally (Figs. 3.5, 3.8). By 1915-1920 a water intake tunnel extended out a distance of 856 m and a stamp sand conveyor belt 527 m into Grand Traverse Bay ([134]). As a crosscheck on discharge, our estimated total discharge at Gay (i.e., 22.7 Tg) corresponds closely to the total of 21.8 Tg reported by Babcock and Spiroff (unpubl.).

Erosion studies using LiDAR and aerial photographs- From a combination of the 2008 LiDAR bathymetry profiles and several aerial photographs (Fig. 3.8), we estimated the mass of stamp sand eroded from the pile through time, and the portion left along the shoreline site (see Methods; Table 3.2). Graphing the values, the time course for mass lost through time from the original tailings pile was clearly nonlinear (Fig. 3.9a). The best fit was obtained with an exponential decay function (Table 3.3, $y = 7.646 \times 10^{16} e^{-x/53.82}$ - 1.42, where x is in calendar years; $R^2 = 0.993$). With the exponential decay model, the zero intercept (indicating when the pile will be gone) was around 2073. The 95% confidence intervals fit around the nonlinear regression trend indicate uncertainty in decades (Table 3.3; 2041 to > 2080). Of the 22.8 Tg stamped and discharged by the Mohawk and Wolverine Mills (Table 3.1), an estimated 15.8 Tg (69.3%) remained on the Gay tailings pile in 1938. Estimating mass erosion through time (Table 3.2), we found that only 3.07 Tg (13.5%) of the original discharged mass was still n the pile in 2008. By 2008, yearly erosion loss was

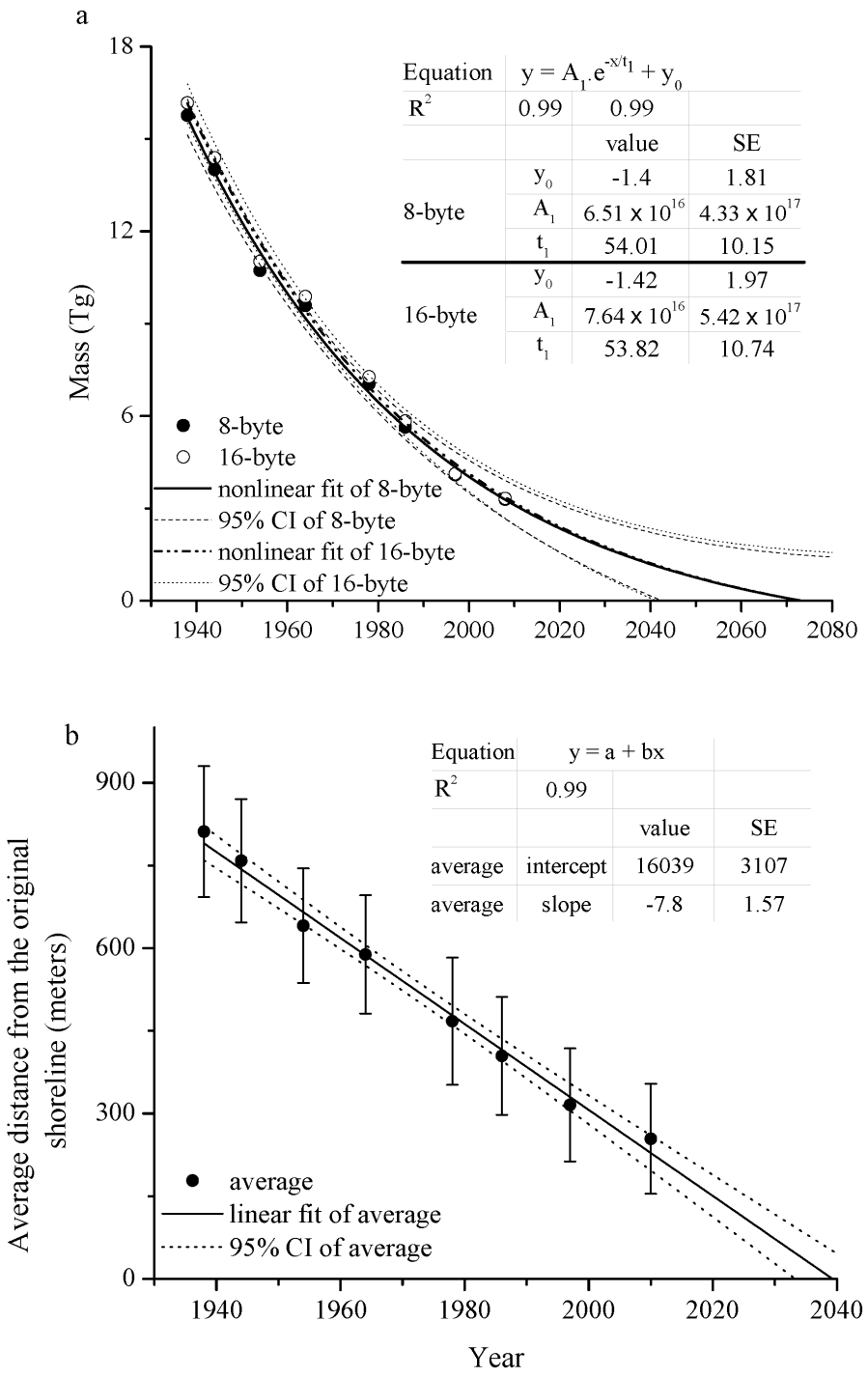

Figure 3.9: Erosion of mass from the primary tailings pile: (a) loss of mass in teragrams from the Gay tailings pile through time is an exponential decay function (8- and 16-byte equations converge, Table 3.3), with a zero intercept around 2074; (b) in contrast, shoreline erosion in meters appears nearly linear, with a mean intercept around 2040 (Table 3.3).

about 42,050 m^3 of stamp sands, or about 0.069 Tg. A second estimate of mass erosion loss came from log10 transformation of volumes see Methods; Table 3.3). As expected for exponential decay, the log10 transformation allowed a linear fit to the data points (Table 3.3; n = 8; $y = 20.01978x + 41.1879$; $R^2 = 0.993$). The linear regression produced a zero intercept of 2082, with 95% confidence intervals of 2077-2091.

A third way of estimating erosion from the Gay pile was to calculate meters of shoreline lost each year, using four transect lines across the pile, each at right angles to the shoreline (Fig. 3.5; Table 3.3). These measurements, derived from georegistered aerial photographs, show that the loss in meters of shoreline each year has remained nearly constant through time (Fig. 3.9b, $y = 27.86x$, $R^2 = 0.990$), i.e., around 7.9 m yr^{-1}. The four transect lines gave zero estimates between 2021 and 2050 (Table 3.3). The nearly constant loss of shoreline per year is intriguing. The nonlinear erosion of mass through time is associated with the greater water depth (and stamp sand volume per slice) occupied by stamp sands back in 1938 (5 m) relative to the lesser depth (2 m) occupied today. While the exact mechanism that produced such a nice exponential decay curve is uncertain, deeper waters along the coastline are subject to stronger currents (Keweenaw Current; [43]; [193]). Another possible contributing factor to a nonlinear mass loss recently is that the northern part of the pile is becoming better shielded behind the natural shoreline (Fig. 3.2), protecting it against the strong southerly currents during winter storms. The distance that stamp sands have moved along beaches in Grand Traverse Bay is only one-third the distance along the more energetic west coast (from Freda to Redridge, 21 km of movement;

Table 3.3
Regression equations for erosion of the Gay tailings pile (time is x, as the year, e.g., 1998). Equation variables and constants, including R^2 values, x-intercept (date of zero stamp sand mass), and 95% confidence limits for dates around the zero mass intercept are given. Nonlinear mass erosion equations are included below, whereas log10-transformed version is the last entry under linear.

				Linear				
No.	Source			Slope	R^2	x-intercept	Lower limit	Upper limit
1	Distance line 1			27.6	0.99	2021	2016	2026
2	Distance line 2			27.9	0.99	2039	2033	2046
3	Distance line 3			28.0	0.99	2044	2037	2052
4	Distance line 4			27.9	0.99	2050	2043	2059
5	Average distance			27.8	0.99	2038	2033	2046
6	Log10 of mass+1 (linear fit)			20.019	0.99	2082	2077	2091
				Nonlinear				
Equation	Source	y_0	A_1	t1	R^2	x-intercept	Lower limit	Upper limit
$y=A\_1\times e^{(-x/t1)}+y\_0$	8-byte nonlinear	21.42	6.5131016	54.01	0.99	2073	2042	2080
$y=A\_1\times e^{(-x/t1)}+y\_0$	16-byte nonlinear	21.42	7.6431016	53.82	0.99	2073	2041	2080t

whereas from Grand Traverse, the value is about 7.4 km; [95]).

Although pre-mining and mining-era bathymetry maps are rare for Grand Traverse Bay, depths and contours were obtained from a 1906 map (see Methods). Although primitive, the depth contours allowed estimates of stamp sand mass underneath the above-water volume measured by LiDAR (Fig. 3.10). Once the total volume of stamp sand along the shoreline was estimated, the amount that had eroded into the bay by 2008 was indirectly calculated, essentially by difference. Pixel calculations estimated the mean depth for the entire shoreline (pile + southern redeposited portion) as 2.94 m (SD = 1.07). For the entire shoreline (pile + southern portion), the above-water total mass was estimated from the 2008 LiDAR as 4.53 Tg, whereas the mass under the shoreline edge was estimated using the 1906 contours as 7.15 Tg, giving a total shoreline mass of 11.68 Tg. Both the 2008 above-water thickness on the Gay pile and the complete shoreline stamp sand thickness

map are shown in Fig. 3.10. Two regions of shoreline contain much larger amounts of underwater stamp sands, the Coal Dock region and a secondary region just south of the primary pile. In retrospect, the Coal Dock was constructed in one of the deepest shoreline regions, 5-7 m deep.

A final estimate from the 2008 LiDAR concerned road use of stamp sands. Starting in the 1950s, a certain amount of stamp sand was removed by the Keweenaw Road Commission from the inland side of the Gay pile, for application on roads during winter. However, given the high resolution of LiDAR and the clear gouges left on the pile by the Road Commission, we could estimate the road application loss as 1.01 Tg of the Gay pile total (4.4%). So of the 22.7 Tg originally discharged onto the pile, 11.68 Tg (51.5%) was redeposited along the shoreline, and 1.01 Tg (4.4%) was removed for road application. By difference, the remaining 10.01 Tg (44.1%) moved into Grand Traverse Bay to spread as an underwater cover (Table 3.4).

Underwater bottom features- The CHARTS LiDAR images resolved several intriguing underwater features (Fig. 3.11). Considering the combination of instrument spatial resolution and the low altitude of overflights in this project, the amount of detail in collected images was orders of magnitude higher than that obtained from routine geospatial imagery platforms. LiDAR penetrated 2.5 times deeper than natural light, to 22 m. Progressing southward from offshore of the Gay tailings pile, we found: (1) a bedrock shelf escarpment of Jacobsville Sandstone with long stamp underwater “sand dunes” parallel to

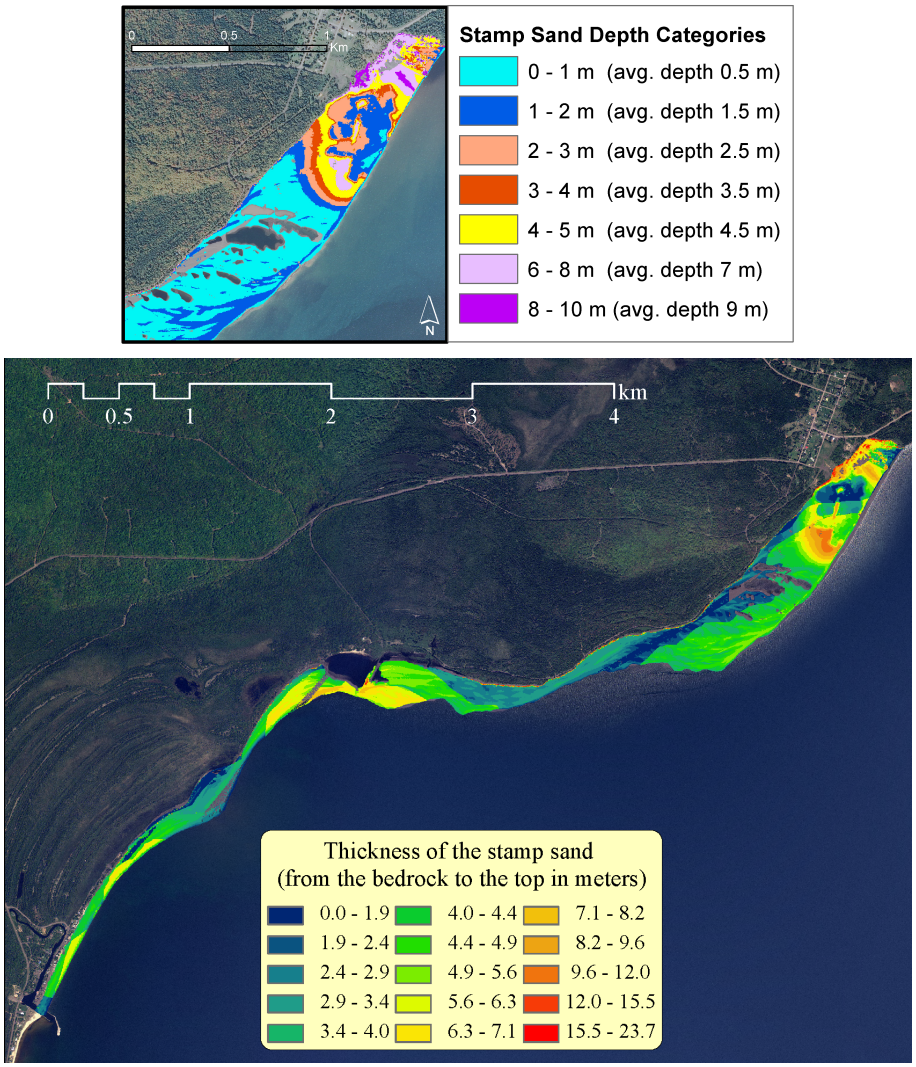

Figure 3.10: Thickness of coastal stamp sands: (a) thickness of above-water stamp sand on the main Gay tailings pile (from 2008 LiDAR); (b) total thickness (above + below water) of coastal stamp sands, bedrock to top of above-water portion (2008 LiDAR abovewater plus 1906 underwater bathymetry depth). Depths are color coded. The large gray-black objects in redeposited stamp sands south of the Gay pile are a series of ponds.

shore; (2) a submersed trough, which seemed to be an ancient riverbed, east of the Buffalo Reef region; (3) the raised promontory of bedrock and cobbles that form Buffalo Reef; and finally (4) a relatively low-gradient underwater sandy terrain south of the Traverse River that ended in a series of small comblike eastward-directed channels. Toward the north,

Table 3.4
At the time of the 2008 overflight, estimated mass of stamp sands remaining on pile, redeposited along shoreline south of original pile, and washed into Grand Traverse Bay (by difference).

Stamp sand estimate	Estimated mass	
	Tg	%
Original discharged mass (1901-1932)	22.79	100
Gay pile (total 2008)	3.07	13.5
Shoreline (above portion 2008)	4.53	19.9
Shoreline (below portion 2008)	7.15	31.4
Total shoreline (original pile+redeposited onshore 2008)	11.68	51.5
In Keweenaw Bay (difference)	10.01	44.0

immediately south of the Tobacco River, the coast seemed mostly an erosion environment, with steep bedrock scarps and migrating underwater "dunes" of stamp sands, whereas toward the south, past the Coal Dock, it seemed a depositional environment. In the southern region, the redeposited stamp sands formed recent additions onto the series of Nipissing beach ridges.

In the middle of Grand Traverse Bay, Buffalo Reef is composed of two separate rises, slightly displaced from each other (eastern promontory is shifted northward). A deep cleft (underwater canyon) runs through the structure. The displacement in the two underwater ridges suggests an old fault, subsequently eroded into a narrow canyon between the two peaks at the same time that the river channel (trough) was eroded. The erosion happened before Buffalo Reef became submersed more recently along the coast. The underwater canyon and trough suggest low water levels in Lake Superior thousands of years ago.

In Fig. 3.12, a "hill shade" technique (ArcMap 9.3, Spatial Analyst; [82]) has been

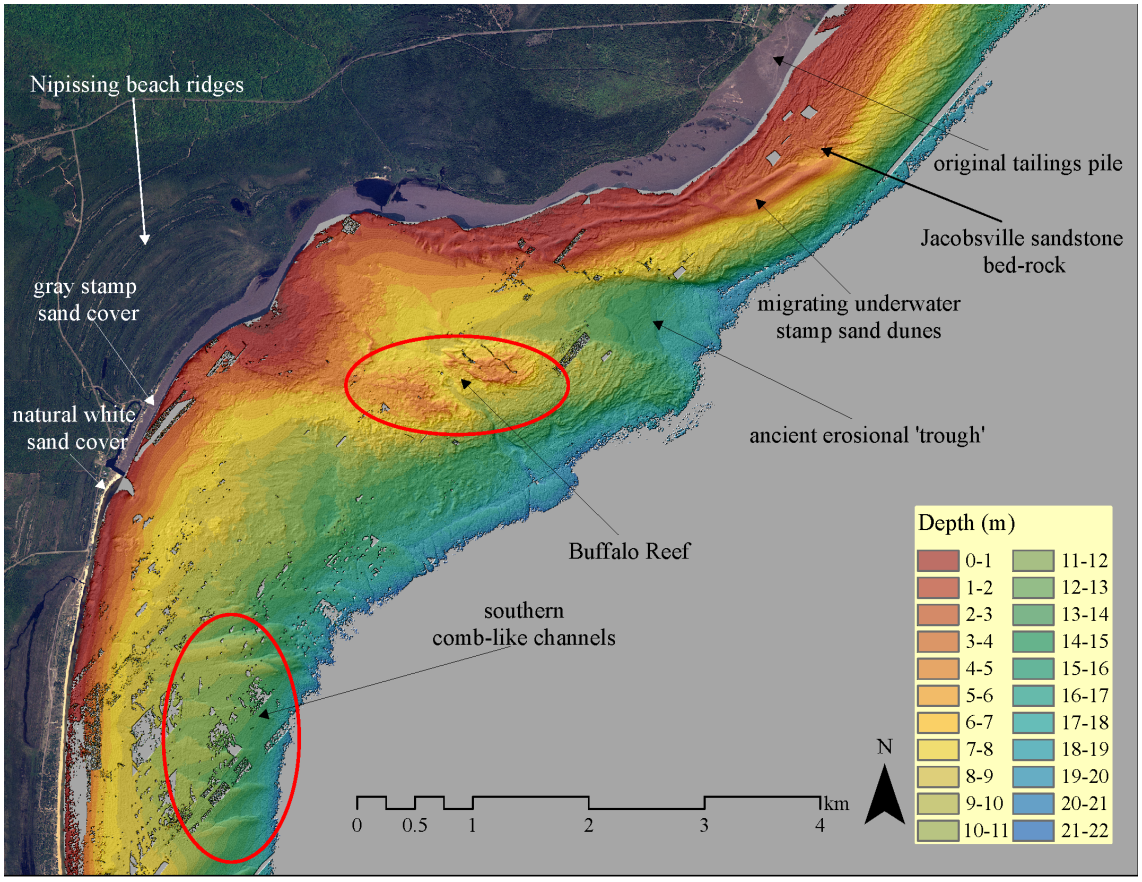

Figure 3.11: Contour-colored LiDAR bathymetry of Grand Traverse Bay juxtaposed against terrestrial aerial photo image (2005 NAIP). LiDAR reveals several prominent bottom features (Jacobsville bedrock, migrating "dunes" of stamp sand, ancient river "trough", the twin promontories of Buffalo Reef split by a cleft, and the southern "comblike" channels), whereas MSS highlights the terrestrial Nipissing beach ridges. Irregular black patches on substrate contours are no-data regions.

applied to highlight underwater benthic surfaces on the LiDAR map. There are several regions in this figure that have intriguing characteristics.The area in rectangle No. 1 reveals underwater stamp sand "dunes" migrating south- and westward. Ground-truth sampling (black dots) confirmed that these "dunes" were composed of coarse stamp sands. The "dunes" appear to stretch out until they reach the northern portion of the trough, off the Coal Dock. One could interpret the structures as ribbons of coarse sand transported

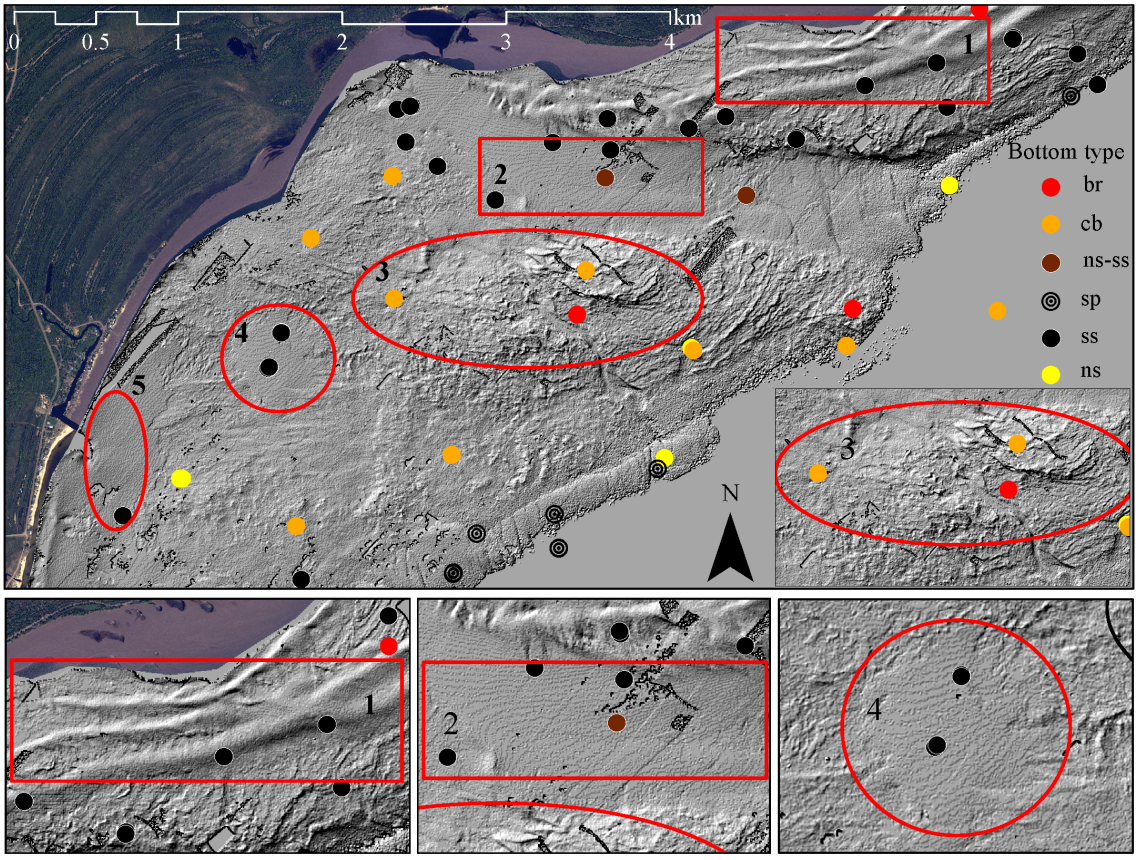

Figure 3.12: "Hill shade" technique highlights bathymetric structures. Note the funneling of underwater stamp sand "dunes" (No. 1 inset) into the upper regions of the "trough" north of Buffalo Reef. The western upper trough stretches are covered by stamp sands and appear smooth (No. 2 inset) in contrast to the lower reaches that resemble riverbed eroded Jacobsville Sandstone. On Buffalo Reef (No. 3), regions of bedrock and cobbles are evident as coarse bottom irregularities. Other topographic lows to the west of Buffalo Reef (No. 4, No. 5) also seem filled with stamp sands. Ground-truth sample sites indicate red (br, bedrock), orange (cb, cobble), deep brown (ns-ss), gray (sp, salt and pepper), black (ss, stamp sand), red yellow (ns, natural sand).

via strong wave action and powerful coastal currents across bedrock to the trough edge, where they spill over into the upper and middle reaches. The trough (rectangle No. 2) seems a 3-km-long structure, scoured to a depth of 2 m below surrounding bedrock. The lower reaches of the trough appear to be bedrock, as eroded bedding planes of Jacobsville

Sandstone cut across the surface. Recognition of the trough now explains why the Coal Dock region was anomalously deep, i.e., it coincided with the upper reaches of an old eroded river channel. It is possible that the Coal Dock effectively served as a groin during erosion of the main pile, deflecting migrating stamp sands into the upper reaches of the trough.

Buffalo Reef is elevated above the local coastal margin slope, with topographic irregularities suggesting bedrock and coarse cobble. The reef seems weathered by wave action out of Jacobsville Sandstone into a southeastwarddirected promontory. The underwater trough (Figs. 3.11, 3.12) lies to the immediate northeast. The upper reaches of the trough surface texture seem unusually smooth, suggesting stamp sand filling (rectangle No. 2). Filling was verified by Ponar sampling. At the middle of the trough, there is a mixture of stamp sand and natural sand (brown dots, Fig. 3.12). Thus, the LiDAR map suggests that nearly half of the trough's bottom is covered by stamp sand. Shipboard Ponar sampling also indicates size sorting of stamp sand and natural sand in the upper and middle reaches of the trough. Stamp sand near the shoreline is coarse grained, resembling above-water coastal sand, whereas deeper samples contain much more silt and clay. This attribute is expected from wave energy gradients, as finer material will settle in the deeper, lower-energy regions.

Toward deeper coastal regions, we find salt-and-pepper textures in top sediments (Fig. 3.12). These patterns show a sprinkling of coarse stamp sand particles on top of

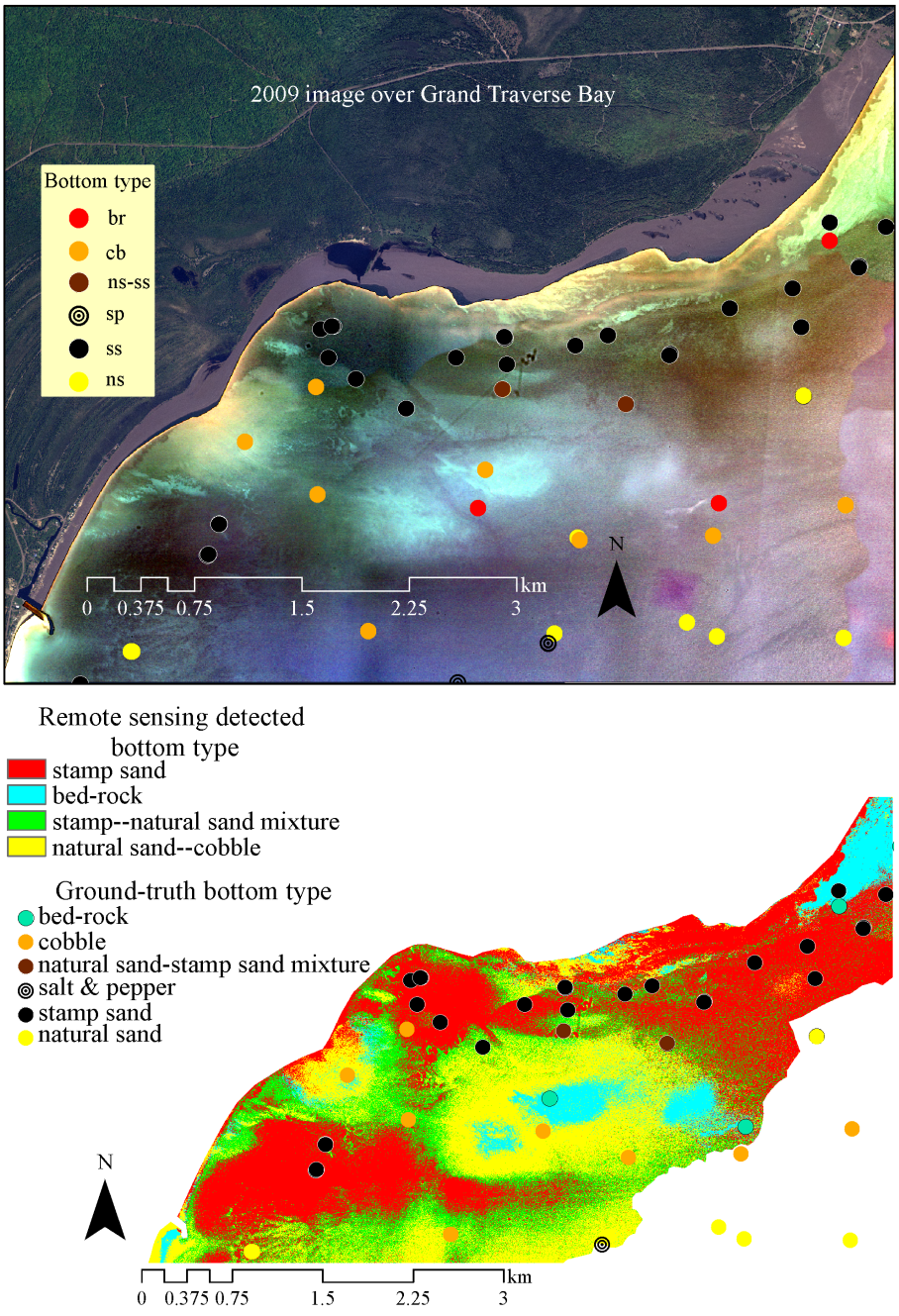

Figure 3.13: (a) A processed 3-band (2009 USDA) image of nearshore Grand Traverse Bay, and (b) the subsequent substrate classification. The 3-band image contrasts bottom coverage by high-albedo bedrock and cobble regions (blue, yellow) with low-albedo stamp sand cover (red). Ground-truth benthic ship samples are color-coded circles (bedrock, cobble, natural sand mixed with stamp sands, salt and pepper, stamp sand, natural sand).

fine deep-water brown silt and clay mud. The patterns could arise if winter ice carried coarse stamp sands from beaches into deeper waters, where melting released the particles to sprinkle upon the typical finer lake silt-clay sediments. Stamp sand particles increase in top sediments, a pattern expected if the stamp sand source is getting closer, as stamp sands migrate down the coast.

MSS classification: stamp sand moves into trough and threatens Buffalo Reef- An analysis of substrate spectra (Fig. 3.3a,b) reveals that the stamp sands are visibly darker than most of the materials against which they would be juxtaposed in nature. Moreover, significant differences exist between stamp sands and background materials in the high ends of the green portion of the spectrum and especially into the red portion of the spectrum.

Buffalo Reef margins include cobble-covered outlying regions that lead to a Jacobsville Sandstone bedrock promontory of $\sim$ 3.1 km^2, divided by the steep crevice. High-resolution LiDAR showed that the reef has two lobes, a 2.0-km^2 plus a smaller 1.1-km^2 region. North of Buffalo Reef there is an underwater promontory that may also have helped divert stamp sands southward into the trough. Along the promontory, however, there is a low depression where migrating stamp sands may have broken through and moved westward. In polygons No. 4 and No. 5 (Fig. 3.12), there are closed depressions filled with coarse stamp sand (black dots, sediment sampling sites).

We used a 3-band aerial photo image from a 2009 USDA NAIP overflight to map

underwater substrates see Methods). Figure 3.13 illustrates the depth-compensated color image and the subsequently derived substrate classification map. In the depth-compensated ([119]) image, stamp sands stretch as irregular patches along the shoreline and in front of, and behind, Buffalo Reef (Fig. 3.13a). Migrating underwater stamp sand dunes show up as orange ribbons parallel to the shoreline, below the Gay pile and western redeposited stretch. Around the Coal Dock, the ribbons spread out to intercept the trough north of Buffalo Reef. Figures 3.11, 3.12 also revealed the slight northern ridge that may have deflected westward migrating sands into the trough and through a low-lying ridge. Indeed, low-gradient "flat" bottom can be seen in Fig. 3.12 (insets No. 4, No. 5), where ground-truth stations confirm stamp sand. In the image, there are also reaches of exposed Jacobsville Sandstone bedrock below the Gay pile, and cobble and bedrock stretching out around Buffalo Reef (Fig. 3.12).

Buffalo Reef is a productive spawning area for whitefish (*Coregonus clupeaformis*) and lake trout (*Salvelinus namaycush*) potentially threatened by movement of stamp sands ([44]). Transgression of moving stamp sands into cobble fields that surround Buffalo Reef is not conducive to normal hatching of fish eggs, for the sands may fill crevices or may be toxic for eggs or newly hatched larvae ([44]). An enlargement of the trough illustrates relatively smooth sands extending down halfway along the slope, forming small ripples along the surface (Fig. 3.12; inset No. 2). Below the halfway point, there are bedding features of Jacobsville Sandstone that suggest eroded hard rock substrates. Based on our substrate map, tribal concerns are fully justified, as stamp sand appears to have encircled three-fourths of Buffalo Reef (Fig. 3.13b).

3.5 Conclusion

Evaluation of LiDAR and MSS data- One aim of this study was to evaluate the effectiveness of the airborne CHARTS sensor system for generating environmentally useful information for coastal zones of large lakes. Working with aerial photography, the above-water LiDAR mapping allowed us to reconstruct erosion of the original tailings pile and to quantify the fate of migrating stamp sand. Bathymetric LiDAR maps (Figs. 3.11, 3.12) revealed intriguing geomorphic structures and processes occurring along the coastal shelf, e.g., ancient riverbeds and fault scarps. LiDAR bottom reflectance also provided singleband information on irregular to smooth bottom types (wave-form measure of "rugosity", not discussed here). The substrate classification corresponded closely with independent sonar and underwater video substrate maps done by NWRI ([23]). However, for the first time, the extent of stamp sand underwater cover could be determined.

The CASI 1500 is a hyperspectral scanner that was used here in a multispectral mode (MSS 8-band; i.e., broadband). Justification for this approach is evident in the ASD hyperspectral reflectance measurements of retrieved submersed sediments (Fig. 3.3a,b). Signatures of above- and below-water sediments exhibited broad spectral differences without the distinct spectral peaks commonly evident in terrestrial vegetation studies. The broad spectral bands used further served to provide more integrated energy in the measured signal, increasing the signal-to-noise ratio and likely achieving greater depth penetration.

Bottom classifications resulting from MSS, CASI, and bathymetric LiDAR showed good agreement with submersed sediment samples retrieved as part of the ground-truth effort. We must note, however, that some spatial difficulties were encountered immediately off the mouths of the Tobacco and Traverse waters, where exiting humic-stained waters created false-bottom readings.

We also need to point out that an airborne scanner imaging system does not represent an instantaneous or synoptic view of the overflight area. The sensor may take hours, or even days, to fly the adjoining flight lines. Different tracts along the scan line will have different bidirectional reflectance angles relative to the sun, resulting in sun glint commonly occurring in certain parts of the scan. Over the time of the overflight, cloud and wind (sea state) conditions may change and water level may also change (in seiche or tidally influenced areas). These artifacts require significant effort to remove and correct. This study also incorporated a significant level of ground- truth data collection to characterize bottom and water column optical properties. One could ask if the extra effort is worthwhile relative to truly synoptic imagery obtainable from satellites. The answer probably is investigation specific, whether enhanced detail is necessary to reveal important properties or to allow precise calculations.

Ecosystem effects- This study revealed that the time course of events associated with unmitigated legacy mining caused progressive environmental effects that continued for over a century and to this day. As wave erosion of the original pile proceeded, the coarse fraction

was moved from the original 0.9-km^2 deposition cone southward as a sorted black sand lens to cover an estimated 1.3 km^2 of white Jacobsville Sandstone beach sands ([185]) and to spread over 5.1 km^2 of bay bottom sediments. Our estimate of 1.3-km2 shoreline beach stamp sands is less than the 2.3-km^2 estimate of Rasmussen et al. ([157]) because the latter calculation used the discredited geographic coordinate reference system for area measurements. So over the 110 yr since discharge, the total surface area of shoreline covered by stamp sands increased 178% (original pile now 0.3 km^2, beach sands 1.3 km^2 = 1.6 km^2), whereas the underwater surface area of bay bottom sediments covered by submersed sands increased 567%. Stamp sands have now moved 7.4-8.1 km south from Gay, extending to the northern seawall of the Traverse River, where they affect the beachfront community.

Ecosystem effects are not restricted to wave-propagated movement of the coarse fraction (stamp sands). In winter, drifting pack ice may incorporate coastal stamp sands and accelerate movement of stamp sand constituents along beaches or across the shelf ([34]). Sediment trap studies of dispersing "slime clay" fractions from the Freda-Redridge stamp sands, off the western coast of the Keweenaw Peninsula, found copper (Cu) concentrations between 50 and 2,000 μg g^{-1} with elevated Cu concentrations (100-340 μg g^{-1}) 20-80 km down-current from the discharge site ([178]). Serious dispersal is also occurring in Keweenaw Bay, as stamp sands move along the beach. Clay-sized particles winnow out of the original tailings pile or from ground-up sands, and disperse widely across bay waters. The clay-sized particles move southward via long-shore currents, ending up in

deep-water Keweenaw sediments and in the mid-bay Keweenaw Trough. The enhanced Cu concentrations appear in sediment core profiles (Fig. 3.1; [90], [89]; [68]). The long-distance movement of the slime clay fraction explains high correlations between mining-associated metals (Cu, Ag, Hg) in Keweenaw deep-water sediment profiles ([89]). A deep-water NOAA sediment core kilometers off Gay recorded buried maxima over 330 μg g^{-1}, relaxing back to 220 μg g^{-1} in surface strata ([90]), both above state probable effects concentration levels (149 μg g^{-1}).

Potential environmental effects of stamp sands in Grand Traverse Bay are expected to be high. Previous knowledge is available on the elemental composition and toxicity of stamp sands. In stamp sands, Cu occurs at toxic levels for aquatic systems and there is a secondary suite of metals (Ag, As, Cd, Co, Cr, Hg, Mn, Ni, Pb, Zn) that often flag aquatic protection levels ([123]; [130]; [95]). Stamp sand concentrations of Cu are high, averaging 10 to 100 times greater than other regional source materials or natural sediments, with elevated Cu:Zn ratios ([91]; [84]). Slime clay fractions (< 1 μm) also tend to be enriched in metals (Cu 2.83x, Zn 3.43x, As 1.33x) above coarse fractions, due to higher surface : volume ratios plus an absorbing rime of Fe and Mg ([91]).

Our estimates of stamp sands discharged into Keweenaw Bay from three major mills (Mass, Mohawk, Wolverine; Table 3.1) are 25.8 Tg. Stamp sands from Gay have been characterized by several methods, including atomic absorption ([85]); neutron activation ([91]), and inductively coupled plasma mass spectrometry ([130], [95]). Early studies of Cu

concentrations in Gay coarse stamp sand found values ranging between 1620 and 5486 μg g^{-1} (mean 2697 μg g^{-1}, n = 7; [92], [95]), whereas more recent sampling studies by the Michigan Department of Environmental Quality (MDEQ) on the Gay tailings pile found Cu concentrations 1500-13,000 μg g^{-1} (mean 2863 μg g^{-1}; n = 274) and only slightly lower, 710-5300 μg g^{-1} (mean = 1443 μg g^{-1}; n = 24) for the southern redeposited beach sands ([130]). Metals in the secondary suite at the main Gay pile averaged concentrations of Ag 0.4-7.7 μg g^{-1} (mean 1.8), As 1.0-15.5 μg g^{-1} (mean 1.5), Cr 18-52 μg g^{-1} (mean 28.8), Co 16-36 μg g^{-1} (mean 22.9), Hg 0.06-0.11 μg g^{-1} (mean 0.027), Ni 20-48 μg g^{-1} (mean 31), Pb 5.1-6.1 μg g^{-1} (mean 2.6), and Zn 48-120 μg g^{-1} (mean 74.7; [130]). If the average concentration of copper in tailings is 2860 μg g^{-1}, the discharges released about 74 x 103 kg of copper into Keweenaw Bay. At the current erosion rate (0.069 Tg in year 2008), this corresponds to 198 x 103 kg Cu yr^{-1} loading from just the main pile.

Toxicity of stamp sand environments- In 2003, MDEQ obtained 274 soil samples and 10 groundwater samples from the main ("northern") pile and 24 surface soil samples from redeposited stamp sand piles south of the main pile ("southern site"; [130]). At the northern site, the following number of samples exceeded Groundwater Surface Water Interface Criteria (GSWIC) levels. In the 274 soil samples: aluminum 271, chromium 265, cobalt 271, copper 274, manganese 159, nickel 168, silver 216, and zinc 242. In the 10 groundwater samples, the number exceeding the GSWIC risk criteria levels: chromium 5, copper 10, manganese 5, nickel 8, silver 8, and zinc 8. The following 24 surface soil samples exceeded GSWIC levels at the southern site: aluminum 20, chromium 19, cobalt

24, copper 24, manganese 7, nickel 8, silver 9, and zinc 10.

Groundwater seepage through coastal stamp sands is another concern. The reworked beach stamp sands created numerous shallow coastal ponds south of the primary tailings pile (Figs. 3.2,3.8). At Gay, groundwater samples from stamp piles contained Cu concentrations of 670 μg L^{-1} ([85]) and 250-22,000 μg L^{-1} ([130]). Dissolved Cu concentrations in pond waters ranged between 10 and 2400 μg L^{-1} ([85]; [118]). Pond waters were found to be toxic to most aquatic organisms ([90]; [118]). Native *Daphnia pulex* suspended in Gay stamp sand pools survived only 2-12 d, depending upon local dissolved Cu concentrations. That *Daphnia* would die rapidly is not surprising because toxicity thresholds (LC50) for freshwater organisms usually lie between 25 and 600 μg L^{-1} (ppb) dissolved Cu. Native *D. pulex* were found sensitive to Cu concentrations above 12 μg L^{-1}, i.e., far below existing concentrations in pools ([118]).

Considerable evidence is also available on copper in sediments contaminated with stamp sands. MDEQ ([130]) samples offshore of the Gay stamp sands found copper concentrations in bay sediments varying between 1400 to 4400 μg g^{-1} (mean 3020 μg g^{-1}, n 5 5). The latter value is very close to pure stamp sands, suggesting little admixture with Tobacco River or Traverse River sediments. Submersed regions immediately around nearshore stamp sand piles on the Keweenaw Peninsula are generally characterized by reduced diversity of benthic macroinvertebrates ([102]; [103]). Freshly worked stamp sand and lake sediments are toxic to *Daphnia* and mayflies (*Hexagenia*) because they release Cu

across the pore-water gradient ([123]). Additional laboratory toxicity experiments with slime-clay-rich lake sediments from the Keweenaw Waterway and Torch Lake showed that solid-phase sediments and aqueous fractions (e.g., interstitial water) associated with the slime-clay sediments were lethal to several taxa of freshwater macroinvertebrates: chironomids (*Chironomus tentans*), oligochaetes (*Lumbriculus variegates*), amphipods (*Hyalella azteca*), and cladocerans (*Ceriodaphnia dubia*). Moreover, the observed toxicity was due to copper, as opposed to other metals (principally zinc and lead) present in the sediments ([162]; [185]). However, toxicity to benthic organisms was not predictable based solely on total copper concentrations in the sediments, but appeared related to bio-available copper, the fraction freely dissolved in the sediment interstitial water ([9]).

Threat to Buffalo Reef and rivers- Buffalo Reef is recognized in the Atlas of the Spawning and Nursery Areas of the Great Lakes, Volume 2 ([70]). The Great Lakes Indian Fish and Wildlife Commission (GLIFWC) conducted fisheries assessments on the reef between 1986 and 2002, documenting that it is an important spawning reef for whitefish and lake trout ([44]). Stamp sand movement is of concern to the Keweenaw Bay tribal council, as tribal members maintain a commercial whitefish and lake trout fishery in Keweenaw Bay. Harvest of these fish is an important cultural and economic activity, as GLIFWC helps tribal members promote and market the health benefits of traditional foods ([128]). Impairment of reef habitat could lead to a decline in important fish species, infringement upon federally guaranteed treaty reserved rights, and negatively affect the health of the tribal population that consumes these resources. NWRI Shipek grab samples and our Ponar samples in

the area immediately north of Buffalo Reef showed the area to have some stamp sands, raising immediate concerns for fish spawning ([23]; this investigation). Along the coastline, another concern about shoreline dispersal of stamp sands is interference with migration of fish up streams or rivers for spawning (e.g., rainbow smelt [*Osmerus mordax*], white sucker [*Catostomus commersoni*], rainbow trout "steelhead" [*Oncorhynchus mykiss*]) or impairment of stream or river mouth habitats.

Global concerns about coastal tailings discharges- Between 1850 and 1968, copper ore processing on the Keweenaw Peninsula discharged around 360 Tg of stamp sand tailings along shorelines, connecting waterways, and into interior lakes and rivers ([90]). As mentioned earlier, the Grand Traverse discharges were of such magnitude that they literally changed the shoreline. Ecosystem effects are pervasive, as tailings have now spread along half the above-water beach and $<$ 22-m below-water benthic environments of the bay. Another well-documented Great Lakes case that affected Lake Superior sediments involved discharge of taconite (iron) tailings north of Duluth, Minnesota. Taconite plants mix iron ore with clay, producing a pellet suited for blast furnaces. Most operating mines on the U.S. and Canadian sides are inland, with tailings piles located near open-pit excavations. However, between 1955 and 1980, 500 Mt of taconite tailings were sluiced into Silver Bay, Minnesota. Iron-rich sediments moved into the Duluth Basin, beyond the confines of the 23.3-km^2 permitted dumping site. Small asbestiform particles (cummingtonite) from the discharge subsequently spread along the coast down to the Duluth water intake site and over three western basins of Lake Superior (Duluth, Chefswet, and Thunder Bay Basins).

The affected area eventually extended over 100 km from the original discharge site ([51]; Cook et al. unpubl.). The Clean Water Act of the U.S. and Canada now bans coastal mining discharges. However, lingering effects come from tailings pond failures. At Elliot Lake uranium mining operations, $>$ 30 tailings pond failures were recorded, prompting the International Joint Commission to describe the drainage system as a major source of radium contamination in the Great Lakes ([190]).

Yet what we discuss here are not historic curiosities confined to the Great Lakes, but rather examples of a substantial problem present around the world. There are numerous cases of past and present mine disposal into freshwater and marine coastal environments (i.e., several examples are listed in Table 3.5). Coastal disposal sites are widely spread across North America (Canada, U.S.A.), South America (El Salvador, Chile), Northern Europe (Norway, Britain), Mediterranean (Spain, Turkey), Africa, Indonesia, Papua New Guinea, Philippines, and Melanesia (Toga). Despite great expressed concern ([126]; [135]), marine coastal deposition continues to be advocated in recent mining methods bulletins ([50]; [60]; [191]).

Table 3.5
Mine tailings discharges into coastal environments around the world. Site location, dominant geological mineral property, and publication sources are listed.

Location	Tailings	Years	Dominant metal or mineral	Source
Freda-Redridge, Keweenaw Peninsula, Michigan, U.S.A.	39.2 Tg	1901-1947	Copper	Kerfoot et al. 2009
Gay, Keweenaw Peninsula, Michigan, U.S.A.	22.5 Tg	1901-1932	Copper	Kerfoot et al. 2009
Silver Bay, Minnesota, U.S.A.	500 Tg	1955-1980	Iron	Cook et al. 1974
Rupert Inlet, British Columbia, Canada	353 Tg	1971-1995	Copper	Burd 2002
Britannia Beach, Howe Sound, north of Vancouver, British Columbia, Canada	44 Tg	1904-1974	Copper, zinc	Chretien 1997
Ensenada Chapaco Bay, north-central Chile	2,612,103 kg d^{-1}	1978-1994	Iron tailings (pelletization)	Lancellotti and Stotz 2004
Chanaral Bay, Atacama Region, Chile	150 Tg	1938-1974	Copper, arsenic	Castilla and Nealler 1978; Andrade et al. 2006
Qaumaujuk and Agfardlikavsa Fjords, Greenland	11.8 Tg	1973-1990	Lead, zinc, silver	Asmund et al. 1994
Rize, Black Sea, Turkey	2,880,103 kg d^{-1}	1994-2000	Copper, arsenic, lead	Berkun 2005
Chameis Bay, Namibia, Africa	366 Tg	1970-2006	Diamonds	Smith 2006
Elizabeth Bay, Namibia, Africa	7 Tg	1991-1998	Diamonds	Smith et al. 2002
Calancan Bay, Marinduque Island, Luzon, Philippines	200 Tg	1975-1991	Copper	Marges et al. 2011
Buyat Bay, North Sulawesi, Indonesia	1,841,103 kg d^{-1}	1996-present	Gold	Edinger et al. 2008
Toga, Melanesia, Western Pacific	2.5 Tg yr21	1990s	Phosphate; Cd, Pb, Cu in tailings	Gnandi

The incentive for discharging into rivers, embayments, or the ocean goes beyond the old-school engineering "dilution is the solution". Advocacy utilizes the following arguments. On-land tailings disposal generally involves the construction of a dam in stream drainage, or an enclosure on gently sloping terrain, that is used to impound tailings. These containment structures are often the largest surface feature of a mine, flooding hundreds of hectares, and adversely affecting the terrestrial environment. Moreover, tailings impoundments are usually left in place after mining has ceased and require perpetual inspection and maintenance. These impoundments are prone to severe climatic and seismic events, leading to unexpected catastrophic failure and widespread environmental "catastrophes" (e.g., "Aznalcollar Disaster", Guadalquivir Estuary, Spain [[72]]; "Marcopper Mining Disaster", Calancan Bay, Marinduque Island, Philippines [[124]]). Along the Mediterranean coast, there are $>$ 230 tailings dams in the Spanish province of Almería alone, dating back to Roman times ([126]). As an alternative, mining documents suggest that tailings discharged along coastal margins have minimal terrestrial effects and disappear underwater, moving "out of sight, out of mind". Our point is that, unattended, they will move across large regions of bays, greatly expanding environmental effects beyond the area of the original tailings deposition.

Given the global incidence of coastal mine discharges, and concern over how long these effects will play out over extended time periods, one can easily envision how combined LiDAR and MSS or hyperspectral coastal imaging provides valuable information regarding the spread of past mining discharges along shallow stretches of coastal shorelines

and ecosystem effects. The ability to discriminate between sediment types has equal value in studies of coastal tailings impoundment failures. However, if the discharges are placed, or move, into waters > 22-35 m, beyond reflectance limits, then alternative tracking methods must be employed. Concerns about stamp sand migration from the Gay pile, aided by preliminary LiDAR and MSS imagery, spurred the United States Army Corps of Engineers Detroit District Office, in February 2011, to approve a US$8-9 million dollar Keweenaw Stamp Sands Ecosystem Restoration Plan for Grand Traverse Bay.

3.6 Acknowledgments

The LiDAR project was a collaborative effort between Bruce Sabol and Mark Graves at the Engineer Research and Development Center-Environmental Laboratory (ERDC-EL, Vicksburg, Mississippi), the Joint Airborne LiDAR Bathymetry Technical Center of Expertise (JALBTCX, Kiln, Mississippi), Detroit District Corps of Engineers, faculty and students from Biological Sciences, Chemistry, and Geological Engineering, Mining and Sciences at Michigan Technological University (Michigan Tech, Houghton, Michigan), and research scientists at Michigan Technological Research Center (MTRI; Ann Arbor, Michigan). Primary funding came from the Army Corps of Engineers ERDC-EL laboratory and was provided by the System Wide WaterResources Program (Steve Ashby, program manager) at Vicksburg. Efforts were also aided by a National Science Foundation, Ocean Sciences 97-12872 grant to W.C.K., and a U.S. Environmental Protection Agency Region

V Grant to the Baraga Tribal Council passed through to W.C.K. Support for the Compact Hydrographic Airborne Rapid Total Survey (CHARTS) flight and initial data processing was provided by the Corps National Coastal Mapping Program managed by Jennifer Wozencraft at the JALBTCX Center. We also thank Mike Donofrio, Mike Sladewski, Esteban Chiriboga, and especially J. Biberhofer for sharing details of the National Water Research Institute and Great Lakes Indian Fish and Wildlife Commission sonar mapping and sediment sampling efforts in Grand Traverse Bay. Lucille Zelazny aided preparation of figures, and Jamey Anderson sieved stamp sand samples.

Chapter 4

Using LiDAR to reconstruct the history of a coastal environment influenced by legacy mining[1]

Foad Yousef[a], **W. Charles Kerfoot**[a,*], **Colin N. Brooks**[b], **Robert Shuchman**[b,c], **Bruce Sabol**[d], and **Mark Gravese**[d]

[a]Lake Superior Ecosystems Research Center and Department of Biological Sciences, Michigan Technological University, Houghton, MI 49931, USA

[b]Michigan Tech Research Institute, Michigan Technological University, Ann Arbor, MI, 48105 USA

[c]Department of Geological and Mining Engineering and Sciences, Michigan Technological University, Houghton, MI 49931, USA

[d]U.S. Army Engineer Research and Development Center (ERDC-Environmental Laboratory), Vicksburg, MS 39180, USA

[*]Corresponding author: wkerfoot@mtu.edu

Index words: remote sensing, LiDAR, coastal erosion, tailing piles, Nipissing dunes, Lake Superior

Running head: LiDAR Lake in Superior

E-mail addresses: fyousef@mtu.edu (F. Yousef), wkerfoot@mtu.edu (W.C. Kerfoot), cnbrooks@mtu.edu (C.N. Brooks), shuckman@mtu.edu (R. Shuchman), Bruce.M.Sabol@usace.army.mil (B. Sabol), Mark.R.Graves@usace.army.mil (M. Graves)

[1]The material contained in this chapter was previously published in *Journal of Great Lakes Research* 2013, doi = 10.1016/j.jglr.2013.01.003

4.1 Abstract

LiDAR (Light Detection and Ranging) data can be used to create fine scale digital elevation and bathymetric models (DEMs). Here we examine natural coastal erosion in Grand Traverse Bay, Michigan, a part of Keweenaw Bay in Lake Superior, and discuss how a variety of geological features (submersed river bed and channels associated with the Houghton Low; Nipissing dunes) interact with long-term sediment accumulation patterns. The geological features also modify migrating tailings from a legacy mining site. The combination of LiDAR derived images and aerial photographs allowed us to reconstruct the historical movement of tailings along the coastline. A total of 22.8 million metric tons (Mt) of stamp sand were discharged into the coastal environment off Gay, MI. Over a span of 80 years, beaches to the southwest of Gay have progressively received 7.0 Mt (30.7%) of the mass eroded from the original pile, whereas 11.1 Mt (48.7%) have moved into the bay. The total amount accumulated along the beaches now greatly exceeds the mass remaining on the original tailings pile (3.7 Mt; 16.2%). Bathymetric differences between two LiDAR surveys (2008 and 2010) were also used to estimate the mass, and to track the movement of migrating underwater stamp sand bars. These bars are moving southwesterly towards Buffalo Reef, creating a threat to the lake trout and lake whitefish breeding ground.

4.2 Introduction

Airborne LiDAR Bathymetry (ALB) or airborne light detection and ranging (LiDAR) is a remote sensing technique for measuring water depths with an airborne scanning pulsed laser beam ([73]). The technique is well suited to nearshore mapping in clear water because it provides the three-dimensional data needed to create a digital terrain model with $\pm$10 - 50 centimeters (cm) vertical accuracy for topographic and bathymetric mapping ([81]). Compared with passive remote sensing systems (e.g. aerial photos, Landsat), which are quite limited with respect to the depth to which they can measure, active LiDAR technology can penetrate up to three times Secchi depth, i.e. considerably beyond passive light penetration. Modern LiDAR systems reach up to a maximum of 50 meters (m) in very clear, marine water, and between 20-35 m in clear coastal waters ([67]). Commercial topographic LiDAR systems operate at a pulse repetition frequency of at least 20,000 Hz and a footprint diameter of 15-20 cm. A topographic LiDAR operating in the infrared (IR) band can image the water surface, but cannot penetrate it. An ALB system, however, operates at a lower pulse-repetition frequency than the topographic LiDAR [up to 3000 hertz (Hz)], with a footprint diameter of 2 m (Table 4.1). In the CHARTS ALB system used here (Table 4.1), the LiDAR sensor records the time difference between two signals (an infrared wavelength that reflects off the lake surface, and a green water-penetrating wavelength that returns from the bottom sediments) to derive measurements of water depth. As opposed to SHOALS (Scanning Hydrographic Operational Airborne LiDAR Survey), CHARTS

(Compact Hydrographic Airborne Rapid Total Survey), and LADS (Laser Airborne Depth Sounder) sensors, the newer USGS EAARL (Experimental Advanced Airborne Research LiDAR) and CZMIL (Coastal Zone Mapping and Imaging LiDAR) bathymetric LiDARs do not utilize an infrared band (Table 4.1).

Table 4.1
Characteristics of typical topographical and bathymetrical LiDAR sensors and Lake Superior water level information for June of 2008 and July of 2010.

	Beam Frequency (nm)	Pulse repetition (kHz)	Pixel size (m)	Vertical accuracy (m)	Horizontal accuracy (m)	Lake Superior water level (m)
Topographic LiDAR	1064	20	0.15-0.20	$\pm$0.10-0.50	$\pm$0.6-5	
Bathymetric LiDAR	532	3	$\sim$2	$\pm$0.10-0.50	$\pm$0.6-5	
2008 LiDAR	1064 (IR)	9	2	$\pm$0.30	$\pm$3	183.4
Topo/Bathy	532 (green)	1	2	$\pm$0.30	$\pm$3	
2010 LiDAR	1064 (IR)	1	2	$\pm$0.30	$\pm$3	183.2
Topo/Bathy	532 (green)	1	2	$\pm$0.30	$\pm$3	

During coastal surveys using CHARTS, the aircraft travels over water at about 60 m per second, pulsing two varying laser beams toward earth through an opening in the plane's fuselage. The first wavelength (green) is intended for lakebed detection because of its water penetration ability, whereas the second wavelength (infrared) allows sensing of the water surface, which behaves as a near opaque surface at this wavelength (4.1). The LiDAR sensor records the time difference between the two signals to derive measurements of water depth. Today, airborne LiDAR bathymetry and topographic LiDAR are used as standard tools for coastal mapping around the globe. Flood maps, shoreline mapping, monitoring of coastal erosion, and habitat protection are only a few of the applications ([73]; [151]). Marine applications of blue-green laser techniques to mapping underwater structures include: 1) mapping of coral reefs relative to fish assemblages ([182]); 2) coral reef extent and structure ([189]; [30]), 3) characterization of Atlantic barrier islands ([145]), 4) studies of Gulf of Mexico estuaries ([29]; [145]), 5) quantification of hurricane effects ([192]), and 6) studies of sea turtle nesting on beaches ([176]). Freshwater applications include surveys of erosion patterns along braided streams ([27]; [99]), Great Lakes coastal erosion ([98]), and evidence for ancient lakes ([121]). Here we use a combination of aerial photography and LiDAR derived images to uncover historical events that influenced Great Lakes coastal environments and investigate how these historical features interact with recent anthropogenic events (tailings pile erosion).

The investigation deals with historic features along Grand Traverse Bay (also locally termed "Big" Traverse Bay), a small coastal portion of Keweenaw Bay, Lake Superior (Fig.

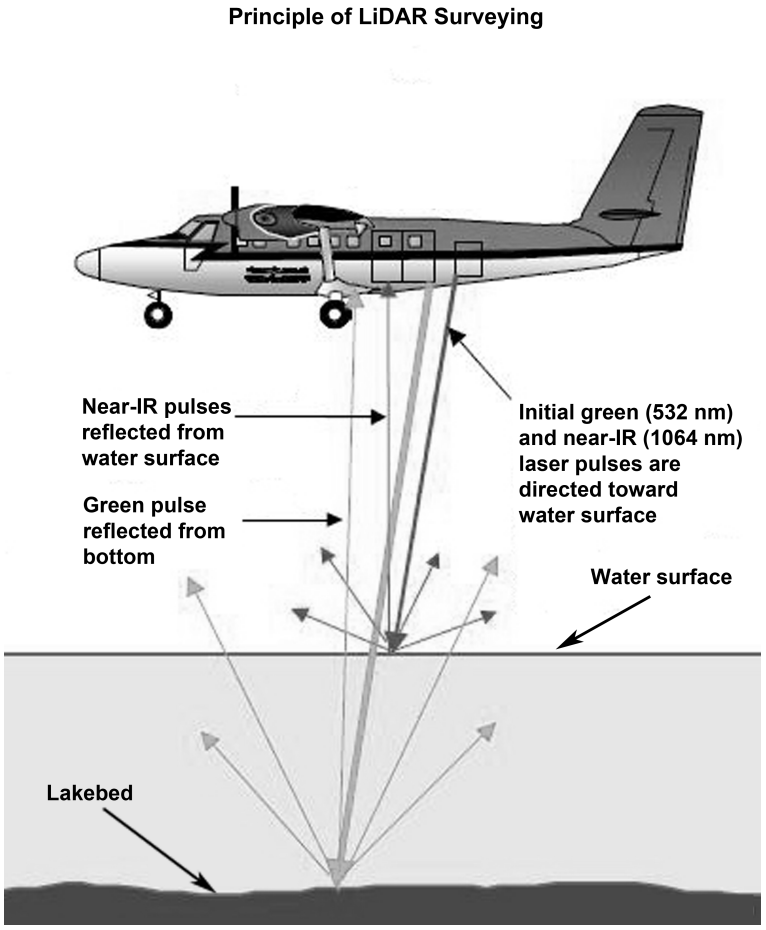

Figure 4.1: Data recording during an overflight of the bathymetric LiDAR system (modified from LaRocque and West 1990).

4.2). Several of the features mark geologic events that are thousands of years old, yet they still influence sedimentation patterns. Other perturbations are much more recent. Severe anthropogenic disturbances to the Keweenaw Peninsula took place within the past 160 years. Between 1850-1929, the Keweenaw mining district was the second largest producer of copper in the world, largely from native copper ([139]; [18]). Native copper came from two principle kinds of ore in the Portage Lake Volcanic Series: basalt lava flows (amygdule deposits) and inter-bedded sediments (conglomerates). The ore was crushed with early

gravity and later giant steam-driven stamps to release the native copper and silver ([33]; [19]). Over 140 mines worked the central deposits and over 40 mills processed stamp rock ([90]). Smelters produced 4.4 million metric tonnes (Mt) of copper, whereas stamp mills sluiced around 360 Mt of copper-rich stamp tailings into rivers and waterways, including 64 Mt directly onto Lake Superior shorelines and 25 Mt into Keweenaw Bay ([96], [95], [98]; [101]). Along the 8.5 km stretch of Grand Traverse Bay in Keweenaw Bay, two stamp mills at Gay (Mohawk and Wolverine Mills) discharged a total of 22.7 Mt of stamp sand onto a single pile (Fig. 4.2; [98]).

Stamp sands discharged off Gay have dispersed as 'black sand' beach deposits between the original tailings pile and the Traverse River (Fig. 4.2). One of the major concerns in this region is the intrusion of stamp sands around and onto Buffalo Reef, located off the Coal Dock location in mid-bay. Buffalo Reef is an important lake trout and whitefish spawning ground [Great Lakes Indian Fish and Wildlife Commission (GLIFWC), [45]]. Impairment of reef habitat could lead to a decline in important fish species, infringement upon federally guaranteed treaty reserved rights, and a health impact on the tribal and non-tribal population that consumes these resources.

Here we use a combination of aerial photography and LiDAR derived images to measure how post-Pleistocene erosion features interact with migrating stamp sands to threaten Buffalo Reef and the natural beach stretches on Grand Traverse Bay. With LiDAR technology, we discovered new post-Pleistocene underwater features that contribute to, and

help direct, natural sediment transport. We estimated several historical erosion rates related to stamp sand mass, namely movements and region-specific erosion/accretion patterns that are superimposed upon natural sedimentation patterns in the bay. Relative to stamp sand dispersion, we wanted to quantify: 1) where and how fast the original tailings pile was eroding, 2) how much stamp sand was being deposited along shoreline stretches (original tailings pile to Traverse River), and 3) how erosion or accretion dynamics were different in various parts of the coastal region.

In terms of technological advances, we also wanted to know if coastal LiDAR data could be used to indirectly or directly estimate the mass of stamp sand that is migrating underwater in the bay? Moreover, where there are underwater masses, are there also indications of recent movement? Underwater movement bears on issues related to toxic effects of stamp sands on benthic organisms ([102]; [103]) and encroachment onto Buffalo Reef ([23]; [98]). Are there techniques that provide more direct and precise estimates of these movements? In a broader context, to what degree can the complimentary use of aerial photography and LiDAR expand studies of beach erosion relative to mine tailing restoration and remediation efforts?

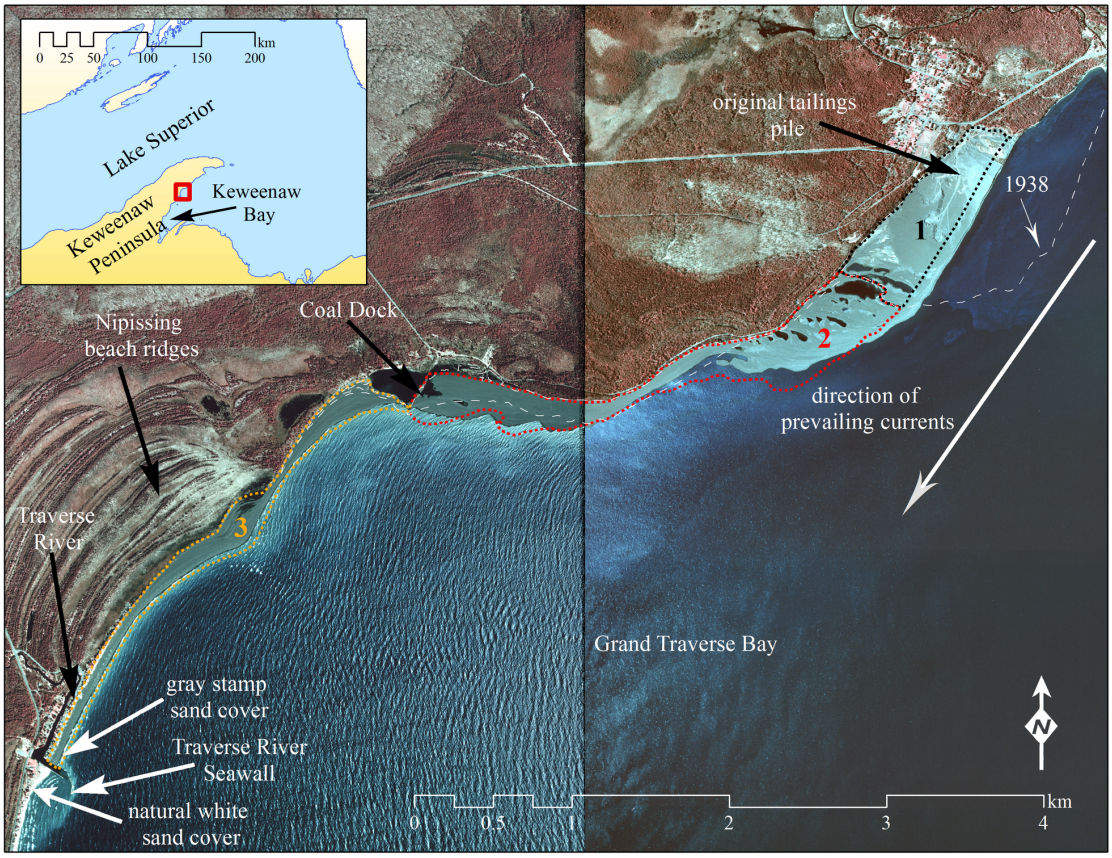

Figure 4.2: Inset gives location of the study site relative to Lake Superior, Keweenaw Bay, and the Keweenaw Peninsula. The aerial photo shows the coastline of Grand Traverse Bay in 1998. Labels indicate local features, including the original tailings pile off Gay, the Coal Dock location, and the Traverse River Army Corps Seawall. The white dashed line represents the boundary of coastal stamp sands indicated on the original 1938 aerial image. The numbers represent the 2010 boundaries of the three coastal stamp sand sections: original stamp sand pile (#1), the Coal Dock region (#2), and the Traverse River section (#3). Note the difference between redeposited stamp sands (grey) and natural sands (white) along the beach stretch. Arrow shows the prevailing direction of alongshore currents.

4.3 Methods

LiDAR image processing. Studies were carried out along the southern shoreline of Lake Superior, on the Keweenaw Peninsula (Fig. 4.2). In this investigation, LiDAR was used principally for producing DEMs (Digital Elevation Models). During the week of 23 June 2008, CHARTS aerial overflights of the Grand Traverse Bay coastline portion of Keweenaw Bay were carried out by the Joint Airborne LiDAR Bathymetry Technical Center of Expertise (JALBTCX). The pulse rates were 1 kilohertz (kHz) at 532nm and 9 kHz at 1064nm with a scan of 20o off nadir side to side from an altitude of 400 m. Using the GIS-referenced high-resolution LiDAR DEM data set, we constructed 2 m resolution LiDAR bathymetric maps down to the maximum penetration depth of 22 m. The CHARTS LiDAR had a vertical accuracy of $\pm$30 cm. Simultaneously, the location and the orientation of the laser source were determined by the Global Positioning System (GPS) and Internal Navigation Units (INU), respectively. We used a Trimble (GeoXT) GPS unit to determine the true height of stamp sand bluffs in order to verify the LiDAR derived height estimates. The results were close, within $\pm$0.4 m.

We also used the NOAA (National Oceanic and Atmospheric Administration) 2010 Great Lakes Restoration Initiative (GLRI) bathymetric LiDAR data in our analysis. The data were collected between July and August by the Fugro LADS Mk II system along the Lake Superior coast of Minnesota, Wisconsin and Michigan.

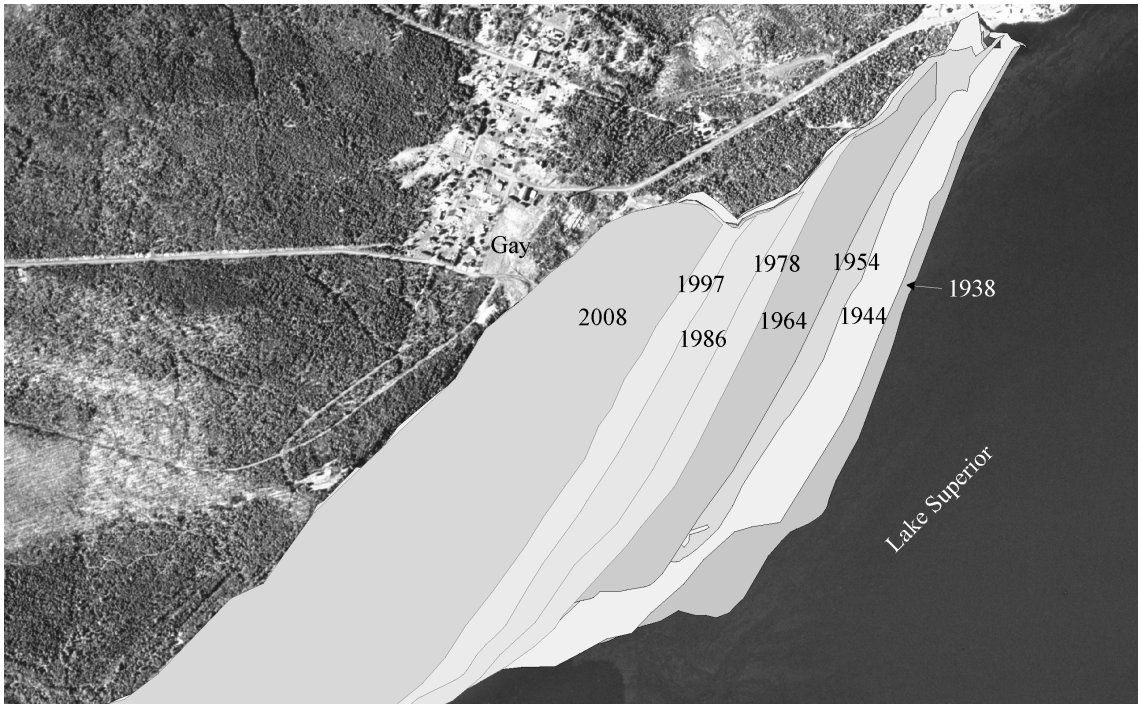

Figure 4.3: Erosion of the Gay tailings pile through time, starting with 1938. The extent of the tailing pile in each aerial photo is labeled with the date of image collection. The region labeled as 2008 represents the remaining pile.

The 2008 LiDAR data were received in strip form. Each strip was taken during a single overpass. ENVI 4.7 was used for the entire image processing procedure. The strips were mosaicked and re-projected. The original coordinate system was Geographical Lat/Long, yet for further distance, aerial, and volume calculations the data were re-projected to a Universal Transverse Mercator (UTM; projection= WGS84, zone=16) coordinate system. The raw mosaicked image needed to be assigned to values of depth, which was done by comparing the LiDAR derived image with a georeferenced aerial photo from 2008. The land-water interface was used as "zero" depth.

The 2010 LiDAR data were downloaded from Digital Coast website (Digital Coast

NOAA, [1]). The data were collected using the LADS Mk II bathymetric LiDAR survey system that acquires bathymetric/topographic data at 1kHz. The original coordinated system for the received data was International Great Lakes Datum 85 (IGLD85), which measures the height above mean sea level. In order to distinguish between below and above water level, the water level elevation (183.2 m, Fugro LADS Mk II) was subtracted from the entire scene, which in return produced a topo/bathy map of the study site. Finally, the 2010 image was color-coded for 5 meter depth intervals to help identify underwater features more easily.

Aerial photograph processing. The original boundaries of the Gay, MI, tailings pile were determined from a georegistered 1938 aerial photo of the region. ArcMap 9.3 was used to digitize the tailings boundary ([82]). Seven additional mosaicked aerial photos (taken between 1944 and 2008) were used as the baseline to determine stamp sand boundary changes through time (Fig. 4.3). The polygons were digitized and re-projected to UTM coordinate system for further geometrical measurements.

Reconstructing the original pile dimensions and mass, and coastline losses underwater to the bay. The Mohawk and Wolverine Mills were located at Gay, MI (Fig. 4.2). They were operated as twin mills with a single pumping plant and joint superintendent. Stamp rock was hauled from the mines to the stamping mills over a rail distance of 21-27 kilometers (km) ([48]; [134]). Gay operations required construction of a Coal Dock (Fig. 4.2) and a short connecting rail line. The Coal Dock extended 100 m

into Grand Traverse Bay and was 5.7 m deep at its end ([48]). Both mills utilized Nordberg Stamps, Harding ball and Chilean mills to crush the amygdule basalt bedrock, releasing copper. By 1932 the two stamp mills sluiced a combined 22.8 Mt of stamp sand tailings onto one enormous pile that covered about 0.9 square kilometers (km^2) ([95],[98]).

To calculate the volume and mass of the original stamp sand pile, three estimates were needed: 1) the thickness of the original pile (the total of below and above water portions), 2) the area of the original stamp sand pile, and 3) the average weight of stamp sand per unit of volume. The input for 'area' came from aerial photos, whereas LiDAR provided estimates of 'thickness'. A 1938 aerial photo provided details about the original extent of the stamp sand pile.

An estimate of below-water mass was still required. To reconstruct the below-water portion of the original pile, the pile was separated into two regions. The two regions were the eroded section and the area under the existing stamp sand pile. The bathymetric LiDAR data were used to estimate the below-water depths of the eroded section (with an assumption of fairly constant water level; 183.3 m; Detroit District Corps). To estimate the depth of the stamp sand in the second region, currently covered by stamp sand, the slope change of bedrock from the LiDAR bathymetric map adjacent to the pile was used and the slope extrapolated under the existing pile.

To reconstruct the above-water portion of the original stamp sand pile, we considered the same two regions, i.e., the portion that is currently covered with stamp sand and the

eroded portion. The LiDAR DEM provided the height of the stamp sand pile in 2008. The elevation of the eroded portion was estimated via extending the height of known landmarks (remaining sluiceways) determined from the 2008 LiDAR DEM. The underwater volume was added based on estimated depth to bedrock.

Landmark reconstruction allowed us to calculate the volume and mass of the pile in 1938. Procedures employed a pixel spatial resolution of 3 meters and an area of 9 m^2. Multiplying area by height gave an estimate of volume of stamp sand for each pixel. Integration provided an estimate of total volume in cubic meters. Moist bulk density of the Gay stamp sands soil was estimated at between 1.35 to 1.65 grams per cubic centimeter (g cm^{-3}) or 1350 kg m^{-3} to 1650 kg m^{-3} [U.S. Department of Agriculture's Natural Resource Conservation Service ([4])]. Based on preliminary measurements, we decided to use the bulk density value of 1650 kg m^{-3}, and calculated the mass for each eroded slice. Plots showed the erosion to be nonlinear, very close to an exponential decay curve. Because the function appeared proportional, values were converted into logarithms.

Estimating pile erosion onto offshore vs. onshore (beach) locations. It is possible that the Coal Dock (Fig. 4.2; southwestern extent of Region #2) served unintentionally as a groin during the 1932-1938 erosion of the main pile, accumulating migrating stamp sands. Further to the south, after construction and lengthening, the Army Corps seawall (Fig. 4.2; southwestern extent of Region #3) on Traverse River intentionally served as a barrier for migrating stamp sands, causing beach widening since the 1970's. Until recently

(2010-11), the Traverse River Seawall prevented incursion of black sands onto the natural white sands of the lower bay. Now there is over-topping. Because of the migration barriers, we examined erosion/accretion patterns along the different shoreline regions.

To estimate the amount of stamp sand lost underwater to Grand Traverse Bay, the mass of stamp sand accumulating along various coastal regions was subtracted from the total tailings discharge. The height of above water portion of the stamp sand was retrieved from the 2008 LiDAR DEM data. Underwater depth estimates along the coast came from a Lake Superior Coast Chart, No. 4 (soundings 1906) and were used to estimate stamp sand thickness below the water level. First, we digitized the 1906 near-shore contours to a series of polygons with different depths and then rasterized these polygons to the same pixel size as in the LiDAR derived images (3m pixels). The product was a raster image with pixel values that were representing water depth in 1906. Total stamp sand thickness was then calculated by adding the under- and above-water thickness values for each pixel. To calculate the volume, each vertical column was multiplied by the area of the pixel ($9m^2$). For calculating the "total mass" layer of the entire coastal stamp sand, the volume layer was multiplied by the average weight of the stamp sand (1650 kg m^{-3}; i.e. 1.65 metric tonnes m^{-3}). Coastal stamp sand boundary polygons were divided into three sections (1= original tailings pile, 2= Coal Dock section, and 3= Traverse River section; see Fig. 4.2). The mass of the stamp sand located inside the section boundary was extracted from the "total mass" raster layer. This process was repeated for every aerial photo polygon to calculate the mass of the stamp sand associated with each of these regions through time and finally

these estimates were plotted against time.

Onshore versus offshore dynamics: To estimate the offshore versus onshore stamp sand deposition, we assumed that stamp sand eroded from the original pile was either deposited southwestward onto the shore along the Coal Dock or Traverse River stretches, or was dispersed out into Grand Traverse Bay. The total amount of stamp sand gain on the Coal Dock or Traverse River stretches (for the period between two aerial photos, Table 4.2) was subtracted from the mass eroded off the original pile (for the same period of time), giving the amount of stamp sand lost to offshore bay waters. In other words, the portion of eroded stamp sand that was not deposited onto the shore was calculated by difference to be dispersed across the offshore underwater region of the bay. Finally, the calculated deposition values to both onshore and offshore regions were plotted and regressed against time.

Mass of the underwater stamp sand bars and interpolation method. Migrating underwater stamp sand bars were discovered in the 2008 LiDAR bathymetric scene and confirmed with aerial photos, and ground-truth sampling. They are located just southwest of the original stamp sand pile at nearshore depths (shoreline to 10 m). In an attempt to determine the mass of these bars, we used a first order slope change analysis to generate the floor of the natural bottom depth beneath the bars. This layer was then subtracted from the height of the underwater bars (LiDAR bathymetric data), giving the volume of the bars, which was then converted into mass. The high resolution LiDAR bathymetric data provided

us with surrounding "true depth" values that were used for interpolation. After tuning the "map prediction" option under **Geostatistical Analyst/Kriging** methods in **ArcGIS 9.3** ([2]), the final predicted bottom map was produced and rasterized.

Change detection map for underwater stamp sand bar profiles. The change detection map is simply a difference map of the pixel values between 2008 and 2010 LiDAR-derived images that helps us to understand the possible movements, erosion, and also accretion on the underwater stamp sand bars. Prior to calculating the difference map, we tried to remove the false differences caused by errors in vertical georectifications. The two maps were regressed over areas that had not changed much during the period between 2008 and 2010. For this purpose, we used depth values over Buffalo Reef (Fig. 4.4), which we assumed had "zero" changes since 2008 (due to its rocky nature). The result (not presented here) showed a 0.53 meter background difference which later was subtracted from the 2008 LiDAR derived image The Change Detection\Compute Difference Map module under basic tools of ENVI 4.7 ([3]) was used for the entire processing operation. We also compared and graphed the selected 2008 and 2010 depth profiles of the underwater stamp sand bars. For calculations and figures, recall that LiDAR resolution was $\pm$30 cm in the vertical and, with resampling, $\pm$3 m in the horizontal.

4.4 Results

General Traverse Bay Erosional Features. The Gay, MI, tailings discharges are superimposed on and interacting with coastal features indicative of post-glacial events, such as submersed erosional structures (river beds, narrow canyon cuts, reefs) and depositional features (Nipissing Beach ridges, natural sand fields). Several long-term erosional features are evident in the above water and underwater 2010 NOAA LiDAR scenes (Fig. 4.4, 4.5). Grand Traverse Bay is underlain by late Precambrian to early Cambrian Jacobsville Sandstone ([125]) that is laid bare by coastal erosion along the shelf margin. The irregular bedding planes that mark the Jacobsville Sandstone bedrock formation are very evident in high resolution LiDAR imagery. Bedrock stretches are prominent along the northern coastal reaches and off Gay, MI, on the outer raised portions of Buffalo Reef, and at the extreme southern margin of the bay, where emerging rock bluffs are encountered. In Grand Traverse Bay, the coastal bedrock seems to be eroding from the northeastern bare rock regions and is being deposited along the southwestern basin as natural white beach sand. The coarse-grained, high albedo reflectance of the natural white beach sand suggests historical origin from eroding Jacobsville Sandstone (Fig. 4.2). Additional eroded Jacobsville Sandstone sediments are contributed by two rivers: the Tobacco River to the northeast and the Traverse River to the southwest.

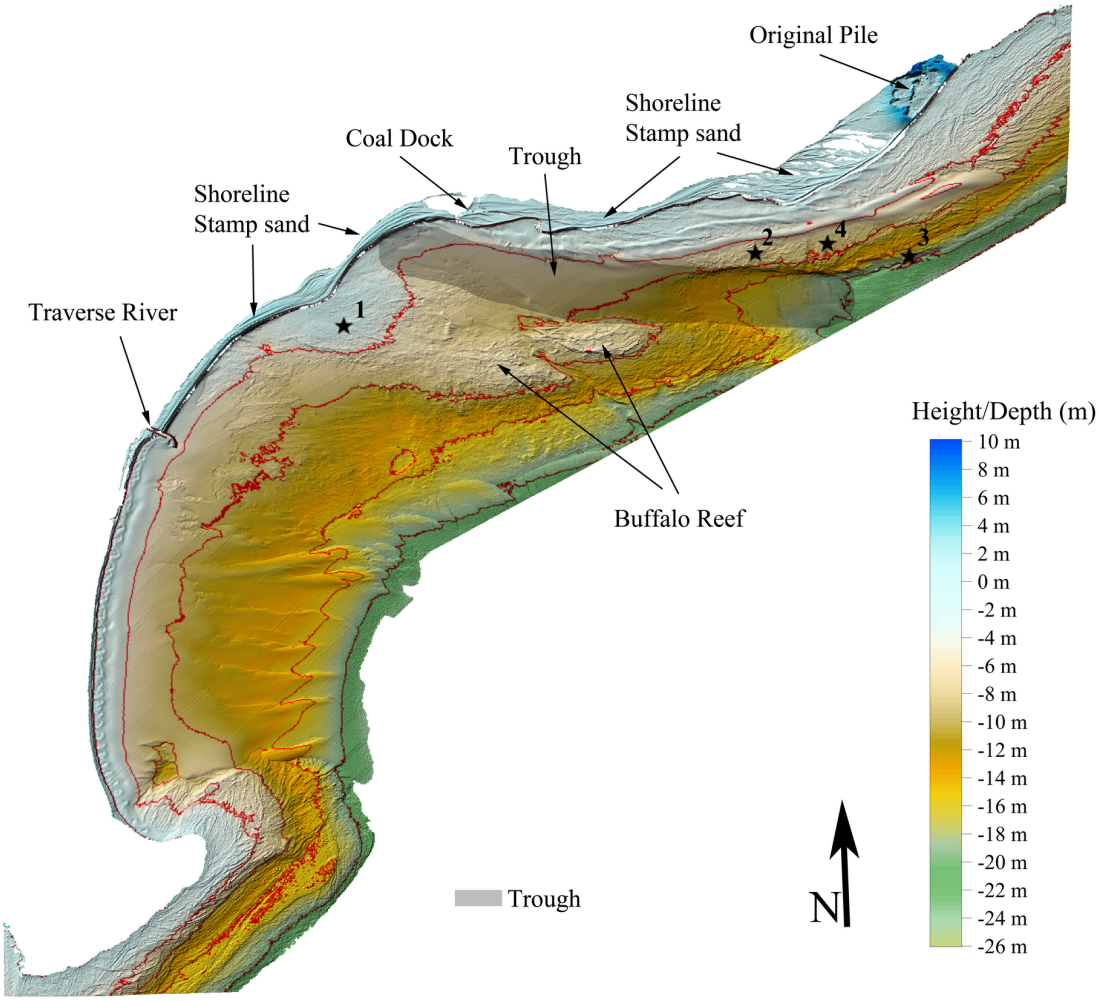

Figure 4.4: 2010 LiDAR bathymetric/topographic map of Grand Traverse Bay viewed from above (nadir). Superimposed red contour lines are at 5m intervals. Note the underwater stamp sand bars moving across Jacobsville Sandstone bedrock on the coastal shelf. Darkened region marks the location of the 'trough', a relict riverbed, northeast of Buffalo Reef. Notice the "comb-like" raised ridges in broad natural sand stretches south of the Traverse River. Solid star symbols correspond to the location of underwater video camera pictures in Figure 4.9.

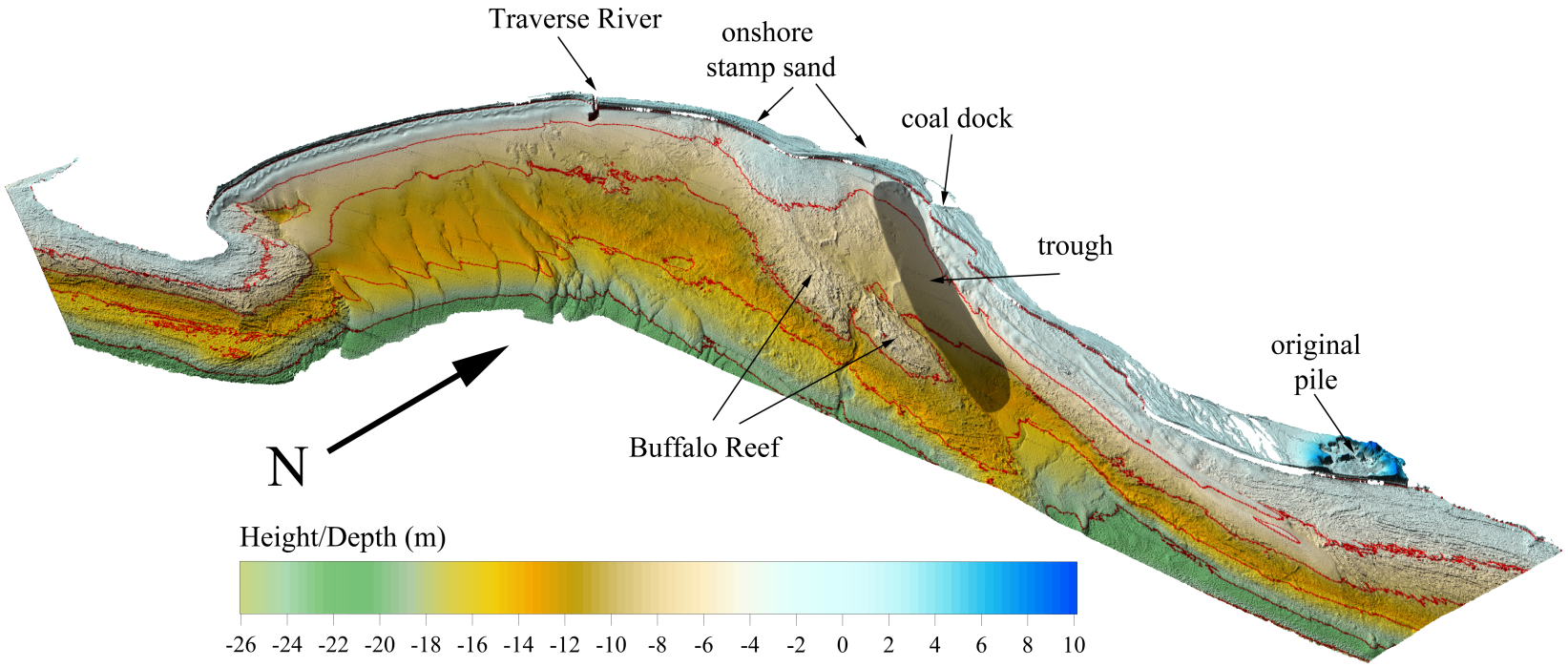

Figure 4.5: 2010 LiDAR bathymetric/topographic map of Grand Traverse Bay from an oblique view. Notice the sharp underwater canyon (dark linear feature) that splits Buffalo Reef into two halves. In the southern portion of the bay, see the band of natural fine sediments hypothesized to be moving into deeper waters.

In the Bay, there are two natural catchment areas for eroded sediments: 1) a 2-3m deep, but broad, 'trough' (highlighted in Fig. 4.4) that cuts across bedrock northeast of Buffalo Reef, and 2) sand fields across the southwestern basin of the Bay (Fig. 4.4, 4.5). The trough appears to be a now-submersed riverbed cut through the bedrock in early post-glacial times, following a terrestrial channel evident across the Keweenaw Peninsula in detailed DEM studies. A second, smaller erosional feature is a narrow and steep canyon that cuts through Buffalo Reef to the south, apparently eroded along a small displacement fault (Fig. 4.5), as the canyon falls along a line of misalignment between the eastern and western sections of the reef.

Before tailings were discharged into Grand Traverse Bay, wave action and southwestward-directed currents eroded sediment from the Jacobsville Sandstone coastal shelf. The sediments accumulated in the trough and moved into the southwestern basin margin of the Bay, adding onto a Nipissing series of coastal dunes (Fig. 4.2) that developed as water depths were dropping.

The LiDAR derived images revealed previously unsuspected bay-wide details about past and present sediment movements. White sand has accumulated along the southwestern bay stretch as a long sandy beach (Fig. 4.4, 4.5). Underwater, the natural fine-grain sandy and silty sediments appear to be superimposed upon the broken Jacobsville Sandstone bedrock, appearing as a relatively thick smooth layer punctuated by numerous erosional channels alternating with modest rises. Ground-truth Ponar sampling of sediments showed

that the smooth bottom sediments in the southwestern basin were almost exclusively naturally eroded material, uncontaminated from anthropogenic stamp sands ([98]). From the vertical perspective, the southwestern basin sediments give the appearance of a comb-like structure (Fig. 4.4). From an oblique perspective, we postulate that the sand and silt layers are moving out of the bay as if on a wide 'conveyor belt' (Fig. 4.5). To our knowledge, this type of progressive mass movement of natural sediments has not been previously described in the Great Lakes. We propose that all these general depositional features were fully developed before the anthropogenic tailings were deposited in Grand Traverse Bay.

Primary Tailings Pile Erosion. The white sands in the southwestern portion of the bay, past the Traverse River break-wall, contrast with the almost grey to black low albedo reflectance of recently deposited 'stamp sand' dunes, derived from copper ore tailings (Fig. 4.2; [98]). In LiDAR derived coastal images, to the northeast and above water off the small town of Gay, MI, is the location of the original main tailings pile. At present, the pile remnants resemble a conical rim, as deep gouges in the middle mark stamp sand removal by the Keweenaw Road Commission (Fig. 4.4). Above the water surface and to the southwest of the pile are redeposited stamp sand beach stretches. These above-water environments contain depressions occupied by seepage ponds and show long dunes of stamp sands either deposited in rows and/or drifting across the surface (Fig. 4.2, 4.4). Compilations from company records (Michigan Tech Archives) give an estimated 22.8 Mt discharged onto the pile from the two working stamp mills between 1900 and 1932 ([95]; [98]). Our estimated

Table 4.2
Mass of the stamp sands (million metric tonnes, Mt) associated with different sections of the shoreline through time [sections: 1) Original Pile; 2) S. end of original pile to Coal Dock; 3) Coal Dock to Traverse River]. Estimated decimal places are set by the 95% C.L. around the respective regressions (i.e. 95% C.L. = ±0.3 Mt for the original pile regression; ±0.3 for the Coal Dock portion; and ±0.1 for the Traverse River portion).

Year	Original Pile	Coal Dock	Traverse River
1938	17.8	1.6	0.2
1944	16.0	1.8	0.3
1954	12.3	2.3	0.8
1964	11.2	2.6	1.0
1978	8.2	2.6	1.7
1986	6.7	3.1	1.9
1997	5.2	3.5	2.2
2008	3.7	4.5	2.6

mass on the pile in 1938, the time of the first aerial photograph, was around 18 Mt (Table 4.2).

Using a 1906 bathymetric map and 2008 LiDAR over-flight to estimate bottom contours, and seven aerial images to measure erosional slices across the pile through time (Fig. 4.3), we estimated that erosion of the Gay tailings pile was greatest early in the record and has declined recently. As mentioned in the Methods, to handle the nonlinearity, we decided to log-transform (natural log, ln) the mass erosion values. The resulting fit was exceptional (R^2=0.99). The regression fit to log-transformed data was plotted versus time and used to predict 1) the rate of erosion and 2) the "zero" mass intercept date (Fig. 4.6a, Table 4.3). The predicted "zero" mass date was 2062, with ±95% C.L. of 2054 and 2071.

Table 4.3
Regression values for stamp sands eroded off of original pile (section 1) and deposition onto onshore/offshore locations (sections 2-3), including mass dynamics for erosion into bay (by difference).

Fit type	No.	Regression	Y-intercept	Slope	R^2	X-intercept	LL	UL
Linear	1	Ln of mass +1 of original stamp sand pile loss (section 1)	46.59	-0.02	0.99	2062	2054	2071
	2	Mass deposited on Coal Dock region (section 2)	-66.17	0.035	0.93	-	-	-
	3	Mass deposited on Traverse River region (section 3)	-66.97	0.035	0.99	-	-	-
	4	Eroded from original pile onto onshore	-213.67	0.11	0.98	-	-	-
	5	Eroded from original pile into offshore	-135.73	0.07	0.90	-	-	-
Polynomial 2^{nd} order	6	Eroded from original pile into offshore $y = A + B^x + C.x^2$	A=-6304.94	B=6.275 C=-0.001	0.98	-	-	-

From the 2008 LiDAR derived image and 1906 bathymetry map (see Methods), we could also estimate the accumulation history of redeposited beach sands along various sections of the coast (Table 4.4). The entire mass of stamp sand redeposited along the coastline was estimated as 7.0 Mt., which amounts to 30.7% of the original mass of stamp sand discharged onto the pile (22.8 Mt). Given the LiDAR high resolution and the clear gouges left on the pile by the Road Commission, we could also estimate that winter road application and bed construction removed about 1.01 Mt of the Gay, MI, pile total mass (4.4%). So of the 22.8 Mt originally discharged onto the pile, 3.7 Mt (16.2%) remain on the pile, 7.0 Mt (30.7%) were redeposited along the shoreline, and 1.01 Mt (4.4%) were removed by the County Road Commission. By difference, the remaining 11.1 Mt (48.7%) has moved out into Grand Traverse Bay, spreading across the underwater substrates.

Table 4.4
Estimated amount of stamp sand deposited on shoreline and offshore into Keweenaw Bay (by difference). Percentage is relative to amount originally discharged on Gay pile (22.8Mt).

Estimate of stamp sand	Mass(Mt)	%
Original discharged mass (1901-1932)	22.8	100
Stamp sand removed by Road Commission	1.0	4.4
Remaining stamp sand on Gay pile (total 2008)	3.7	16.2
Stamp sand redeposited on beach	7.0	30.7
Total shoreline (pile + beach, 2008)	10.8	47.4
Deposited in Keweenaw Bay (by difference)	11.1	48.7

Contrasting Various Erosional Patterns Through Time. Given the excellent time resolution afforded by the combination of aerial and LiDAR imagery, we could also estimate beach stamp sand accumulation patterns and, by difference, examine how much has moved progressively underwater into the bay through time. Both the Coal Dock and

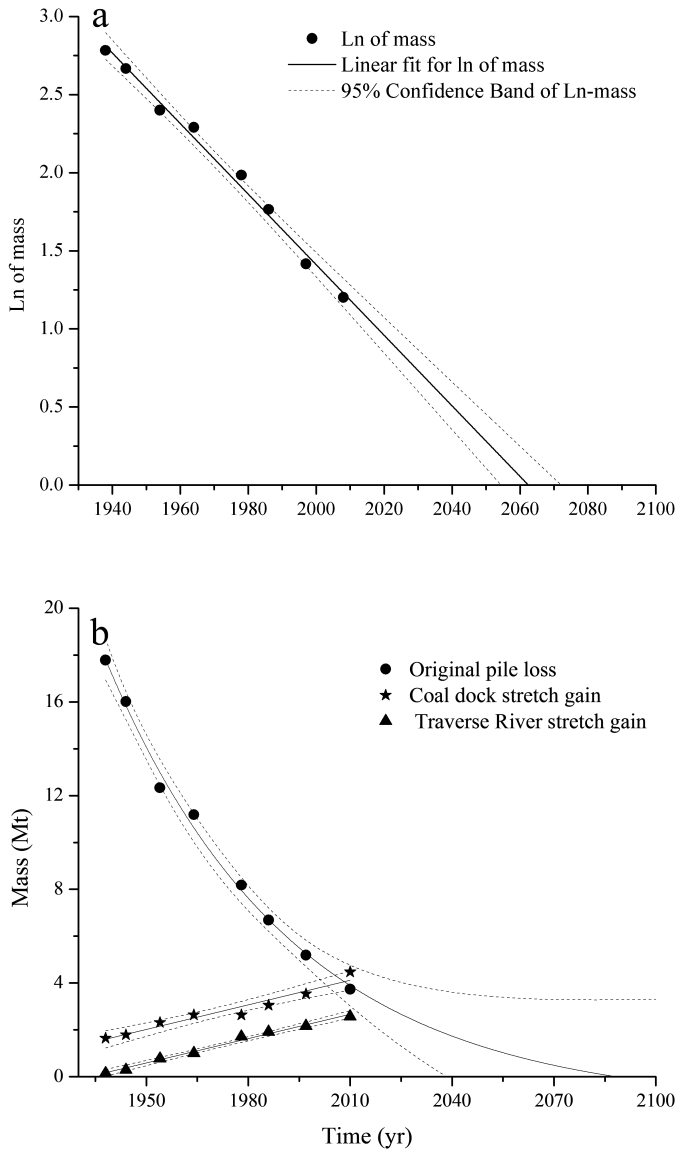

Figure 4.6: Erosion of the Gay tailings pile through time: A) Log-transformed mass remaining on the Gay tailing pile through time, starting with 1938. Notice that the regression (solid line) X-intercept is 2062, with ±95% confidence intervals; B) Mass dynamics on different coastal regions: squares document nonlinear erosion (loss) from Gay tailings pile through time; circles represent mass redeposited in the Coal Dock region; and triangles are the mass redeposited in the Traverse River region. The latter two regions conform closely to a linear accumulation of stamp sand mass through time. The numbers associated with each line represent the coastal stretch on Figure 4.2.

Traverse Bay Seawall appear to have acted as groins, retaining migrating stamp sand on their upstream sides. Patterns of deposition along different stretches of the beach (original pile to Coal Dock section; Coal Dock to Traverse River section) were compared to the erosion of the original tailings pile (Fig. 4.7).

As mentioned earlier, the mass of the original tailings pile shows a nonlinear, proportional (exponential decay) loss of stamp sands through time. The historical erosion is pronounced enough, that now the mass of stamp sand in the original pile (3.7 Mt) is far less than the combined amount along the shoreline to the south of the pile (7.0 Mt). The Coal Dock stretch is holding 4.5 Mt of stamp sand. Along the shoreline beach, accumulation over time in the original pile-Coal Dock section appears to fit a linear function (Fig. 7; Table 3; R^2=0.93). The mass of stamp sand in the Coal Dock to Traverse River section (2.57 Mt; section 3) also shows an increasing linear trend with a time delay (Fig. 4.7; Table 4.3; R^2=0.99). That the functions are positive should be no surprise, since the eroded stamp sands are pushed southwestward by a combination of strong southward-directed waves and currents. Both curves show simple (linear) trends with nearly identical slopes (Coal dock section slope = 0.034, S.E. = 0.003; Traverse River slope = 0.033, S.E. = 0.001).

Using the combination of aerial photos and LiDAR derived images, we could also estimate the time course of loss into the bay by difference. Total redeposition onto the shoreline shows a linear, increasing trend ($P<0.05$, Table 4.3), whereas erosion into offshore regions of Lake Superior from 1938 to 2008 shows an accumulation curve that

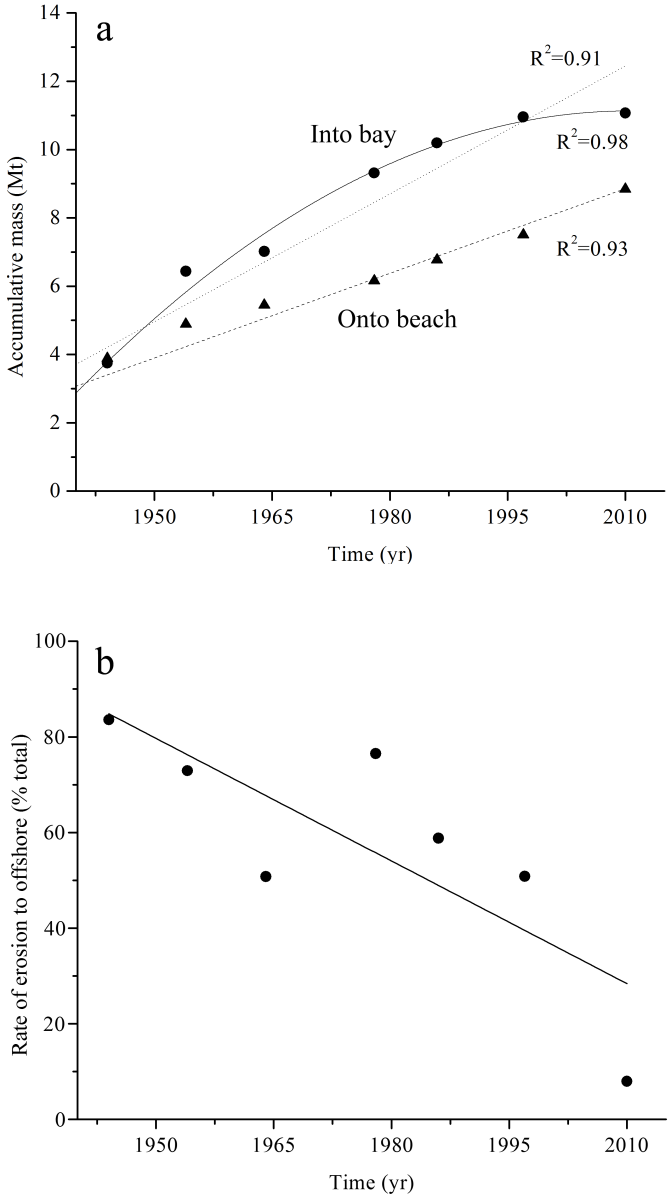

Figure 4.7: Total accumulative mass of stamp sand eroded to onshore and offshore regions between 1938 and 2008: A) offshore trends (circles) are fit with both linear (dotted line) and polynomial (solid line) functions, whereas the onshore (beach; solid triangles) accumulation is fit with a linear (dashed line) equation (Table 4.3). B) Running two-point estimate of % loss from the 1938 tailings pile total (18 Mt) to the bay; approximates the slope of the polynomial regression. That is, the percentage of mass lost to the bay from the remaining pile (total) is declining through time. The R^2 values of various regressions are given next to the lines

reaches an asymptote (Fig. 4.7a; Table 4.3). Notice from both accumulation curves that more material has moved into the bay than has accumulated along the beaches. Moreover, most of the eroded stamp sand from the original tailings pile is now being re-deposited and moved across the bay bottom. When treated as a series of two-point estimates, the declining rate for transfer of sediments into the bay is very evident (Fig. 4.7b). Presumably much of the declining rate is due to the dwindling amount at the source, i.e. the original tailings pile. One might argue that the original erosion of the tailings pile was heavily influenced by a combination of strong waves and offshore currents, whereas the movement along the beach was largely due to wave action aided by weaker long-shore currents.

Migrating Underwater Stamp Sand Bars. LiDAR derived imagery also revealed intriguing details associated with stamp sand spread into the bay and along the coast towards Buffalo Reef. Underwater stamp sand bars off Gay (Fig. 4.4, 4.8) have a distinct appearance that can distinguish them from surrounding Jacobsville Sandstone bedrock. They have smooth slopes and rounded edges. LiDAR imagery revealed that underwater bars spread out from the original tailings pile and are aligned in a northeast to southwesterly direction, stretching out over the Jacobsville Sandstone shelf (Fig. 4.4, 4.5). These long bars have southwestern ends that appear to dump into the 'trough' north of Buffalo Reef. The migrating piles were confirmed as composed of stamp sands by ground-truth Ponar samples ([98]) and lie at water depths of 0 to 10 meters. At present, the bars near the original tailings pile cover an area of about 1.08 km^2 (more than the original pile) and are especially pronounced on the 2010 NOAA LiDAR derived images. After processing the

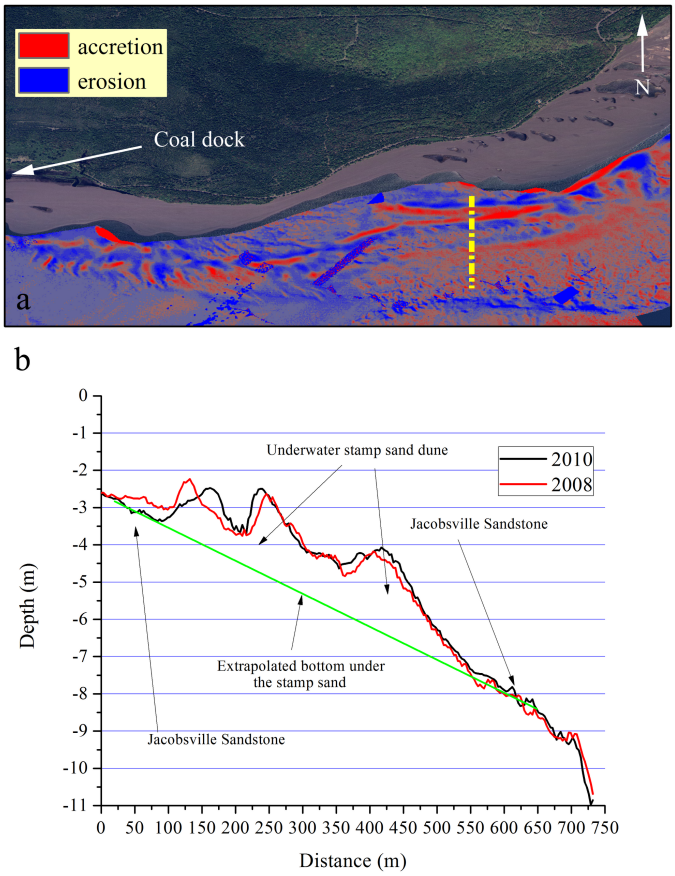

Figure 4.8: Change detection maps of sand bar movement: A) Map represents changes in the erosion (loss; bright blue) and deposition (bright red) patterns between 2008 and 2010 LiDAR images at underwater region east of Coal Dock. The yellow line marks the transect line for detailed height measurements of individual bars. B) Along the transect, the black line represents the height of the selected profile in 2010, whereas the red line represents the height of the same profile in 2008. The green solid line represents the interpolated bottom. Note relative shifts in the dune positions. Recall that the vertical resolution is ± 30 cm, whereas the horizontal resolution is ± 3 m.

imagery and recalculating the thickness of the underwater stamp sand, we estimated the mass of stamp sand in the large bars is about 0.6 ($\pm$ 0.1) Mt, about 6% of the total mass of stamp sand lost to the offshore region.

Bars that are closer to the shoreline have steeper slopes compared to those that lie in deeper waters. The shallow-water stamp sand bars are also narrower (Fig. 4.8a). The results from the change detection analysis showed that underwater bars in the shallow regions move more than deeper bars, inching rapidly towards greater depths (Fig. 4.8b). The boundaries and overall shape of the large, deeper bars did not appear to change as much. However, the deeper, larger bars showed slight stamp sand accumulation between 2008 and 2010 and evidence for internal, lateral movement. The deeper, larger bars, appears to progressively creep from northeast to southwest (loss, bright blue; deposition, bright red), especially evident along the southwestern ridges (Fig. 4.8a).

Depth profiles (Fig. 4.8b) of stamp sand bars in 2008 and 2010 also confirm the overall pattern. The location of the depth transect is marked with a straight light line in Fig. 4.8a. The shallow water bars show more movement than the bars in deeper waters. Moreover, the deeper bars appear to remain in place and tend to accumulate stamp sand. Our general interpretation of these difference patterns is that they indicate that bars in shallow water are moved progressively into deeper waters, where they coalesce with the larger bars. On the other hand, the large bars show active lateral movement, as sands erode from northeasterly faces and are deposited onto southwesterly faces. Evidence whether the large bars eventually creep down over the Jacobsville Sandstone coastal shelf into deeper waters, or move laterally into the trough near Buffalo Reef, will require longer-duration LiDAR monitoring.

Figure 4.9: Underwater camera images of various bottom substrates in Grand Traverse Bay: #1) top left, natural cobble field, #2) top right, cobbles and boulders covered by natural sand, #3) bottom left, stamp sands creeping across natural Jacobsville Sandstone bedrock, and #4) bottom right, stamp sands moving into a cobble field. Encrypted data gives: date, time, station name and number, and the station geographical coordinate in UTM, Zone = 16. Sites of photos are shown in Figure 4.4. Taken from Biberhofer and Procopec (2008, [23]).

4.5 Discussion

In Grand Traverse Bay, LiDAR-based erosion and deposition calculations for stamp sand movement revealed some very interesting features and deposition patterns. The original stamp sand pile was sluiced into a historical erosional zone, whereas the Coal Dock and Traverse River stretches fell into historical depositional zones (Nipissing Beach deposits).

Two prominent natural catchment regions for eroded sediments included an old eroded riverbed (the 'trough') northeast of a mid-bay reef (Buffalo Reef). The prominent reef and a groin-like anthropogenic shoreline structure (the Coal Dock) served to capture migrating sands, diverting them into the 'trough'. The small canyon in Buffalo Reef may have formed at the same low water stage when the 'trough' was cut. Similar channel cutting patterns near Thunder Bay ([28]) suggest a drop of Lake Superior water levels during the Houghton Low (7,900-8,100 years before present; yrs B.P.). Overflow from glacial Lakes Agassiz or Ojibway associated with retreat of the Laurentide Ice Sheet are suspected additional sources of water. After about 6,400 yrs B.P., glacial rebound lifted the North Bay outlet sill above the Sault Ste. Marie sill and set about the onset of the Nipissing transgression.

Regarding the Nipissing sequence, there is considerable debate about how the sequence relates to climate, with emerging evidence that the last 4,000 yrs of water level fluctuations in Superior have been influenced by wetter and drier periods ([26]; [32]; [166]). Johnston et al. ([87]) found that the southwestern beach ridges in Grand Traverse Bay were deposited between 3800 to 900 yrs B.P. In the sequence, a single ridge formed every 36 years, with indications of changing rates of water lowering. The sequence indicates that relative lake levels lowered about 4.5 m between 3800 to 1200 yrs B.P., then actually increased 0.7 m between 1200 to 900 yrs B.P. Moreover, changes in mean grain-size in the lake-ward ridges indicate larger wave action between 1200 to 900 yrs. B.P., suggesting a shift in the predominant wind direction after 1200 yrs B.P. ([87]). An earlier study, Rasmussen et al. ([157]), pointed out that the natural beach breadth has

increased along the redeposition region since 1938, but this is due almost exclusively to accumulation of anthropogenic tailings (stamp sands) deposited on top of existing natural beach, augmenting beach mass. The Traverse River seawall has blocked further southward migration of stamp sand since the early 1970's, although recent overtopping (2010-2011) has finally breached this barrier. Our analysis of aerial photos between 1978 and 2008 shows an increased beach width of about 3 meters per year. At present, the coastal mass of redeposited stamp sand in the Coal Dock region exceeds what is left at the original tailings pile site. Recall that the adjacent natural Nipissing beaches had a progradation rate of 0.7 ± 0.1 m per year ([87]). So the accumulation of stamp sands today is almost 4.3 times faster than the natural past maximum sand accumulation on the Nippising beach ridges. Just by measuring stamp sand-traveling distance/year by regression studies, we were also able to predict the distance that stamp sand might have traveled in the absence of the Traverse River Seawall, i.e. about 1.5 km more to the south over natural sand beaches. Although the Army Corps Traverse River Seawall caused an increase in the accumulation of stamp sand (increased beach width), it also proved an effective barrier, temporarily halting southward migration of stamp sand.

Surface waves, nearshore and offshore currents, along with winter storms, are major factors reshaping shorelines all around the world ([158]; [159]; [146]). The combination of LiDAR, aerial photography, and bathymetric maps permitted calculations of historic stamp sand mass deposition and erosion. Our observations document that the original tailings pile experienced an exponential decay in erosion through time (Fig. 4.6), with almost all

of the mass traveling southwestward. We suggest that placement of the original tailings pile in deep water off Gay contributed to rapid initial erosion once operations ceased, since the pile was deeper along the offshore margin and exposed to maximum wave action and strong alongshore currents.

Surface waves, alongshore currents, and winter ice all have created scour and moved material in Grand Traverse Bay ([185]; [95], [98]). Prevailing currents along the eastern coastline of the Keweenaw Peninsula flow predominantly southward, parallel to isobaths ([154]; [43]; [193]). Measurements by Sloss and Saylor ([154]) documented periodically strong (1.0-5.0 cm/s^{-1}) summer and fall southward alongshore flows. In other studies, Hawley ([74]) and Churchill et al. ([47]) found that surface wave currents had a seasonal component, strongest in Lake Superior during late autumn to winter.

Churchill et al. ([47]) also caution that high-frequency motions in internal waves could be of fundamental importance in generating bottom stress at locations where the seasonal thermocline intersects bottom strata. Clearly, winter shoreline wave action and ice also move stamp sands down-drift and out into the bay ([34]; [185]). During December to March, creation of a nearshore ice complex would seem to protect the coastline against wave erosion. However, during winter storms, sediments accumulate in layer-cake fashion on top of nearshore ice complexes, subsequently contributing to beach loading during spring melting ([34]). Salt-and-pepper deposition of stamp sands on top of fine deep-water sediments suggests recent ice rafting and deposition during spring melt ([98]). Whether the

latter pattern is due to progressive movement of stamp sands along the coast during winter storms or to changing patterns of ice drift is unclear.

Concern about underwater stamp sand migration involves encroachment of stamp sands onto Buffalo Reef. Not only do stamp sands have high copper concentrations (1,500-13,000 micrograms (μg) g-1; mean 2,863 μg g^{-1}; n=274; [130]; [95], [98]), the Keweenaw Bay Tribal Community is concerned that stamp sands will fill in the scattered cobble fields that surround the reef, compromising depressions that normally shield eggs deposited by lake trout and lake whitefish ([45]). Evidence that both processes are of genuine concern come from underwater photos of moving stamp sands (Fig. 4.9; from [23]) and from prior toxicity tests of stamp sands ([123]; [118]; [185]). The images depict 1) undisturbed fields of natural cobbles, 2) stamp sands moving over Jacobsville Sandstone bedrock, and 3) stamp sands invading cobble fields. In the detailed LiDAR-derived bottom surfaces of Grand Traverse Bay (Figs. 4.4, 4.5), stamp sands moving out of the 'trough' appear to be moving into the cobble fringe north of Buffalo Reef, creating a flatter area.

Southwestward movement and deposition of stamp sands along the shoreline also increases the risk of encroachment onto Buffalo Reef during winter storms and extreme weather conditions. Change detection analysis showed that underwater stamp sand bars move toward the 'trough' and deposit stamp sands into that depression. Profiling the underwater bars also provide valuable information on the displacement of the bars between 2008 and 2010. As is evident from the change detection map, the underwater stamp sand

bars migrate into deeper waters where they coalesce into large bars that creep laterally, emptying into a broad 'trough' northeast of Buffalo Reef. Preliminary calculations of 'trough' surface and volume give 1,275,400 m^2 and 4,205, 200 m^3, respectively. If the remainder of the stamp sand pile is converted into cubic meters, there are around 2,120,000 m^3, roughly half of the calculated volume of the trough. At the present rate of erosion, about 55,000 m^3 of stamp sands are moving across bedrock towards the trough each year. From the LiDAR images, the shallow portion of the trough now seems full, with overtopping moving southwestward into some of the cobble fields around Buffalo Reef.

In the past, the land-water interface has posed characterization problems. On the shoreline side, before the advent of the Global Positioning System (GPS) and LiDAR, shoreline position analysis and beach profiling were based largely on historical aerial photographs and topographic maps ([82];[138]; [88]). Along the nearshore water margin, traditional shipboard sonar survey methods encountered significant limitations, such as shallow-water hazards, shoals, currents, and marine tides ([73]). However, high-resolution LiDAR has now become a preferred option, as it allows simultaneous mapping of nearshore bathymetry, navigational canals, remote and shallow harbors, wetlands, and shoreline erosion. In a single LiDAR survey (8h), aircraft can cover a study area that would require a week or more for a vessel to survey. Also, when classifying the bottom, LiDAR amounted to 10% (or less) the cost for shipboard surveys ([31]).

Here the ability of LiDAR to map topographic and bathymetric features

simultaneously in fine details (spatial resolution 2-3 meters and ±30cm vertical accuracy; [155]) was a significant advantage. Additional SONAR transects (NWRI; KBIC tribal projects) served as an important complement ([23]). Because the LiDAR depth-sounding technique depends upon laser penetration of waters, optical water clarity was the most critical property of Lake Superior waters, allowing 22 m depth penetration. River inflow, resuspended sediments, and air bubbles are a few factors that increase light attenuation in the water column and hinder maximum penetration ([88]). Fortunately, the low productivity of Lake Superior means that imagery is not as compromised by phytoplankton blooms, benthic periphyton films and aquatic macrophyes as are the coastal stretches of the lower Great Lakes.

4.6 Concluding Remarks

In Lake Superior, high water clarity allowed excellent high-resolution mapping of coastal bathymetric features to a depth of 22 m. We discovered several previously unrecognized post-Pleistocene erosional features (e.g., river bed channel, narrow canyon through Buffalo Reef) and revealed what appears to be a conveyor-belt movement of natural sediments out of the lower bay. Discharge of tailings onto the coastal shelf margin off Gay between 1900-1932 provided the opportunity to trace anthropogenic stamp sand movements in Grand Traverse Bay and to see how these migration patterns interacted with the post-Pleistocene features. Using a combination of aerial photographs and LiDAR derived

imagery, we quantified an 80-year record of specific mass erosion and deposition dynamics. The fact that century-long estimates of pile erosion fit a simple exponential decay function and that sediment accumulation along two separate stretches of coastal beach fit a simple linear function is very intriguing. At present, progressive encroachment by stamp sands is threatening Buffalo Reef, a critical lake trout and whitefish breeding ground, by filling up a trough in front of the reef and spilling over into the cobble beds around the reef. With its great spatial resolution, LiDAR derived imagery is giving us a much better understanding of the fate of "legacy" mining discharges. Given that global climate change is modifying shoreline ice cover and storm frequency/magnitude patterns in the Great Lakes (Schwab et al., 2006; Austin and Colman, 2007), we would expect that these coastal erosion patterns will show departures in the near future.

4.7 Acknowledgements

Primary funding came from the Army Corps of Engineers ERDC-EL laboratory and was provided by the System Wide Water Resources Program (Dr. Steve Ashby, program manager) at Vicksburg. Efforts were also aided by a National Science Foundation OCE 97-12872 grant to WCK, and a U.S. Environmental Protection Agency Region V Grant to the Baraga Tribal Council passed through to W.C.K. Support for the CHARTS flight and initial data processing was provided by the Corps National Coastal Mapping Program managed by Dr. Jennifer Wozencraft at the JALBTCX Center. We thank Dave Schwab,

NOAA GLERL, Ann Arbor, for assistance on the NOAA LiDAR series overflight and coastal forecast information. We also thank Esteban Chiriboga, and especially Hans Biberhofer for sharing details of the National Water Research Institute and Great Lakes Indian Fish and Wildlife Commission sonar mapping and sediment sampling efforts in Grand Traverse Bay. We also want to recognize the data processing support provided by Michael Sayers and Nathaniel Jessee at MTRI. Lucille Zelazny aided preparation of figures.

References

[1] Digital coast noaa.

[2] Economic and social research institute, arcdesktop.

[3] Environment for visualizing images. visual information solutions.

[4] U.s. department of agriculture?s natural resource conservation service.

[5] Laboratory culture of zebra (dreissena polymorpha) and quagga (d. bugensis) mussel larvae using estuarine algae. *Journal of Great Lakes Research*, 22(1):46 – 54, 1996.

[6] Great lakes cladophora in the 21st century: same algae?different ecosystem. *Journal of Great Lakes Research*, 36(2):248 – 255, 2010.

[7] F. Ackermann. Airborne laser scanning-present status and future expectations. *J. Photogram. Remote Sens.*, 54:64–67, 1999.

[8] S. Andrade, J.Moffett, and J. A. Correa. Distribution of dissolved species and suspended particulate copper in an intertidal ecosystem affected by copper mine tailings in northern chile. *Mar. Chem.*, 101:203–212, 2006.

[9] G. T. Ankley, V. R. Mattson, E. N. Eonard, C. W. West, and J. L. Bennett. Predicting the acute toxicity of copper in freshwater sediments:evaluation of the role of acid volatile sulfide. *Environ. Toxicol. Chem.*, 11:315–320, 1993.

[10] G. Asmund, P. G. Broman, and G. Lindgren. Managing the environment at the black angel mine, greenland. *Int. J. Surf. Min., Reclam. Environ.*, 8:37–40, 1994.

[11] J.A. Austin and S.M. Colman. Lake Superior summer water temperatures are increasing more rapidly than regional air temperatures: A positive ice-albedo feedback. *Geophys. Res. Lett.*, 34:5, 2007.

[12] Richard P. Barbiero, David B. Bunnell, David C. Rockwell, and Marc L. Tuchman. Recent increases in the large glacial-relict calanoid limnocalanus macrurus in lake michigan. *Journal of Great Lakes Research*, 35(2):285 – 292, 2009.

[13] R.P. Barbiero, B.M. Lesht, and G.J. Warren. Evidence for bottom-up control of recent shifts in the plagic food web of Lake Huron. *J. Great Lakes Res.*, 37:78–85, 2011.

[14] R.P. Barbiero, K. Schmude, B.M. Lesht, C.M. Riseng, G.J. Warren, and M.L.

Tuchman. Trends in Diporeia population across the Laurentian Great Lakes 1997-2009. *J. Great Lakes Res.*, 37:9–17, 2011.

[15] Dmitry Beletsky, James H. Saylor, and David J. Schwab. Mean circulation in the great lakes. *Journal of Great Lakes Research*, 25(1):78–93, 1999.

[16] Dmitry Beletsky and David J. Schwab. Modeling circulation and thermal structure in lake michigan: Annual cycle and interannual variability. *Journal of Geophysical Research: Oceans*, 106(C9):19745–19771, 2001.

[17] Dmitry Beletsky, David J. Schwab, Paul J. Roebber, Michael J. McCormick, Gerald S. Miller, and James H. Saylor. Modeling wind-driven circulation during the march 1998 sediment resuspension event in lake michigan. *Journal of Geophysical Research: Oceans*, 108(C2), 2003.

[18] C.H. Benedict. *Red metal: The Calumet and Hecla story*. University of Michigan Press, 1952.

[19] C.H. Benedict. *Lake Superior Milling Practice*. Michigan College of Mining and Technology, Houghton., 1955.

[20] D.E. Bentil, B.M. Osei, C.D. Ellingwood, and J.P. Hoffmann. Analysis of a schnute postulate-based unified growth model for model selection in evolutionary computations. *Biosystems*, 90(2):467 – 474, 2007.

[21] Trisha Bergmann, Gary Fahnenstiel, Steven Lohrenz, David Millie, and Oscar Schofield. Impacts of a recurrent resuspension event and variable phytoplankton community composition on remote sensing reflectance. *Journal of Geophysical Research: Oceans*, 109(C10), 2004.

[22] M. Berkun. Submarine tailings placement by a copper mine in the deep anoxic zone of the black sea. *Water Res.*, 39:5005–5016, 2005.

[23] J. Biberhofer and C.M. Procopec. *Delineation and characterization of aquatic substrate features on or adjacent to Buffalo Reef, Keweenaw Bay, Lake Superior*. Environment Canada National Water Resource Institute (NWRI), Technical Note AERMB-TN06, 2008.

[24] Bopaiah A. Biddanda and James B. Cotner. Love handles in aquatic ecosystems: The role of dissolved organic carbon drawdown, resuspended sediments, and terrigenous inputs in the carbon balance of lake michigan. *Ecosystems*, 5:431–445, 2002.

[25] C.E. Binding, J.H. Jerome, R.P. Bukata, and W. G. Booty. Trends in water clarity of the lower Great Lakes from remotely sensed aquatic color. *J. Great Lakes Res.*, 33:828–841, 2007.

[26] R.K. Booth, S.T. Jackson, and T.A. Thompson. Paleoecology of a northern Michigan lake and the relationship among climate, vegetation, and Great Lakes water levels.

Quater. Res., 57:120–130, 2002.

[27] Z.H. Bowen and R.G. Waltermire. Evaluation of light distancing and ranging (LiDAR) for measuring river corridor topography. *J. Paleolimnol.*, 38:33–41, 2002.

[28] M. Boyd, J.T. Teller, Z. Yang, L. Kingsmill, , and C. Shultis. An 8,900-year-old forest drowned by Lake Superior： hydrological and paleoecological implications. *Journal of Physical Chemistry*, DOI 10.1007/s10933-010-9461-1, 2010.

[29] J. Brock, C. Wright, A. Sallenger, W. Krabill, and R. Swift. Basis and methods of NASA Airborne Topographic Mapper lidar surveys for coastal studies. *J. Coastal Res.*, 18:1–13, 2002.

[30] J.C. Brock, C.W. Wright, T.D. Clayton, and A. Nayegandhi. LIDAR optical rugosity of coral reefs in Biscayne National Park, Florida. *Coral Reefs*, 23:48–59, 2004.

[31] E.D. Brown, J.H. Churnside, R.L. Collins, T. Veenstra, J.J. Wilson, and K. Abnett. Remote sensing of capelin and other biological features in the North Pacific using LiDAR and video technology. *ICES Journal of Marine Science*, 59:1120–1130, 2002.

[32] R.B. Brugam, B. Owen, and L. Kolesa. Continental-scale climate forcing factors and environmental change at Glimmerglass Lake in the Upper Peninsula of Michigan. *Holocene*, 14(6):807–817, 2002.

[33] B.S. Butler and W.S. Burbank. *The copper deposits of Michigan*. United States Geological Survey Professional Paper No. 144, 1929.

[34] J. Budd, W.C. Kerfoot, A. Pilant, and L.M. Jipping. The Keweenaw current and ice rafting: use of satellite imagery to investigate copper-rich particle dispersal. *J. Great Lakes Res.*, 25:642–661, 1999.

[35] Judith W. Budd and Daniel S. Warrington. Satellite-based sediment and chlorophyll a estimates for lake superior. *Journal of Great Lakes Research*, 30, Supplement 1:459–466, 2004.

[36] J.W. Budd, W.C. Kerfoot, S. Green, and M. Julius. News. Technical report, Ocean Color Spectrum 33-34, 2002.

[37] B. J. Burd. Evaluation of mine tailings effects on a benthic marine infaunal community over 29 years. *Mar. Environ. Res.*, 53:481–519, 2002.

[38] L.E. Burlakova, A.Y. Karatayev, and D.K. Padilla. The impact of Dreissena polymorpha (PALLAS) invasion on Unionid Bivalves. *Internat. Rev. Hydrobiol.*, 85(5-6):529–541, 2000.

[39] P.A. Burrough and R.A. McDonnell. *Principles of Geographical Information Systems*. 1998.

[40] J. C. Castilla and E. Nealler. Marine environmental impact due to mining activities of el salvador copper mine, chile. *Mar. Pollut. Bull.*, 9:67–70, 1978.

[41] Y. Cha, C.A. Stow, T.F. Nalepa, and K.H. Reckhow. Do invasive mussels restrict offshore phosphorus transport in Lake Huron? *Environ. Sci. Technol.*, 45(17):7226–7231, 2011.

[42] C. Chen et al. Impacts of suspended sediment on the ecosystem in Lake Michigan: A comparison between the 1998 and 1999 plume events. *J. Geophysical Res.*, 109, 2004.

[43] C. Chen, J. Zhu, E. Ralph, S.A. Green, J. Wells Budd, and F.Y. Zhang. Prognostic modeling studies of the Keweenaw Current in Lake Superior. Part I: Formation and evolution. *J. Phys. Oceanogr.*, 31:379–395, 2001.

[44] E. D. Chiriboga and W. P. Mattes. Buffalo reef and substrate mapping project. Technical report, Administrative Report 08-04. Great Lakes Indian Fish and Wildlife Indian Commission, 2008.

[45] E.D. Chiriboga. *GLIFWCK Buffalo Reef and stamp sand substrate mapping project. Abstract, Remote sensing across the Great Lakes: Observations, monitoring and action*, 2006.

[46] A. R. Chretien. *Geochemical behaviour, fate and impact of Cu, Cd, and Zn from*

mine effluent discharging in Howe Sound. PhD thesis, Univ. of British Columbia, 1997.

[47] J.H. Churchill, A.J. Williams, and E.A. Ralph. Bottom stress generation and sediment transport over the shelf and slope off of Superior's Keweenaw Peninsula. *J. Geophysical Res.*, 109:17, 2004.

[48] D.H. Clarke. *Copper mines of Keweenaw, No. 12*: *Mohawk Mining Company*. Lake Linden, Michigan, 1978.

[49] W.T. Claxton and G.L. Mackie. Seasonal and depth variations in gametogenesis and spawning of dreissena polymorpha and dreissena bugensis in eastern lake erie. *Can. J. Zool.*, 76:2010–2019, 1998.

[50] J. R. Coldwell and E. C. Gensler. Potential for submarine tailings disposal to affect the availability of minerals from united states coastal areas. ofr 101-93. Technical report, U.S. Bureau of Mines, 1993.

[51] P. M. Cook, G. E. Glass, and J. H. Tucker. Asbestiform amphibole minerals: Detection and measurement of high concentrations in municipal water supplies. *Science*, 185:853–855, 1974.

[52] J.B. Cotner, T.H. Johengen, and B.A. Biddanda. Intense winter heterotrophic production stimulated by benthic resuspension. *Limnol. Oceanogr.*, 45:1672–1676,

2000.

[53] N. Cressie. *Analytical and computer cartography*. Prentice-Hall, Englewood Cliffs, NJ, 1993.

[54] N. Cressie. *Fundamentals of geographical information systems*. Wiley, New York, 1997.

[55] P. Crow, S. Benham, B. J. Devereux, and G. S. Amable. Woodland vegetation and its implications for archaeological survey using lidar. *Forestry*, 80:241–252, 2007.

[56] David C Depew, Stephanie J Guildford, and Ralph E.H Smith. Nearshore?offshore comparison of chlorophyll a and phytoplankton production in the dreissenid-colonized eastern basin of lake erie. *Canadian Journal of Fisheries and Aquatic Sciences*, 63(5):1115–1129, 2006.

[57] R. Dermott, M. Munawar, R. Bunnel, S. Carou, H. Niblobk, T.F. Nalepa, and G.A. Messick. Preliminary investigation for causes of the disappearance of Diporeia spp. from Lake Onterio. In: Mohr, L.C., Nalepa, T.F. (Eds.), Proceedings of a Workshop on the Dynamics of Lake Whitefish (Coregonus clupeaformis) and the Amphipod Diporeia spp. in the Great Lakes. *Great Lakes Fishery Commission Technical Report*, 66:203–232, 2005.

[58] B. J. Eadie, D. J. Schwab, R. A. Assel, N. Hawley, M. B. Lansing, G. S. Miller, N. R.

Morehead, J. A. Robbins, P. L. Van Hoof, G. A. Leshkevich, G. A. Leshkevich, T. H Johengen, P. Lavrentyev, and R. E. Holland. Development of recurrent coastal plume in lake michigan observed for first time. *Eos, Transactions American Geophysical Union*, 77(35):337–338, 1996.

[59] E. N. Edinger, K. Azmy, W. Diegor, and P. R. Siregar. Heavy metal contamination from gold mining recorded in porites lobata skeletons, buyat-ratototok district, north sulawesi, indonesia. *Mar. Pollut. Bull.*, 56:1553–1569, 2008.

[60] D. V. Ellis and J. D. Robertson. Underwater placement of mine tailings: Case examples and principles. *Springer*, pages 123–141, 1999.

[61] M.A. Evans, G. Fahnenstiel, and D. Scavia. Incidental oligotrophication of North American great Lakes. *Environ. Sci. Technol.*, 45:3297–3303, 2011.

[62] G. Fahnenstiel, S. Pothhoven, H. Vandergloeg, D. Klrer, T. Nalepa, and D. Scavia. Recent changes in primary production and phytoplankton in the offshore region of southeastern Lake Michigan. *J. Great Lakes Res.*, 36:20–29, 2010.

[63] G.L. Fahnenstiel, R.A. Stone, M.J. McCormick, C.L. Schelske, and S.E. Lohrenz. Spring isothermal mixing in the Great Lakes: evidence of nutrient limitation and nutrient-light interactions in a suboptimal light environment. *Can. J. Fish. Aquat. Sci.*, 57:1901–1910, 2000.

[64] T. Nalepa S. Pothoven H. Carrick D. Scavia. Fahnenstiel, G. Lake michigan lower food web: Long-term observations and dreissena impact. *J. of Great Lakes Res.*, 36(3):1–4, 2010.

[65] S. A. Fitzgerald and W. Grdner. An algal carbon budget for pelagic-benthic coupling in lake michigan. *Limnol. Oceanogr.*, 38(3):547–560, 1993.

[66] R. Frouin, B. A. Franz, and P. J. Werdell. The SeaWiFS PAR product. p. 46-50. In Algorithm Updates for the Fourth SeaWiFS Data Reprocessing, ed. by S. B. Hooker and E. R. Firestone. *NASA/TM-2003-206892*, 22, 2003.

[67] G.C. Guenther. *Digital Elevation Model Technologies and Applications: The DEM Users Manual*. 2nd Edition, D. Maune, ed., American Society for Photogrammetry and Remote Sensing, Chapter 8 : Airborne lidar bathymetry, 253-320, 2007.

[68] S. B. Gewurtz, L. Shen, P. A. Helm, J.Waltho, E. J. Reiner, S. Painter, I. D. Brindle, and C. H. Marvin. Spatial distributions of legacy contaminants in sediments of lakes huron and superior. *J. Great Lakes Res.*, 34:153–168, 2008.

[69] K. Gnandi, G. Tchangbedji, K. Killi, G. Baba, and K. Abbe. The impact of phosphate mine tailings on the bioaccumulation of heavy metals in marine fish and crustaceans from the coastal zone of togo. *Mine Water*, 25:56–62, 2006.

[70] C. S. Goodyear, T. A. Edsall, D. M. Ormsby Dempsey, G. D. Moss, and P. E.

Polanski. Atlas of the spawning and nursery areas of great lakes fishes. u.s. fws/obs-82/52. Technical report, U.S. Fish and Wildlife Service, 1982.

[71] W.W. Gregg. Analysis of orbit selection for seawifs: ascending vs descending node. Technical report, NASA Tech. Memo 104566. Vol. 2, 16 pp, 1992.

[72] J. O. Grimalt, M. Ferrer, and E. Macpherson. The mine tailing accident in aznalcollar. *Sci. Total Environ.*, 242:3–11, 1999.

[73] G.C. Guenther, A.G. Cunningham, P.E. LaRocque, and D.J. Reid. Meeting the accuracy challenge in airborne lidar bathymetry. 2000.

[74] N. Hawley. Sediment suspension near the Keweenaw Peninsula, Lake Superior during the fall and winter 1990-1991. *J. Great Lakes Res.*, 26:495–505, 2000.

[75] R.E. Hecky, R.E.H. Smith, D.R. Barton, S.J. Gulldford, W.D. Taylor, M.N. Charlton, and T. Howell. The Nearshore phosphorus shunt: a consequence of ecosystem engineering b dreissenids in the Laurentian Great Lakes. *Can. J. Fish. Aquat. Sci.*, 16:1285–1293, 2004.

[76] J. D. Hedley, A. R. Harborne, and P. J. Mumby. Simple and robust removal of sun glint for mapping shallow-water benthos. *Int. J. Remote Sens*, 26:2107–2112, 2005.

[77] S.N. Higgins, S.J. Vander Zanden, L.N. Joppa, and Y. Vadeboncoeur. The effects

of dreissenid invasion on chlorophyll and the chlorophyll:total phosphorus ration in north-temperate lakes. *Can. J. Fish. Aquat. Sci.*, 63:319–329, 2011.

[78] Ruth E. Holland. Changes in planktonic diatoms and water transparency in hatchery bay, bass island area, western lake erie since the establishment of the zebra mussel. *Journal of Great Lakes Research*, 19(3):617 – 624, 1993.

[79] E. Todd Howell, Christopher H. Marvin, Robert W. Bilyea, Peter B. Kauss, and Keith Somers. Changes in environmental conditions during dreissena colonization of a monitoring station in eastern lake erie. *Journal of Great Lakes Research*, 22(3):744 – 756, 1996.

[80] W. Humphrey, A. Dalke, and K. Schulten. Preliminary report of Late Holocene lake-level variation in southern Lake Superior: Part 1. *Indiana Geological Survey, Open File Study*, 2000.

[81] J.L. Irish, J.K. McClung, and W.J. Lillycrop. Airborne lidar bathymetry: the shoals system. 103:43–53, 2000.

[82] J.R. Jensen. *Introductory digital image processing, 3rd Ed.* Upper Saddle River, NJ: Prentice Hall, 2005.

[83] J.R. Jensen. *Remote Sensing of the Environment: An Earth Resource Perspective, 2nd Ed.* Upper Saddle River, NJ: Prentice Hall, 2007.

[84] J. Jeong and D. Mcdowell. Characterization and transport of contaminated sediments in the southern central lake superior. *J. Miner. Mater. Charact. Eng.*, 2:111–135, 2003.

[85] J. Jeong, N. R. Urban, and S. Green. Release of copper from mine tailings on the keweenaw peninsula. *J. Great Lakes Res.*, 25:721–734, 1999.

[86] Rubao Ji, Changsheng Chen, Judith Wells Budd, David J. Schwab, Dmitry Beletsky, Gary L. Fahnenstiel, Thomas H. Johengen, Henry Vanderploeg, Brian Eadie, James Cotner, Wayne Gardner, and Marie Bundy. Influences of suspended sediments on the ecosystem in lake michigan: a 3-d coupled bio-physical modeling experiment. *Ecological Modelling*, 152:169–190, 2002.

[87] J. W. Johnston, T. A. Thompson, and S. J. Baedke. Preliminary report of late holocene lake-level variation in southern lake superior: Part 1. *Indiana Geological Survey, Open File Study. Indiana Univ.*, pages 99–18, 2000.

[88] V. Kelmas. Beach profiling and LIDAR bathymetry: an overview with case studies. *Journal of Coastal Research*, 27:1019–1028, 2011.

[89] W. C. Kerfoo, S. L. Harting, J. Jeong, J. A. Robbins, and R. Rossmann. Local, regional and global implications of elemental mercury in metal (copper, silver, gold, and zinc) ores: Insights from lake superior sediments. *J. Great Lakes Res.*,

52:162–184, 2004.

[90] W. C. Kerfoot, S. Harting, R. Rossmann, and J. A. Robbins. Anthropogenic copper inventories and mercury profiles from lake superior: Evidence for mining impacts. *J. Great Lakes Res.*, 25:663–682, 1999.

[91] W. C. Kerfoot and J. A. Robbins. Nearshore regions of lake superior: Multi-element signatures of mining discharges and a test of pb-210 deposition under conditions of variable sediment mass flux. *J. Great Lakes Res.*, 25:697–720, 1999.

[92] W. C. Kerfoot, R. Rossmann, and J. A. Robbins. Elemental mercury in copper, silver and gold ores: An unexpected contribution to lake superior sediments with global implications. *Geochem. Explor. Environ. Anal.*, 2:185–202, 2002.

[93] W.C. Kerfoot, J.W. Budd, B.J. Eadie, H.A. Vanderploeg, and M. Agy. Winter storms: sequential sediment traps record daphnia ephippial production, resuspension and sediment interactions. *Limnol. Oceanogr.*, 49:1365–1381, 2004.

[94] W.C. Kerfoot, J.W. Budd, S.A. Green, J.B. Cotner, B.A. Biddanda, D.J. Schwab, and H.A. Vanderploeg. Doughnut in the desert: late-winter production pulse in southern Lake Michigan. *Limnol. Oceanogr.*, 53(2):589–604, 2008.

[95] W.C. Kerfoot, J. Jeong, and J.A. Robbins. Lake Superior mining and the proposed Mercury Zero-discharge Region. *n M. Munawar Ed., State of Lake Superior.*

Ecovision World Monograph Series, pages 153–216, 2009.

[96] W.C. Kerfoot, G. Lauster, and J.A. Robbins. Paleolimnological study of copper mining around Lake Superior: Artificial varves from Portage Lake provide a high resolution record. *Journal of Coastal Research*, 39:649–669, 1994.

[97] W.C. Kerfoot, F. Yousef, J.W. Budd, S.A. Green, D.J. Schwab, and H.A. Vanderploeg. Approaching storm: Disappearing winter bloom in Lake Michigan. *J. Great Lakes Res.*, 36(3):30–41, 2010.

[98] W.C. Kerfoot, F. Yousef, S.A. Green, R. Regis, R. Shuchman, C.N. Brooks, M. Sayers, B. Sabol, and M. Graves. LiDAR (Light Detection and Ranging) and multispectral studies of disturbed Lake Superior coastal environments. *Limnol. & Oceanogr.*, 57:749–771, 2012.

[99] P.J. Kinzel, C.W. Wright, J.M. Nelson, and A.R. Burman. Evaluation of an experimental LiDAR for surveying a shallow, braided, sand-bedded river. *J. Hydraul. Eng.*, 133:838–842, 2007.

[100] J.T.O. Kirk. *Light and Photosynthesis in Aquatic Ecosystems*. 1994.

[101] J.J. Kolak, D.T. Long, W.C. Kerfoot, T.M. Beals, and S.J. Eisenreich. Nearshore versus offshore copper loading in Lake Superior sediments: Implications for transport and cycling. *J. Great Lakes Res.*, 25:611–624, 1999.

[102] K.J. Kraft. Pontoporeia distribution along the Keweenaw shore of Lake Superior affected by copper tailings. *J. Great Lakes Res.*, 7:258–263, 1979.

[103] K.J. Kraft and R.H. Sypniewski. Effect of sediment copper on the distribution of benthic macroinvertebrates in the Keweenaw Waterway. *J. Great Lakes Res.*, 7(3):258–263, 1981.

[104] R. Kreiss. Lake michigan mass balance. Technical report, Lake Michigan Monitoring Coordination Council, Muskegon, MI., 2004.

[105] D. C. Lam. Simulation of water circulation and chloride transports in lake superior for summer 1973. *J. Great Lakes Res.*, 4:343–349, 1978.

[106] D. A. Lancellotti and W. B. Stotz. Effects of shoreline discharge of iron mine tailings on a marine soft-bottom community in northern chile. *Mar. Pollut. Bull.*, 48:303–312, 2004.

[107] G.A. Lang and G.L. Fahnenstiel. *Great Lakes primary production model-Methodology and use*, 1996.

[108] P.E. LaRocque and G.R. West. *Airborne Laser Hydrography*: *An Introduction. ROPME/PERSGA/IHB Workshop on Hydrographic Activities in the ROPME Sea Area and Red Sea (Kuwait City).* 1990.

[109] Cheegwan Lee, David J. Schwab, Dmitry Beletsky, Jonathan Stroud, and Barry Lesht. Numerical modeling of mixed sediment resuspension, transport, and deposition during the march 1998 episodic events in southern lake michigan. *Journal of Geophysical Research: Oceans*, 112(C2), 2007.

[110] M. A. Lefsky, D. Harding, W. B. Cohen, G. Parker, and H. H. Shugart. Surface lidar remote sensing of basal area and biomass in deciduous forests of eastern maryland, usa. *Remote Sens. Environ.*, 67:83–98, 1999.

[111] Schwab D.J. Muhr G.C. Leshkevich, G.L. Satellite environmental monitoring of the great lakes: A review of noaa's great lakes coast watch program. *Photogrammetr. Eng. Remot. Sens.*, 59:371–379, 1993.

[112] B. M. Lesht, J. R. Stroud, M. J. McCormick, G. L. Fahnenstiel, M. L. Stein, L. J. Welty, and G. A. Leshkevich. An event-driven phytoplankton bloom in southern lake michigan observed by satellite. *Geophysical Research Letters*, 29(8):67–1–67–4, 2002.

[113] Barry M. Lesht, Richard P. Barbiero, and Glenn J. Warren. A band-ratio algorithm for retrieving open-lake chlorophyll values from satellite observations of the great lakes. *Journal of Great Lakes Research*, 39(1):138–152, 2013.

[114] James R. Liebig, Henry A. Vanderploeg, and Steven A. Ruberg. Factors affecting

the performance of the optical plankton counter in large lakes: Insights from lake michigan and laboratory studies. *Journal of Geophysical Research: Oceans*, 111(C5), 2006.

[115] S.E. Lohrenz, G.L. Fahnenstiel, O. Schofield, and D.F. Millie. Coastal sediment dynamics and river discharge as key factors influencing coastal ecosystem productivity in southeastern lake michigan. *Oceanography*, 21:61–69, 2008.

[116] Steven E. Lohrenz, Gary L. Fahnenstiel, David F. Millie, Oscar M. E. Schofield, Tom Johengen, and Trisha Bergmann. Spring phytoplankton photosynthesis, growth, and primary production and relationships to a recurrent coastal sediment plume and river inputs in southeastern lake michigan. *Journal of Geophysical Research: Oceans*, 109, 2004.

[117] R. D. Lytle. In situ copper toxicity tests: Applying likelihood ratio tests to daphnia pulex incubations in keweenaw peninsula waters. *J. Great Lakes Res.*, 25:744–759, 1999.

[118] R.D. Lyttle. In situ copper toxicity tests: applying likelihood ratio tests to Daphnia pulex incubations in Keeweenaw Peninsula waters. *J. Great Lakes Res.*, 25:744–759, 1999.

[119] D. R. Lyzenga. Remote sensing of bottomreflectance andwater attenuation

parameters in shallow water using aircraft and landsat data. *Int. J.Remote Sens.*, 2:71–82, 1981.

[120] R. W. Macdonald, B. Morton, and S. C. Johannessen. A review of marine environmental contaminant issues in the north pacific: The dangers and how to identify them. *Environ. Rev.*, 11:103–139, 2003.

[121] B.H. Mackey, J.J. Roering, and M.P. Lamb. Landslide-dammed paleolake perturbs marine sedimentation and drives genetic change in anadromous fish. *Pnas.org*, doi/10.1073/pnas.1110445108, 2011.

[122] C.P. Madenjian et al. Dynamics of the Lake Michigan food web, 1970-2000. *Can. J. Fish. Aquat. Sci.*, 59:736–753, 2002.

[123] K.W. Malueg, G.S. Schuytema, D.F. Krawczyk, and J.H. Gakstatter. Laboratory sediment toxicity tests, sediment chemistry and distribution of benthic macroinvertebrates in sediments from the Keweenaw Waterway, Michigan. *Environ. Toxicol. Chem.*, 3:233–242, 1984.

[124] M. Marges, G. S. Su, and E. Ragragio. Assessing heavy metals in the waters and soils of calancan bay, marinduque island, philippines. *J. Appl. Sci. Environ. Sanit.*, 6:45–49, 2011.

[125] H.M. Martin. *The centennial geological map of the northern peninsula of Michigan*,

1936.

[126] J. Martinez-Frias. Mine waste pollutes mediterranean. *Nature*, 388:120, 1997.

[127] C. M. Mayer, R. A. Keats, L. G. Rudstam, and E. L. Mills. Scale-dependent effects of zebra mussels on benthic invertebrates in a large eutrophic lake. *Journal of the North American Benthological Society*, 21(4):pp. 616–633, 2002.

[128] Mazina'igan. A chronicle of the lake superior ojibwe, 2007 summer edition. Technical report, Great Lakes Fish and Wildlife Commission, 2007.

[129] C.R. McClain, M.L. Cleave, G.C. Feldman, W.W. Gregg, S.B. Hooker, and N. Kuring. Science quality seawifs data for global biosphere research. Technical report, Sea Technology Reprint, 1998.

[130] MDEQ. *Toxicological evaluation for the Gay, Michigan stamp sand. W.O. No 20083.032.00*. Weston Solutions, Houghton, MI, 2006.

[131] J.L. Mida, D. Scavia, G.L. Fahnenstiel, S.A. Pothoven, H.A. Vanderploeg, and D.M. Dolan. Long-term and recent changes in southern Lake Michigan water quality with implications for present trophic status. *J. Great Lakes Res.*, 36(3):42–49, 2010.

[132] E.S. Millard, D.D. Myles, O.E. Johannsson, and K.M. Ralph. Seasonal phosphorus deficiency of Lake Ontario phytoplankton at two index stations: light versus

phosphorus limitation of growth. *Can. J. Fish. Aquat. Sci.*, 53:1112Ű1124, 1996.

[133] D.F. Millie, G.L. Fahnenstiel, H.J. Carrick, S.F. Lohrenz, and O.M.E. Schofield. Phytoplankton pigment in coastal Lake Michigan: Distribution during the spring isothermal period and relation with episodic sediment resuspension. *J. Phycol.*, 38:639–648, 2002.

[134] C.J. Monette. *Upper Peninsula's Wolverine*. Lake Linden, MI, 1992.

[135] R. Moran, A. Reichelt-Brushett, and R. Young. Out of sight, out of mine: Ocean dumping of mine wastes; the worldŠs oceans, already imperiled, face a new threat. *WorldWatch*, 22(2):30–34, 2009.

[136] A. Morel, Y. Hout, B. Gentili, P.J. Werdell, S.B. Hooker, and B.A. Franz. Examining the consistency of products derived from various ocean color sensors in ocean (Case1) waters in the perspective of a multi-sensor approach. *Remote Sensing of Environment*, 111:69–88, 2007.

[137] A. Morel and R. Smith. Relation between total quanta and total energy for aquatic photosynthesis. *Limnol. Oceanogr.*, 19(4):591–600, 1974.

[138] R.A. Morton and T.L. Miller. National assessment of shoreline changes:part 2. Historical shoreline changes and associated coastal land loss along the U.S. Southeast Atlantic Coast. *USGS. Open-file report*, 1401:40, 2005.

[139] W.A. Murdoch. *Boom copper: The story of the first United States mining boom*. 1943.

[140] T.F. Nalepa, D.L. Fanslow, and G.A. Lang. Transformation of the offshore benthic community in Lake Michigan: recent shift from the native amphipod Diporeia spp. to invasive mussel Dreissena rostrifoemis bugensis. *Freshwater Biology*, 54:466–479, 2009.

[141] T.F. Nalepa, D.L. Fanslow, and S.A. Pothoven. Recent Changes in density, biomass, recuruitment, size structure, and nutritional state of Derissena population in southern Lake Michigan. *J. of Great Lakes Res.*, 36(3):5–19, 2010.

[142] T.F. Nalepa and M.A. Quigley. Distribution of photosynthetic pigments in nearshore sediments of lake Michigan. *J. Great Lakes Res.*, 13:37–42, 1987.

[143] Thomas F Nalepa, David J Hartson, David L Fanslow, Gregory A Lang, and Stephen J Lozano. Declines in benthic macroinvertebrate populations in southern lake michigan, 1980-1993. *Canadian Journal of Fisheries and Aquatic Sciences*, 55(11):2402–2413, 1998.

[144] A. Nayegandhi, J. C. Brock, and C. W. Wright. Classifying vegetation using nasa's experimental advanced airborne research lidar (eaarl) at assateague island national seashore [cd-rom]. *American Society of Photometry and Remote Sensing*, 2005.

[145] A. Nayegandhi, J.C. Brock, C.W. Wright, and M.J. O'Connell. Evaluating a small footprint, waveform-resolving lidar over coastal vegetation communities. *Photogrammetric Engineering & Remote Sensing*, 72:1407–1417, 2006.

[146] R.N. Oldale. Coastal Erosion on Cape Cod : Some Questions and Answers. *Cape Naturalist*, 25:70–76, 1999.

[147] J. O'Reilly, S. Maritorena, D. Siegal, M. O'Brien, D. Toole, F. Chavez, P. Strutton, G. Cota, S.Hooker andC. McClain, K. Carder, F. Muller-Karger, L. Harding, A. Magnuson, D. Phinney, G. Moore, J. Aiken, K. Arrigo, R. Letelier, and M. Culver. Seawifs postlaunch calibration and validation analyses, part 3. Technical report, In Hooker, S.B. and Firestone, E.R. (eds), 2000.

[148] J.E. O'ŠReilly et al. SeaWiFS postlaunch technical report series. Volume 11, SeaWiFS postlaunch calibration and validation analyses, part3. *NASA Technical Memorandum 2000-206892*, 11, 2000.

[149] John E. O'Reilly, Stéphane Maritorena, B. Greg Mitchell, David A. Siegel, Kendall L. Carder, Sara A. Garver, Mati Kahru, and Charles McClain. Ocean color chlorophyll algorithms for seawifs. *Journal of Geophysical Research: Oceans*, 103(C11):24937–24953, 1998.

[150] James J. Pauer, Katherine W. Taunt, Wilson Melendez, Russell G. Kreis Jr., and

Amy M. Anstead. Resurrection of the lake michigan eutrophication model, mich1. *Journal of Great Lakes Research*, 33(3):554 – 565, 2007.

[151] S. Pe'eri and B. Long. Lidar technology applied in coastal studies and management. *J. Coastal Research*, 62:1–5, 2011.

[152] S.A. Pothoven and C.P. Madenjian. Changes in consumption by Alewives and Lake Whitefish after Dreissenid mussel invasions in Lake Michigan and Huron. *North American Journal of Fisheries Management*, 28:308–320, 2008.

[153] D. Pozdnyakov, R. Shuchman, A. Korosov, and C. Hatt. Operational algorithm for the retrieval of water quality in Great Lakes. *Remote Sensing of Environment*, 97:352–370, 2005.

[154] P.W. Sloss and J.H. Saylor. *Large-Scale Current Measurements in Lake Superior. NOAA Technical Report ERL 363-GLERL 8*. Great Lakes Environmental Research Laboratory, Ann Arbor, MI, 1976.

[155] N.D. Quadros, P.A. Collier, and C.S. Fraser. Integration of bathymetric and topographic Lidar: A preliminary investigation. *The International Archives of the Photogrammetry, Remote Sensing and Spatial Information Sciences*, B8:1299–1304, 2008.

[156] Great Lakes Water quality Board. Great lakes water quality, 1977 annual report.

Technical report, INTERNATIONAL JOINT COMMISSION, Windsor, Ontario, 1977.

[157] T. Rasmussen, R. Fraser, D.S. Lemberg, and R. Regis. Mapping stamp sand dynamics: Gay, Michigan. *J. Great Lakes Res.*, 28:276–284, 2002.

[158] D.J. Reed. Patterns of sediment deposition in subsiding coastal salt marches, Terrebonne Bay, Louisiana: the role winter storms. *Estuaries*, 12:222–227, 1989.

[159] R.G. Dean and K.A. Darlymple. *Water wave mechanics for engineers and Scientist*. 2nd series of ocean engineering, 1991.

[160] S. Roe and H.J. MacIsaac. Deep-water population structure and reproductive state of quagga mussels (dreissena bugensis) in lake erie. *Can. J. Fish. Aq. Sci.*, 54:2428–2433, 1997.

[161] B. Sabol, E. Lord, and K. Reine Snd D. Shafer. Comparison of acoustic and aerial photographic methods for quantifying the distribution of submersed aquatic vegetation in sagamore creek, nh. doer-e23. Technical report, U.S. Army Engineer Research and Development Center, 2008.

[162] M. K. Schubauer-Berigan, J. R. Dierkes, P. D. Monson, and G. T. Ankley. ph-dependent toxicity of cd, cu, ni, pb, and zn to ceriodaphnia dubia, pimephales promelas, hyalella azteca and lumbriculus variegates. *Environ. Toxic. Chem.*,

12:1261–1266, 1993.

[163] David J. Schwab and Dmitry Beletsky. Relative effects of wind stress curl, topography, and stratification on large-scale circulation in lake michigan. *Journal of Geophysical Research: Oceans*, 108(C2), 2003.

[164] D.J. Schwab, B.J. Eadie, R.A. Assel, and P.J. Roebber. Climatology of large sediment resuspension events in southern Lake Michigan. *J. Great Lakes Res.*, 32:50–62, 2006.

[165] Camilla B. Schwind. Knowledge based language tutoring. *Computer Assisted Language Learning*, 1996.

[166] S. Sharma, G. Mora, J.W. Johnston, and T.A. Thompson. Stable isotope ratios in swale sequences of Lake Superior as indicators of climate and lake level fluctuations during the Late Holocene. *Quatern. Sci. Reviews*, 24:1941–1951, 2005.

[167] R. Shuchman, A. Korosov, C. Hatt, D. Pozdnyakov, J. Means, and G. Meadows. Verification and application of a bio-optical algorithm for Lake Michigan using SeaWiFS: a 7-year inter-annual analysis. *J. Great Lakes Res.*, 32:258–279, 2006.

[168] R. A. Shuchman, M. Sayers, G. L. Fahnenstiel, and G. Leshkevich. A model for determining the satellite-derived primary productivity estimates for lake michigan. *Journal of Great Lakes Research*, 2013.

[169] G. Smith, G. Mocke, R. Van Ballegooyen, and C. Soltau. Consequences of sediment discharge from dune mining at elizabeth bay, namibia. *J. Coast. Res.*, 18:776–791, 2002.

[170] G. G. Smith. Assessment of the cumulative effects of sediment discharges from on-shore and near-shore diamond mining activities on the bclme. Technical report, Natural Resources and the Environment, CSIR, 2006.

[171] M. Sprung. *The other life: an account of present knowledge of the larval phase of Dreissena polymorpha*. In: Nalepa, T.F., Schloesser, D.W. (Eds.) Zebra Mussels: Biology, Impacts, and Control. CRC Press, Boca Raton, FL, 1993.

[172] Jonathan R. Stroud, Barry M. Lesht, David J. Schwab, Dmitry Beletsky, and Michael L. Stein. Assimilation of satellite images into a sediment transport model of lake michigan. *Water Resources Research*, 45(2), 2009.

[173] Richard P. Stumpf. Applications of satellite ocean color sensors for monitoring and predicting harmful algal blooms. *Human and Ecological Risk Assessment: An International Journal*, 7(5):1363–1368, 2001.

[174] R.P. Stumpf, R.A. Arnone, Jr. R.W. Gould, P.M. Martinolich, and V. Ransibrahmanakul. A partially coupled oceanŰatmosphere model for retrieval of water-leaving radiance from seawifs in coastal waters. algorithm updates for the

fourth seawifs data reprocessing:. Technical report, SeaWiFS Postlaunch Technical Report Series, vol. 22, 2003.

[175] R.P. Stumpf, V. Ransibrahmanakul, K. Hughes, R. Sinha, S. Ramachandran, and H. Gu. Esdim progress report: The evaluation of the atmospheric correction algorithms for processing seawifs data. Technical report, Project 392N-SeaWiFS Regional Pathfinder: Reproducing Validation, and Exploitation of SeaWiFS Ocean Color Data, 2000.

[176] T.A.Long, J. Angelo, and J.F. Weishampel. LiDAR-derived measures of hurricane- and restoration-generated beach morphodynamics in relation to sea turtle nesting behavior. *Intern. J. Remote Sensing*, 32(1):231–241, 2011.

[177] K.P.B. Thomson, J. Jerome, and W.R. McNeil. Optical properties of the Great Lakes (IFYGL). *Proc. Conf. Gt. Lakes Res.*, 17:811–822, 1974.

[178] N. R. Urban, X. Lu, Y. Chai, and D. S. Apul. Sediment trap studies in lake superior: Insights into resuspension, cross-margin transport, and carbon cycling. *J. Great Lakes Res.*, 30:147–161, 2004.

[179] A.H. Vanderploeg, T.F. Nalepa, D.J. Jude, E.L. Mills, K.T. Holeck, J.R. Liebig, I.A. Grigorvich, and H. Ojaveer. Dispersal and emerging ecological impacts of Ponto-Caspian species in the Laurentian Great Lakes. *Can. J. Fish. Aquat. Sci.*,

59:1209–1228, 2002.

[180] H.A. Vanderploeg, T.H. Johengen, P.J. Lavrentyev, C. Chen, G.A. Lang, M.A. Agy, M.H. Bundy, J.F. Cavaletto, B.J. Eadie, J.R. Liebig, G.S. Miller, S.A. Ruberg, and M.J. McCormick. Anatomy of the recurrent coastal sediment plume in Lake Michigan and its impacts on light climate, nutrients, and plankton. *J. Geophys. Res.-Oceans*, 112, 2007.

[181] H.A. Vanderploeg, J.R. Liebig, T.F. Nalepa, G.L. Fahnenstiel, and S.A. Pothoven. Dreissena and the disappearance of the spring phytoplankton bloom in Lake Michigan. *J. Great Lakes Res.*, 36(3):50–59, 2010.

[182] B.K. Walker, K.B. Lance, and R.E. Spieler. Relationship of reef fish assemblages and topographic complexity on southeastern Florida coral reef habitats. *J. Coastal Res.*, 53:39–48, 2009.

[183] D.S. Warrington. Great lakes chlorophyll and turbidity estimates using seawifs (sea-viewing wide field-of-view sensor) imagery. Master's thesis, Michigan Technological University Houghton, MI., 2001.

[184] C. W. West, V. R. Mattson, E. N. Leonard, G. L. Phipps, and G. T. Ankley. Comparison of the relative sensitivity of three benthic invertebrates to copper contaminated sediments from the keweenaw waterway. *Hydrobiologia*, 262:57–68,

1993.

[185] Weston Solution of Michigan, INC. *Migrating stamp sand migration plan technical evaluation*. Report prepared for Michigan Department of Environmental Quality, Remediation and Redevelopment division, 2007.

[186] R.G. Wetzel and G.E. Likens. *Limnological Analyses 3rd ed*. Springer, 2000.

[187] S.W. Wilhelm. *Field methods in the study of toxic cyanobacterial blooms: results and insights from Lake Erie research. In: Hudnell, H.K. (Ed.), Proceedings of the Interagency, International Symposium on Cyanobacterial Harmful Algal Blooms.* Advances in Experimental Medicine and Biology, 2008.

[188] L. Wilkinson. *version 10.0*. 2000.

[189] C.W. Wright and J.C. Brock. *EAARL: A lidar for mapping shallow coral reefs and other coastal environments*, 2002.

[190] G. Wynn. Canada and arctic north america: An environmental history. Technical report, ABC-CILO, 2007.

[191] P. L. Younger. Towards regulatory criteria for discharging iron-rich mine water into the sea. *Mine Water Environ.*, 27:56–61, 2008.

[192] K. Zhang, D. Whitman, S. Leatherman, and W. Robertson. Quantification of beach changes caused by hurricane Floyd along Florida's Atlantic coast using airborne Laser surveys. *J. Coastal Res.*, 211:123–134, 2005.

[193] J. Zhu, C. Chen, E. Ralph, S.A. Green, J.W. Budd, and F.Y. Zhang. . Prognostic modeling studies of the Keweenaw Current in Lake Superior. Part II: Simulation. *J. Physical Oceanogr.*, 31:396–410, 2001.